November 2019

PREDICTIVE SIMULATION OF HUMAN MOVEMENT AND APPLICATIONS TO ASSISTIVE DEVICE DESIGN AND CONTROL

Vinh Nguyen

PREDICTIVE SIMULATION OF HUMAN MOVEMENT AND APPLICATIONS TO ASSISTIVE DEVICE DESIGN AND CONTROL

A Dissertation Presented

by

VINH Q. NGUYEN

Submitted to the Graduate School of the

University of Massachusetts Amherst in partial fulfillment

of the requirements for the degree of

DOCTOR OF PHILOSOPHY

September 2019

Department of Mechanical and Industrial Engineering

PREDICTIVE SIMULATION OF HUMAN MOVEMENT AND APPLICATIONS TO ASSISTIVE DEVICE DESIGN AND CONTROL

A Dissertation Presented

by

VINH Q. NGUYEN

Approved as to style and content by:

_____
Frank C. Sup IV, Chair

_____
Xian Du, Member

_____
Brian R. Umberger, Member

_____
Sundar Krishnamurty, Department Head

Mechanical and Industrial Engineering

DEDICATION

I dedicate this to my parents, Sang Nguyen and Tuong Nguyen, and my wife, Loan Pham, for their unconditional love and support!

ACKNOWLEDGMENTS

First, I want to express great appreciation to my advisor, Professor Frank Sup IV, for his countless advising and guidance in the past five years. He has always been supportive and patient in his mentoring. I feel so lucky to have had him as an advisor.

I am deeply grateful to Professor Brian Umberger for his advising during my Ph.D. research. He has always been a great source of knowledge. Every time I spoke to him, I have learned something new.

I would also like to thank Professor Kourosh Danai who served as a committee member in my Master thesis and Ph.D. proposal. I learned lots of data analysis and modeling through his course. Thank Professor Xian Du for his feedback and comments on my dissertation and to be a part of the committee in my final defense.

Later, I would like to thank my friends and colleagues that I have worked with, Andrew, Mark, Russell, Ryan, and Jonaz. It has been wonderful working with them. I would like to thank all of my labmates, Punith, Qiandong, Soumitra, Julio, Ericber. My graduate school would not be so joyful without them. They have always offered me help when I needed: giving me a hand doing experiments, hanging out with me when I was bored, lending me money when I was broke, and so much more. I will probably miss those guys a lot after graduation.

I cannot thank enough to all of my family members, especially my parents and my wife, for their unconditional love and support. Knowing that my family always stands right next to me has given me more courage and strength to pursue my dreams.

I would also like to express my gratitude to the Vietnam Education Foundation (VEF) for their fellowship that allowed me to start my graduate school in the early days. VEF had opened the door from which I have been seeing the world.

This work was also supported by the National Science Foundation (IIS-1526986), the Defense Advanced Research Projects Agency (D16PC0092), and National Institute on Disabilities, Independent Living and Rehabilitation Research (90BI0033-01-00).

ABSTRACT

PREDICTIVE SIMULATION OF HUMAN MOVEMENT AND APPLICATIONS TO ASSISTIVE DEVICE DESIGN AND CONTROL

SEPTEMBER 2019

VINH Q. NGUYEN

B.Sc., HANOI UNIVERSITY OF SCIENCE AND TECHNOLOGY

M.Sc., UNIVERSITY OF MASSACHUSETTS AMHERST

Ph.D., UNIVERSITY OF MASSACHUSETTS AMHERST

Directed by: Professor Frank C. Sup IV

Predictive simulation based on dynamic optimization using musculoskeletal models is a powerful approach for studying biomechanics of human gait. Predictive simulation can be used for a variety of applications from designing assistive devices to testing theories of motor controls. However, one of the challenges in formulating the predictive dynamic optimization problem is that the cost function, which represents the underlying goal of the walking task (e.g., minimal energy consumption) is generally unknown and is assumed a priori. While different studies used different cost functions, the qualities of the gaits with those cost functions were often not provided. Therefore, this dissertation evaluates and examines different cost function forms for dynamic simulation of human walking. The problem of the walking cost function determination was cast as a bilevel optimization, which was solved using a nested evolutionary approach. The results showed cost functions based on a weighted combination of muscle-based performance criteria (e.g., metabolic cost, muscle fatigue), gait smoothness, and gait stability led to better walking solutions compared to any cost functions only based on muscle performance criteria. Further evaluations of the walking cost functions were done in the simulation cases of human walking augmented with assistive devices such as prosthesis and exoskeleton. The simulations of augmented walking were comparable to the experimental results, which suggests the potential of using the simulation approach to address problems of finding assistive device design and control.

TABLE OF CONTENTS

LIST OF TABLES

Table Page

LIST OF FIGURES

Figure Page

CHAPTER 1

INTRODUCTION

Modeling and simulation of musculoskeletal systems play an important role in studying the biomechanics of human movements. The simulation approach has been used to estimate variables that are difficult or impossible to measure (e.g., muscle forces, muscle controls, and joint torques) in human movements such as walking (Umberger 2010)(Koelewijn and van den Bogert 2016) and pedaling (Kaplan and H. Heegaard 2001)(Gidley, Marsh, and Umberger 2019). In addition, the simulation approach can be used to predict the human movements when experimental data is unavailable (Anderson and Pandy 2001)(Lin, Walter, and Pandy 2018). Recently, simulation approach has been used to predict human walking augmented by assistive devices such as prosthesis (Handford and Srinivasan 2018)(Handford and Srinivasan 2016). These predictive simulations, which are often formulated as a dynamic optimization problem can give valuable insights into rehabilitation and assistive device design and control. However, in formulating the dynamic optimization problem for walking, the cost function, which represents the underlying goal of the movement such as walking with minimial energy consumption, is generally unknown. Previous studies often made assumptions of the cost functions, which may greatly affect the predicted results. In this chapter, the current state-of-the-art modeling and simulation approach is first discussed. The problems and objectives of this dissertation are then presented.

1.1 Simulation approaches

Two approaches for biomechanical analysis are commonly used in the literature (Figure 1.1). The first approach is inverse dynamics. Given the measured motions, inverse dynamics results in the joint moments and forces (Otten 2003)(Winter 2009)(Dumas et al. 2009)(Serrancolí et al. 2016). The accuracy of inverse dynamics depends on the accuracy of the experimental data (Winter 2009). The second approach is forward dynamics. Given the control inputs such as

muscle excitations, forward dynamics results in the motion of the system (Otten 2003)(Erdemir et al. 2007). Therefore, forward dynamics can be set up without the experimental data (e.g., measured kinematics). However, a major challenge of forward dynamics is that the control inputs (e.g., muscle excitation) are usually unknown. Because the human body is over-actuated with multiple muscles crossing a joint, solving for the muscle excitation is challenging. This redundancy problem is often solved through optimization technique, which is based on the idea that human movements contain some optimality aspects such as minimizing energy cost, maximizing movement smoothness (Ralston 1976)(Flash and Hogan 1985).

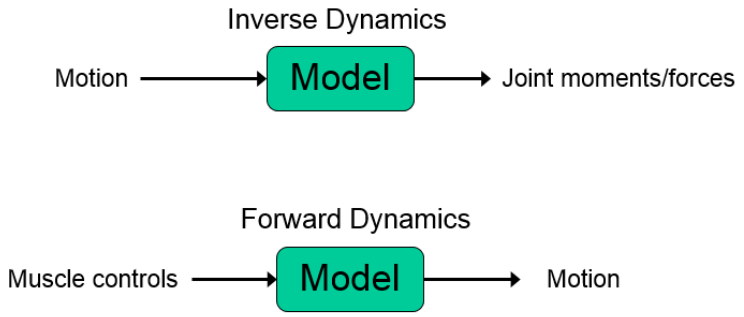

Figure 1.1: Forward dynamics and inverse dynamics

Optimization approaches for solving the muscle excitation can be divided into two groups, namely: static optimization and dynamic optimization. In static optimization, the muscle excitation is solved based on the resultant joint force/torque at a specific time step. The cost function in the optimization problem is, therefore, time-independent. There is no solving for the dynamic equation of the system over time involved (Patriarco et al. 1981)(Crowninshield and Brand 1981)(Thelen and Anderson 2006)(Luc, David, and Cahou 2002), which helps reduce the required computation cost. However, there are some potential drawbacks of static optimization. For example, time-dependent cost functions, such as total metabolic cost over a duration, which are sometimes desired cannot be included. Second, the dynamics of the musculoskeletal model over time does not involve, which may potentially lead to sudden and unrealistic changes in the result. Some studies have developed algorithms based on static optimization that improves the

abovementioned disadvantages such as computed muscle control algorithm (Thelen, Anderson, and Delp 2003) (Thelen and Anderson 2006), forward static optimization (Shourijeh, Mehrabi, and McPhee 2017). Nevertheless, a disadvantage of static optimization is that it relies on the experimental human data.

Different from static optimization, dynamic optimization is formulated as an optimal control problem, which requires solving for the dynamic differential equation representing the musculoskeletal model over time. Note that in the biomechanics literature, the term dynamic optimization is commonly used in place of optimal control (Umberger and Miller 2017). In this dissertation, dynamic optimization and optimal control are used interchangeably. Eq. 1.1 shows a typical dynamic optimization problem: minimize a cost function J, subject to the dynamic equation of the system (e.g., human body) (Eq. 1.1-b), and some constraints (Eq. 1.1-c).

$$\min_{\boldsymbol{x},\boldsymbol{u}} J(\boldsymbol{x}(t), \boldsymbol{u}(t), t) \tag{1.1-a}$$

$$\text{Subject to: } \dot{\boldsymbol{x}}(t) = f(\boldsymbol{x}(t), \boldsymbol{u}(t), t) \tag{1.1-b}$$

$$C_{lb} \leq C(\boldsymbol{x}(t), \boldsymbol{u}(t), t) \leq C_{ub} \tag{1.1-c}$$

where $\boldsymbol{x}(t) \in R^l$ is the state (e.g., joint angles, joint velocities) with l representing the dimension of the state, $\boldsymbol{u}(t) \in R^m$ is the muscle control (muscle excitation) with m representing the dimension of the control, t is the time, and C is the constraint, C_{lb} and C_{ub} are lower and upper bounds, respectively. In the dynamic optimization, the cost function J can be minimizing a performance criterion such as energy walking cost, and a tracking term representing the difference between the behaviors of the model and the human data. This problem is referred to as a *data-tracking problem* (Lee and Umberger 2016). When the tracking term is removed from the cost function, the dynamic optimization becomes independent from the experimental data, and the problem is referred to as a *predictive problem* (Anderson and Pandy 2001)(Ackermann and van den Bogert 2010). Being able to formulate a predictive problem is an important advantage that makes the dynamic optimization to be capable of predicting human movements (Anderson and

Pandy 2001)(Ackermann and van den Bogert 2010). Although dynamic optimization possesses the expensive computation challenge, the approach has been extensively used in studying human locomotion (Miller et al. 2011)(Fey, Klute, and Neptune 2012)(Anderson and Pandy 2001)(Ackermann and van den Bogert 2010). Therefore, this dissertation will focus on the dynamic optimization approach.

1.2 Musculoskeletal model

One of the first steps in the simulation is to create the musculoskeletal model, which captures the dynamics of the human body. The process of modeling the human musculoskeletal model is time and effort consuming. Therefore, some software packages have been developed to facilitate the process such as OpenSim (Delp et al. 2007) and SIMM/Dynamics Pipeline (Delp and Loan 2000). Due to the high complexity of human body with over 200 degrees of freedoms (DOF) and over 600 muscles (Prilutsky and Zatsiorsky 2002), studies often simplified the model but allowed the model to capture the dynamic behaviors of interest. In locomotion simulations, the upper body is usually modeled as a single segment that lumps the arms, head and some or all of torso together (Figure 1.2-a) (Anderson and Pandy 2001)(Neptune, Kautz, and Zajac 2001)(Zmitrewicz, Neptune, and Sasaki 2007)(Handford and Srinivasan 2016). The lower body can be allowed to move in the two-dimension (2D) sagittal plane (Zmitrewicz et al. 2007)(Miller et al. 2011)(Koelewijn and van den Bogert 2016) or three-dimensions (3D) (Anderson and Pandy 2001)(Xiang et al. 2009)(Xiang, Arora, and Abdel-Malek 2011)(Miller 2014)(Lin et al. 2018). Each lower limb is commonly modeled with some rigid body segments such as thigh, shank, and foot. These body segments are connected via joints where the rotation centers and the joint axes are usually assumed.

The model can be actuated by muscle-tendon units, which are often modeled based on the Hill-type muscle model (Thelen 2003)(Millard et al. 2013). The number of muscles in the models in the literature ranges from relatively small (13 muscles, (Handford and Srinivasan 2016)), to

medium (24 muscles, (Umberger 2010)), and large (80 muscles, (Lin et al. 2018)) amounts. While the musculoskeletal models actuated by muscles may be complicated, some studies used the model actuated by torque actuators at the joints (Xiang et al. 2011)(Bessonnet 2005)(Xiang et al. 2010) (Figure 1.2-b). However, models actuated by joint torques may not be able to provide the information in muscle level (e.g., muscle forces and muscle activations), which is often in the interest, especially in cases of amputees.

In walking, the feet interact with the ground to produce ground reaction forces (GRFs) that contain important features describing the gait. Studies often model the vertical foot-ground contact by viscoelastic, spring force, and the horizontal friction force by Coulomb friction (Neptune et al. 2001)(Fey, Klute, and Neptune 2013)(Miller 2014)(Koelewijn and van den Bogert 2016).

In general, adding more dynamics details (e.g., more degrees of freedoms, more muscles) into the musculoskeletal model may increase the model accuracy, but at the same time, it will require more computation cost in solving the simulation based on the dynamic optimization (Eq. 1.1). The next section will discuss the current practices of solving the dynamic optimization problem of human movements.

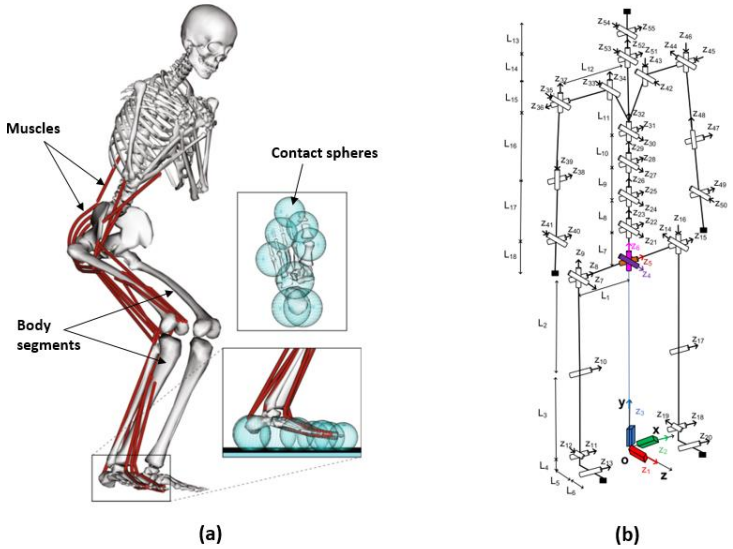

Figure 1.2: Human musculoskeletal models. (a)-Model actuated by muscles (Porsa et al. 2016); (b)-Model actuated by joint torques (Xiang et al. 2010)

1.3 Solving dynamic optimization problems

Dynamic optimization problems are usually solved numerically with direct methods. Direct methods transform the original optimal control problem (Eq. 1.1) into a nonlinear programming problem (NLP) by parameterizing the control, or both control and state, at discrete time steps $0 = t_0 < t_1 < \cdots < t_N = t_f$. The NLP latter is solved by an NLP solver or an optimization algorithm. In the case only control is parameterized, the method is called control parameterization (e.g., single shooting, multiple shooting). If both state and control are parameterized, then the method is called state and control parameterization (e.g., direct collocation, global collocation)(Rao 2009). In the literature, direct collocation and direct shooting methods are often used for simulation of human movements.

1.3.1 Shooting methods

In direct shooting methods, the control variable $\boldsymbol{u}$ is parameterized. The dynamic equation is satisfied by integrating Eq. 1.1-b over time. The shooting methods are often divided into single shooting method and multiple shooting method. In the single shooting method, the dynamic equation is integrated from the beginning t_0 to final time t_f. The cost function is calculated in the same way of integrating the dynamic equation. The process is repeated until the constraints are satisfied, and the cost function is optimized. Single shooting has been used for simulations of walking (Anderson and Pandy 2001)(Umberger 2010) and jumping (Porsa, Lin, and Pandy 2016). Single shooting method generally creates few optimization variables. However, solving the dynamic equation (Eq. 1.1-b) by integrating can be time-consuming, especially when the musculoskeletal model is complicated. In addition, since the dynamic equation is integrated for the whole time interval $[t_0, t_f]$, the method may be highly sensitive to the initial conditions (Rao 2009).

The multiple shooting method minimizes the sensitivity to initial conditions by dividing the time interval $[t_0, t_f]$ into some subintervals (Figure 1.3). Then in each subinterval $[t_i, t_{i+1}]$,

the single shooting method is performed. To fulfill the continuity of state for the whole time interval $[t_0, t_f]$, the initial state at one subinterval must be equal to the final state at the previous subinterval. This requirement can be done by adding equality constraints (Eq. 1.2):

$$\boldsymbol{x}(t_i^-) - \boldsymbol{x}(t_i^+) = 0 \tag{1.2}$$

where $\boldsymbol{x}(t_i^-)$ is the final state at subinterval $[t_{i-1}, t_i]$; and $\boldsymbol{x}(t_i^+)$ is the initial state at subinterval $[t_i, t_{i+1}]$. The multiple shooting method increases the number of optimization variables as now the state at the beginning of each subinterval are also parameters of the optimization problem. However, multiple shooting reduces the sensitivity to the initial conditions as the integration is performed in smaller time intervals. In addition, parallel computing could be performed for multiple subinterval integrations (Diehl et al. 2005). These advantages make the multiple shooting method sometimes favorable over the single shooting method. Multiple shooting has been used in the simulation of human locomotions (Mombaur, Truong, and Laumond 2010)(Handford and Srinivasan 2016). Nevertheless, integration of the dynamic equation as required in the multiple shooting method might still be computationally expensive, especially in cases of highly complex musculoskeletal models.

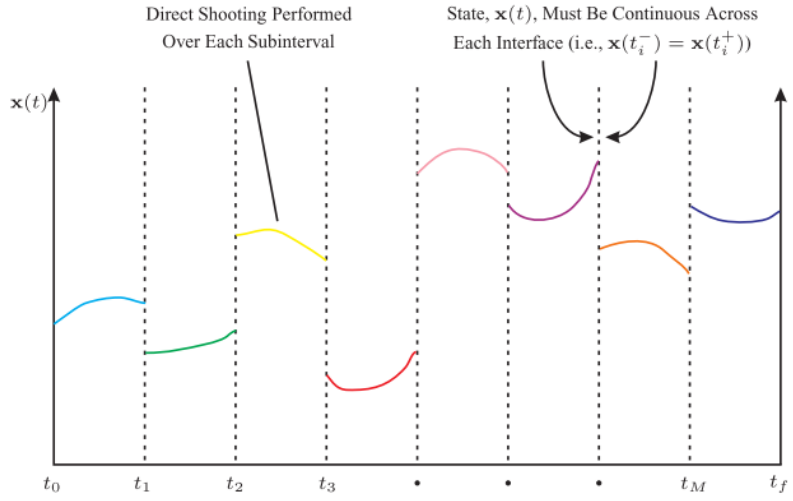

Figure 1.3: Schematic of the direct multiple shooting method (Rao 2009)

1.3.2 Direct collocation method

The direct collocation method avoids the integration of the dynamic equation by approximating the state and control at discrete time steps (nodes) simultaneously. Both state and control are parameterized to at multiple nodes $0 = t_0 < t_1 < \cdots < t_N = t_f$. The differential dynamic equation Eq. 1.1-b is satisfied by imposing equality constraints in the NLP through finite difference such as implicit Euler method (Eq. 1.3) (Lee and Umberger 2016)(Ackermann and van den Bogert 2010).

$$\boldsymbol{x}_{i+1} = \boldsymbol{x}_i + h_i f(\boldsymbol{x}_{i+1}, \boldsymbol{u}_{i+1}, t_{i+1}) \tag{1.3}$$

where $h_i = t_{i+1} - t_i$ is the time interval. Higher order implicit forms such as the mid-point method (Van Den Bogert, Blana, and Heinrich 2011) may potentially improve the accuracy of the results (Betts 2010). However, using higher order forms increases the computation requirement and reduces the sparsity of the NLP (Betts 2010). The direct collocation method generally creates a larger-scale NLP compared to the shooting methods, but the NLP with the direct collocation is usually highly sparse. The sparsity of NLP once being exploited can greatly reduce the computation cost (Lee and Umberger 2016)(Porsa et al. 2016).

To solve the NLP problems, studies usually used gradient-based NLP solvers such as IPOPT (Wächter 2003), SNOPT(Gill, Murray, and Saunders 2005), or fmincon (Matlab, the MathWorks, Inc.). These solvers have been successfully used in different simulations of human movements such as walking and jumping (Ackermann and van den Bogert 2010)(Lee and Umberger 2016)(Porsa et al. 2016)(Lin et al. 2018). Some derivative-free algorithms such as simulated annealing (Zmitrewicz et al. 2007)(Umberger 2010) or Covariance Matrix Adaptation (Dorn et al. 2015) were also used to solve the NLP problems. These derivative-free algorithms may increase the chances to converge to a global optimum. However, these derivative-free algorithms are often more computationally expensive compared to gradient-based algorithms.

1.4 Walking cost function problem

One of the challenges in formulating the dynamic optimization of walking is that the cost function (Eq. 1.1-a) is generally unknown. Studies usually make assumptions about the walking cost function, even though it is known that different cost functions can lead to different simulation results (Ackermann and van den Bogert 2010)(Miller et al. 2011)(Koelewijn, Dorschky, and van den Bogert 2018). It has been observed that human walks in manners that minimize some aspects such as the metabolic energy cost per unit distance traveled (Ralston 1976)(Figure 1.4). Therefore, minimizing metabolic cost per distance traveled has been used in the formulation of the dynamic optimization of walking (Anderson and Pandy 2001)(Brian R Umberger 2010)(Miller 2014)(Lin et al. 2018) (Eq. 1.4). Other studies have used the performance criteria, which are related to the metabolic energy, such as sum of muscle activations or excitations (Eq. 1.5) (Kaplan and H. Heegaard 2001)(Van den Bogert et al. 2012)(Koelewijn and van den Bogert 2016)(Ackermann and van den Bogert 2010) or the sum of muscle stresses (Miller et al. 2011) (Eq. 1.6). These cost functions often allowed to generate human-like walking solutions.

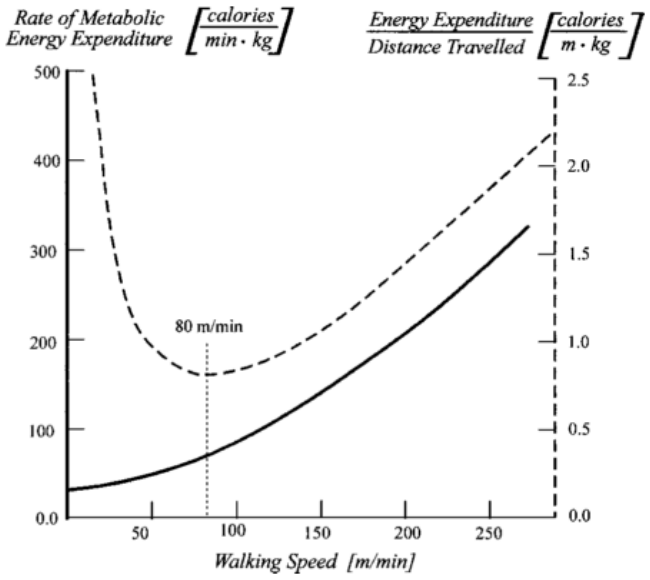

Figure 1.4: Metabolic energy expenditure plotted as a function of walking speed (Anderson & Pandy, 2001)

$$J = \frac{\int_0^{t_f} \dot{E}_{total}^M}{X(t_f) - X(t_0)} \tag{1.4}$$

$$J = \frac{1}{\sum_{i=1}^{m} w_i} \frac{1}{t_f} \sum_{i=1}^{m} w_i \int_0^{t_f} a_i^p(t) dt \tag{1.5}$$

$$J = \frac{1}{t_f} \sum_{i=1}^{m} \left[\int_0^{t_f} \left(\frac{F_i}{PCSA_i} \right)^2 dt \right] \tag{1.6}$$

where $\dot{E}_{total}$ is the rate of metabolic expenditure; $X(0)$ and $X(t_f)$ are the model horizontal positions at the beginning and final time, respectively. a_i is muscle activation of the muscle i^{th} of total m muscles. w_i is the weight associated with the muscle i^{th}. F_i is the force in the muscle i^{th} , and $PCSA_i$ is the physiological cross-sectional area of the muscle i^{th} (Haxton 1944).

Some studies have also suggested that the cost function of walking may be a trade-off among more some performance criteria (Dorn et al. 2015). Therefore, additional performance criteria have been evaluated as parts of the cost functions. These criteria, for example, include joint contact forces (Fey et al. 2012), differences in velocity of the center of mass (CoM) with targeted velocity (Dorn et al. 2015), passive moments applied at joints (Umberger 2010), and rate of changes of ground reaction forces (GRFs) (Rebula and Kuo 2015) (Table 1.1). Rebula and Kuo 2015 showed combining performance criteria can lead to more realistic results (e.g., simulated GRFs were smooth like in human data). However, it is unknown how these criterion terms should be weighted in the cost function. In addition, while different studies used different cost function forms, the quantitative qualities of the gait solutions using those cost functions were often not provided. Therefore, there is a need to evaluate the cost functions used in the literature, and determine the cost function forms that can be used in the dynamic optimization of human walking.

Studies	Cost functions	
	Muscle-based performance criteria	**Other criteria**
(Davy and Audu 1987)	Metabolic cost, muscle fatigue	-
(Anderson and Pandy 2001)	Metabolic cost	-
(Kaplan and H. Heegaard 2001)	Sum of squared muscle excitation	-
(Xiang et al. 2011)	Sum of squared joint torques	-
(Umberger 2010)	Metabolic cost	Passive moments applied at joints
(Ackermann and van den Bogert 2010)	Muscle activation based functions	-
(Srinivasan 2010)	Metabolic cost	-
(Fey et al. 2012)	Metabolic cost	Joint contact forces
(Van den Bogert et al. 2012)	Sum of squared muscle controls	-
(Miller et al. 2011)	Metabolic cost, muscle activation based functions, muscle fatigue	-
(Dorn et al. 2015)	Metabolic cost	Deviation of velocity of center of mass, relative velocity of head and center of mass
(Rebula and Kuo 2015)	Joint torques	Ground reaction force derivative
(Koelewijn and van den Bogert 2016)	Squared muscle excitation	Joint moment asymmetry (amputee)
(Handford and Srinivasan 2016)	Metabolic cost	Prosthesis cost (amputee)
(Uchida et al. 2016)	Sum of squared muscle activation	Torque applied by reserve actuator
(Koelewijn et al. 2018)	Muscle effort based on muscle activation; metabolic cost	-
(Lin et al. 2018)	Metabolic cost	-

Table 1.1: Cost functions in some relevant studies

1.5 Applications of predictive simulation in assistive device design and control

Restoring and improving an individual functional walking ability is in the great interests in the biomechanics and robotics fields. Many assistive devices such as prostheses and exoskeletons have been developed. However, few of them have succeeded to reduce the metabolic cost of walking (Malcolm et al. 2013)(Zhang et al. 2017), or improve stability (Kim and Collins 2015). A possible reason is that the current practice of design and control of assistive

devices is highly time and effort consuming, which prevents quickly exploring different design and control parameters. Some studies have used the simulation approach to facilitate the process of design and control of assistive devices. For example, Fey et al. (Fey et al. 2012) used dynamic optimization with tracking data to optimize the stiffness of a passive prosthesis. Lapre et al. used a forward integration tool to evaluate the performance of a powered ankle prosthesis (Laprè, Umberger, and Sup 2014). OpenSim computed muscle control algorithm (Thelen et al. 2003) was used to simulate human running with assistive devices augmented at different joints (Uchida et al. 2016), and human walking with assistive devices while carrying heavy loads (Dembia et al. 2017). These simulation studies can provide insights into the design and control of the assistive devices. However, a substantial limitation in these studies is the requirement of the experimental data and the assumption that the gait kinematics and kinetics were fixed with the change of the assistive device parameters, even though experimental reports show significant changes in the gait profiles with the assistive device (Galle et al. 2013)(Koller et al. 2015)(Quinlivan et al. 2017).

Simulations based on the dynamic optimization, on the other hand, can be formulated as predictive problems that are independent of experimental data. Recent studies have used predictive simulation to predict human movements augmented by assistive devices. For example, amputee walking on powered prosthesis ankles was generated to examine different control strategies of the ankle prosthesis (Handford and Srinivasan 2018) (Handford and Srinivasan 2016). In these simulations, the gait solutions were found along with the control of the ankle device. Without the need for the experimental data, predictive simulation based on the dynamic optimization may be a promising approach to address the problems of design and control of the assistive device.

1.6 Research objectives

Predictive simulation of human gait based on dynamic optimization is a promising approach that can be used for a variety of applications from rehabilitation to assistive device design and control. However, one of the challenges in formulating the optimization problem is that the cost function is unknown and generally assumed a priori. Therefore, this dissertation is aimed to determine the walking cost function that can be used for generating predictive optimal control of human walking. Our hypothesis is that the cost function can be represented as a weighted combination of some performance criteria (e.g., energy cost, smoothness, stability). The result of the walking cost function may allow prediction of the human gait profiles with more accuracy and reliability. Furthermore, the result may give insights about the motor control of human walking.

In addition, this dissertation develops a simulation tool based on the predictive dynamic optimization for studying the biomechanics of human movement augmented by assistive devices. Simulation studies of able-bodied walking with an exoskeleton, amputee walking with a prosthesis, and upper limb lifting with an exoskeleton are conducted. The simulation results help better understand the biomechanics of human-robotic device interaction. Besides, the results can provide insights into the design and control of assistive devices.

1.7 Dissertation overview

The remainder of this dissertation details the accomplishments of the research objectives. Chapter 2 is adapted from a paper accepted to the journal of Transaction of Neural Science and Rehabilitation (Nguyen, Johnson, et al. 2019). Here, an approach based on bilevel optimization for the walking cost function determination based on the experimental gait data is presented. The bilevel optimization, which consists of two coupled optimization problems, is solved through a nested evolutionary approach. The nested evolutionary approach was shown to effectively solve different bilevel optimization problems, including human walking problems.

Chapter 3 evaluates a variety of cost function forms that can be used for predictive simulation of able-bodied human walking. These cost functions are based on a set of performance criteria such as muscle activation, gait stability, and gait smoothness. With the bilevel optimization approach presented in Chapter 2, parameters of the cost functions were optimized to ensure the best walking solutions with the cost functions. The results showed that the cost function based on muscle-based criteria, gait smoothness, and stability can be used to predict human gaits.

Chapter 4 is adapted from a paper accepted to the IEEE International Conference on Rehabilitation Robotics (Nguyen, Umberger, and Sup IV 2019). Using the cost function found in Chapter 3, predictive simulations of human walking augmented by a powered ankle exoskeleton were generated. The simulation allows to evaluate the performance of the assistive device and provide a generic optimal assistive ankle torque pattern.

Chapter 5 addresses the problem of determining the cost function for the dynamic simulation of amputee walking. Similar to Chapter 3, here, a variety of cost function forms were evaluated. Besides the performance criteria used similar in able-bodied walking as in Chapter 3, minimizing the socket load criterion was examined. The simulations showed that the cost function based on muscle activation, gait smoothness, and gait stability led to the best gait solutions compared to other cost functions. This result suggests that muscle activation, gait smoothness, and stability are all likely important in amputee walking.

In Chapter 6, the effects of inclusion internal dynamics of the robotic actuator in the simulation of augmented human movement were examined. A simulation of an upper limb wearing a powered exoskeleton lifting an object was used. The device actuator, which is based on DC motors, was modeled using various ways with different detail levels. The results showed while the effects of mass and inertia of the actuator may be small, the electromechanical dynamics of the DC motor can significantly affect the simulation results. This chapter's result is

submitted as a paper to the journal the International Journal for Numerical Methods in Biomedical Engineering, which is currently under review.

The final chapter summarizes key findings and conclusions. In addition, suggestions for future works and research directions are discussed.

CHAPTER 2

BILEVEL OPTIMIZATION APPROACH FOR COST FUNCTION DETERMINATION IN DYNAMIC SIMULATION OF HUMAN GAIT

This chapter is adapted from a paper titled *Bilevel optimization for cost function determination in dynamic simulation of human gait* accepted to the journal of Transaction of Neural Science and Rehabilitation (Nguyen, Johnson, et al. 2019).

Predictive simulation based on dynamic optimization using musculoskeletal models is a powerful approach for studying human gait. Predictive musculoskeletal simulation may be used for a variety of applications that range from designing assistive devices to testing theories of motor control. However, the underlying cost function for the predictive optimization is unknown and is generally assumed *a priori*. Alternatively, the underlying cost function can be determined from among a family of possible cost functions, representing an inverse optimal control problem that may be solved using a bilevel optimization approach. In this study, a nested evolutionary approach is proposed to solve the bilevel optimization problem. The lower level optimization is solved by a direct collocation method, and the upper level is solved by a genetic algorithm. We demonstrate our approach to solve different bilevel optimization problems, including finding the weights among three common performance criteria in the cost function for normal human walking. The proposed approach was found to be effective at solving the bilevel optimization problems. This approach should provide practical utility in designing assistive devices to aid mobility, and could yield insights about the control of human walking.

2.1 Introduction

Simulation of musculoskeletal motion via dynamic optimization is a powerful approach for studying the biomechanics of human movement. Inherent in the forward dynamics approach is the ability to formulate the dynamic optimization problem independent of experimental data,

leading to a predictive musculoskeletal simulation. Predictive simulation has been used to study able-bodied walking (Anderson and Pandy 2001)(Umberger 2010) , and more recently to study walking in the case of lower limb loss with a powered prosthesis (Handford and Srinivasan 2016)(Handford and Srinivasan 2018). Indeed, the potential applications to rehabilitation and assistive device design are among the most promising areas for predictive biomechanical simulation. However, in generating a predictive simulation of human walking, the cost function is generally unknown and is usually assumed a priori, even though it is known that different forms of the cost function can lead to different results (Ackermann and van den Bogert 2010)(Miller et al. 2011)(Gidley et al. 2019). In a predictive simulation, the cost function represents the goal of the movement task, such as walking with minimal cost or jumping as high as possible. In all likelihood, the cost function for walking is actually a combination of multiple performance criteria, such as metabolic energy, stability, and smoothness (Dorn et al. 2015). While it has been shown that combining multiple performance criteria, such as rate of force production and mechanical work, leads to more realistic simulations in a simple walking model (Rebula and Kuo 2015), the general form of the cost function and the weighting among terms remain unknown. The problem of determining the cost function may be understood as an inverse optimal control problem, which can be cast as a bilevel optimization (Mombaur et al. 2010)(Sinha, Malo, and Deb 2017).

The bilevel optimization problem consists of two coupled optimization problems: the upper and the lower level, where the lower level optimization results are the constraints on the upper level optimization problem (Sinha et al. 2017). In the case of identifying the cost function for human movements, the lower level represents a complete, single optimization of the movement in question (Bottasso et al. 2006). This problem takes the form of Eq. 2.1-c, d, e to minimize the cost function, subject to the dynamic equation of the musculoskeletal model and some constraints (e.g., joint limits). The upper level adjusts the cost function parameters to

minimize the difference between the solution of the lower level and the experimental data (Eq. 2.1-a, b).

$$\min_{\boldsymbol{w}} e \tag{2.1-a}$$

$$\text{Subject to: } \boldsymbol{w}_{lb} \leq \boldsymbol{w} \leq \boldsymbol{w}_{ub} \tag{2.1-b}$$

$$\min_{\boldsymbol{x},\boldsymbol{u}} J(\boldsymbol{w}, \boldsymbol{x}, \boldsymbol{u}, t) \tag{2.1-c}$$

$$\text{Subject to: } \dot{\boldsymbol{x}} = f(\boldsymbol{x}, \boldsymbol{u}, t) \tag{2.1-d}$$

$$C_{lb} \leq C(\boldsymbol{x}, \boldsymbol{u}, t) \leq C_{ub} \tag{2.1-e}$$

where $\boldsymbol{w} \in R^n$ is the unknown parameter in the cost function for the human movement J, n is the dimension of $\boldsymbol{w}$, e is the error between the solution of the lower level and the experimental data, $\boldsymbol{x}(t) \in R^l$ is the state (e.g., joint positions, joint velocities, muscle lengths and activations) with l representing the dimension of the state, $\boldsymbol{u}(t) \in R^m$ is the muscle control (muscle excitation) with m representing the dimension of muscle control, t is the time, and C is the constraint, C_{lb} and C_{ub} are lower bound and upper bound of the constraint, respectively. Eq. 2.1-d represents the dynamical equation describing the musculoskeletal model. In the case of determining the cost function for human walking, the unknown parameter $\boldsymbol{w}$ can represent any number of parameters in the cost function, such as the exponent of the muscle activation (Ackermann and van den Bogert 2010), or the weights among various performance criteria (Clever and Mombaur 2016). The criteria could be quantities such as muscle activations, gait stability, and movement smoothness. The experimental data that are used to calculate the error, e, would commonly be measured kinematic (e.g., joint angles) and kinetic (e.g., ground reaction force (GRF)) data. Solving the lower level requires generating a complete optimal control simulation of walking (Anderson and Pandy 2001)(Umberger 2010) for a given set of parameter values in the upper level.

Bilevel optimizations are intrinsically difficult as they are nonconvex and non-differentiable even for simple problems (Colson, Marcotte, and Savard 2007). Some solution

approaches have been proposed in the literature. These approaches can be divided into classical and evolutionary approaches (Sinha et al. 2017). Classical approaches, such as single-level reduction with Karush-Kuhn-Tucker (KKT) conditions, and descent methods, mainly focus on well-behaved bilevel problems and relatively small-scale optimization problems. For example, a bilevel optimization was used to find the unknown weights among different performance terms in the cost function for simple models of a human arm and a human leg generating forces in different directions (Bottasso et al. 2006). In this work, a single-level reduction approach was used. The bilevel optimization problems were converted to standard optimization problems that were solved using nonlinear programming (NLP) methods. Similarly, the single-level reduction is used to solve the bilevel optimization of finding the weights for performance terms in the cost function of an arm reaching task (Albrecht et al. 2011). In these cases that used the single-level reduction approach, the lower levels were relatively simple, involving a static optimization problem for arm and leg pushing problems (Bottasso et al. 2006), and a dynamic optimization with a simple arm model (Albrecht et al. 2011). When the lower level is a substantial dynamic optimization problem, with many unknowns and highly nonlinear dynamics, such as human walking simulated with a complex musculoskeletal model, the single-level reduction with KKT conditions will lead to a very large-scale optimization problem that may be difficult to solve.

As alternatives to the classical approaches, evolutionary algorithms have been successfully used for complex bilevel optimization problems (Sinha et al. 2017). A popular approach is the nested evolutionary algorithm. In this approach, some solution candidates (populations) for the upper level are initialized. The lower level problem is solved corresponding to each upper level solution candidate, then the results are used to evaluate and update the population (Sinha et al. 2014). The process is repeated until the termination condition for the upper level is met. The upper optimization problem is solved with a derivative-free algorithm (e.g., genetic algorithm, simulated annealing), while the lower optimization problem may be solved with a classical method (e.g., shooting method, direct collocation) or a derivative-free

algorithm (Mombaur et al. 2010)(Yin 2000)(Zhao and Gu 2006)(Suryan et al. 2016)(Clever and Mombaur 2016). Although effective, a main disadvantage of the nested evolutionary algorithm is that it is computationally expensive, especially when the lower level problem is time-consuming to solve. Fortunately, some evolutionary algorithms are well-suited to parallel implementation for reducing computation time.

In applying bilevel optimization to the problem of human walking using the nested evolutionary approach, the lower level requires generating a full predictive simulation of human walking. The predictive problem has usually been solved through direct methods such as the shooting method (Anderson and Pandy 2001)(Umberger 2010), and direct collocation (Ackermann and van den Bogert 2010)(Lin et al. 2018). These direct methods transform the dynamic optimization problem into a NLP problem (Rao 2009). The NLP problem is then solved by a NLP solver such as SNOPT (Gill et al. 2005) or IPOPT (Wächter 2003). The direct collocation approach results in a highly sparse NLP, and that sparsity can be exploited for computational efficiency. This advantage makes the direct collocation method an attractive choice over the traditional shooting method in biomechanics (Porsa et al. 2016)(Lee and Umberger 2016). Therefore, the direct collocation method may be used to solve the lower level problem in a reasonable time, which makes it practical to solve the bilevel optimization problem with the nested evolutionary approach.

Herein, we propose applying the nested evolutionary approach to solve the bilevel optimization problem of determining the cost function for human walking. The challenge of a potentially prohibitive computational cost was overcome by efficiently solving the lower level problem with the direct collocation method, and implementing parallel computing for a continuous genetic algorithm (GA) for solving the upper level problem. We first demonstrate the use of our approach for a simple bilevel optimization example with a known, analytical solution. Then, the proposed approach was used to determine the weights among performance criteria in a cost function such that predicted walking gaits match as closely as possible to target kinematics

and GRFs. For the walking problems we used both a synthetic gait, where a perfect match to the target is possible, and experimental human gait data, as is typically used in these applications. The objective in both cases was to find the optimal weights among performance criteria based on muscle activation, gait stability, and movement smoothness. The robustness of the proposed approach was evaluated by comparing the quality of the solutions for different, randomly chosen initial guesses.

2.2 Method

The bilevel optimization problem (Eq. 2.1) was solved with a nested evolutionary algorithm. The lower level was solved efficiently with the direct collocation method in which both the state and control variables are parameterized and searched for simultaneously (Lee and Umberger 2016)(Rao 2009). The upper level is solved with a GA that is based on evolutionary theory. GA is derivative-free and has been used for solving a wide variety of optimization problems (Haupt and Haupt 2004)(Mitchell 1998). In addition, GA is ideal for parallel computing implementation, which can significantly reduce the overall computation time (Van Soest and Casius 2003).

2.2.1 Genetic algorithm (GA)

The GA algorithm in this study works directly on the continuous variable $\boldsymbol{w}$ in the upper level (Eq. 2.1). The algorithm consists of several steps: Initializing the population, fitness evaluation, selection, recombination, mutation, and termination checking (Haupt and Haupt 2004). At the beginning, an initial population of candidate solutions for the upper level problem is generated (Eq. 2.2).

$$\boldsymbol{P} = \begin{bmatrix} w_{11} & \cdots & w_{1n} \\ \vdots & \ddots & \vdots \\ w_{q1} & \dots & w_{qn} \end{bmatrix} \tag{2.2}$$

where $\boldsymbol{P}$ is a $q \times n$ matrix. Each row of $\boldsymbol{P}$ represents a candidate solution (individual) for the upper level optimization problem, which is a vector size of n $\boldsymbol{w}_i = [w_{i1}, \dots, w_{in}]$, and $w_{ik} \in [\boldsymbol{w}_{lb}(k),\ \boldsymbol{w}_{ub}(k)]$ with $i = 1, \dots, q$; $k = 1, \dots, n$. In the evaluation step, the fitness of each individual in the population is calculated. Here, $\boldsymbol{w}_i$ will be treated as a constant in the cost function of the lower level optimization (Eq. 2.1-c). The solution of the lower level $\boldsymbol{x}^*(t)$ is used to evaluate the fitness (Eq. 2.3).

$$Fitness(i) = \frac{1}{\varepsilon + e} \tag{2.3}$$

where $Fitness(i)$ is the fitness of the candidate $\boldsymbol{w}_i$; e is the upper level cost function (i.e., error between $\boldsymbol{x}^*(t)$ and the experimental human gait data), and ε is a small positive number to avoid dividing by zero. The fitnesses of multiple individuals are evaluated simultaneously using the Parallel Computing Toolbox in MATLAB (The MathWorks, Inc. version 2017a) on an Intel i9 10-core 3.5GHz CPU to reduce computation time.

The selection step chooses the candidates for the next steps based on stochastic universal sampling which allows weak fitness individuals to have chances to be chosen (Haupt and Haupt 2004). The recombination and mutation steps worked directly with the real variables $\boldsymbol{w}_i$ as described in (Chelouah and Siarry 2000). The algorithm is stopped when there is no significant improvement through some generations or when the number of generations exceeds the maximum number of generations.

2.2.2 Direct collocation

The direct collocation method was used in this study for the lower level problems. The states and controls are discretized along the time axis (Eq. 2.4).

$$\boldsymbol{z} = \left(\boldsymbol{x}_1, \cdots, \boldsymbol{x}_N, \boldsymbol{u}_1, \cdots, \boldsymbol{u}_N, t_f\right) \in R^{N(l+m)+1} \tag{2.4}$$

where N is the number of nodes, t_f is the time final. The dynamic equation (Eq. 2.1-d) is fulfilled using finite differences, such as the Euler or mid-point method (Rao 2009)(Van Den Bogert et al.

2011). The lower level problem then becomes an NLP problem, which is solved with an NLP solver, either IPOPT or fmincon (MATLAB optimization toolbox).

In the problem of human walking, given the unknown parameter $\boldsymbol{w}$ value fixed in the cost function (Eq. 2.1-c), the lower level represents a full optimal control solution for human gait (Ackermann and van den Bogert 2010). In solving this problem, the time final t_N is allowed to change in a suitable range so that the model can choose the optimal stride frequency when the walking speed is fixed. The direct collocation formulation results in a highly sparse NLP problem. This sparsity property is exploited in calculating the derivatives of the constraints to reduce computational cost (Porsa et al. 2016)(Lee and Umberger 2016).

2.2.3 Problem 1: Demonstration for simple example

We first demonstrated our approach by solving a simple bilevel optimization (Problem 1) (Eq. 2.5). The upper level solves for the weight $w \in R^1$. The lower level (Eq. 2.5-c, d, e) is a dynamic optimization, which was used as a test problem in past studies (Vlassenbroeck and Van Dooren 1988)(McAsey, Mou, and Han 2012). To leverage the analytic solution from the past studies for the lower level, the form of the problem is kept the same, and the weight w is introduced to the cost function. With $w = 1$, the lower level has the analytic solution $x(1) = 0.28197$ (McAsey et al. 2012). Therefore, the bilevel problem has an analytic solution $w^* = 1$ for the upper level.

$$\min_{w} e = (x(1) - 0.28197)^2 \tag{2.5-a}$$

$$\text{Subject to: } 0 \leq w \leq 20 \tag{2.5-b}$$

$$\min_{x,u} J = \int_0^1 (x^2 + wu^2)dt \tag{2.5-c}$$

$$\text{Subject to: } \dot{x} = -x + u \tag{2.5-d}$$

$$x(0) = 1 \tag{2.5-e}$$

The problem (Eq. 2.5) was solved numerically with the proposed nested evolutionary approach. The lower level is solved with the direct collocation method with a 50 node grid, and mid-point scheme. For this simple example, the fmincon solver from the MATLAB optimization toolbox is used. The solution found through the proposed approach is compared to the analytic solution.

2.2.4 Applications to human walking

We further demonstrated the use of the proposed nested evolutionary approach on the problem of determining a cost function for human walking (Eq. 2.6). In these applications, the lower level (Eq. 2.6-c, d, e) was an optimal control problem of human walking (Ackermann and van den Bogert 2010). The cost function of the lower level, J, was described as a weighted combination of some performance terms J_i (Eq. 2.6-c).

$$\min_{\boldsymbol{w}} e \tag{2.6-a}$$

$$\text{Subject to: } \boldsymbol{w}_{lb} \leq \boldsymbol{w} \leq \boldsymbol{w}_{ub} \tag{2.6-b}$$

$$\min_{\boldsymbol{x},\boldsymbol{u}} J = \sum_{i=1}^{n} w_i J_i \tag{2.6-c}$$

$$\text{Subject to: } \dot{\boldsymbol{x}} = f(\boldsymbol{x}, \boldsymbol{u}, t) \tag{2.6-d}$$

$$C_{lb} \leq C(\boldsymbol{x}, \boldsymbol{u}, t) \leq C_{ub} \tag{2.6-e}$$

Equation 2.7 provides the details of the specific, multi-objective cost function that was evaluated. The first term, describing muscle endurance, is the sum of muscle activations (a) cubed (Ackermann and van den Bogert 2010)(Miller et al. 2011). The second and third terms represent the stability during walking. Although there are several stability measures in the literature, there seems not to be a widely accepted measure (Bruijn et al. 2013). Some common stability metrics such as margin of stability (Hof, Gazendam, and Sinke 2005), stabilizing and destabilizing forces (Duclos et al. 2009) rely on the base of support, which is not continuous over the gait cycle. These approaches could cause the optimization solvers to fail or get trapped in a

local minimum. Therefore, we proposed a stability measure that includes two terms: the total difference between the position of center of mass (CoM) in the fore-aft direction (CoM_x) and the center of the extended base of support ($midBoS_x$) over the gait cycle, and the total difference between the position of the head in fore-aft direction ($head_x$) and the $midBoS_x$ over the gait cycle. The extended base of support is defined as the convex area that contains the vertical projections of the two feet on the ground. The extended base of support eliminates the discontinuity that would otherwise arise when the feet are not in contact with the ground. The fourth and fifth terms represent jerk cost (third derivative of position, squared), which describes the smoothness of walking. It has been proposed that the central nervous system controls movements so as to produce smooth movement trajectories (Flash and Hogan 1985). The smoothness of walking in this study is defined as the jerk costs for the CoM in the fore-aft (CoM_x) and vertical directions (CoM_y). Without loss of generality, the first weight associated with the endurance term is set to equal to 10. Therefore, the weight vector is $\boldsymbol{w} = [w_1, \quad w_2, \quad w_3, \quad w_4]$. Due to the different dimensions of the quantities in Eq. 2.7, the stability and smoothness terms are scaled to yield reasonably similar magnitudes across terms.

$$
\begin{aligned}
J &= \frac{10}{t_f}\sum_{i=1}^{m}\int_0^{t_f} a_i^3(t)dt + w_1\frac{10^{-1}}{t_f}\int_0^{t_f}(CoM_x - midBoS_x)^2 dt \\
&+ w_2\frac{10^{-1}}{t_f}\int_0^{t_f}(head_x - midBoS_x)^2 dt + w_3\frac{10^{-6}}{t_f}\int_0^{t_f}\left(\frac{d^3CoM_x}{dt^3}\right)^2 dt \\
&+ w_4\frac{10^{-6}}{t_f}\int_0^{t_f}\left(\frac{d^3CoM_y}{dt^3}\right)^2 dt
\end{aligned}
\tag{2.7}
$$

The simulations of walking were generated using a musculoskeletal model implemented in OpenSim Ver. 3.3 (Seth et al. 2011). The model consists of 12 rigid bodies, namely: torso, pelvis, right and left femur, tibia, talus, calcaneus and toes. These bodies were connected through 11 degrees of freedom (DOFs) (three at pelvis relative to the ground, one rotation for each hip, knee, ankle, and metatarsophalangeal joint) (Figure 2.1-a). The model was actuated by 18 muscle

tendon units (nine for each lower limb) that were represented with a Hill-type muscle model (Millard et al. 2013). These muscles and muscle groups were: biarticular hamstring (HAM), biceps femoris short head (BFsh), gluteus maximus (GMAX), iliopsoas (IL), rectus femoris (RF), vasti (VAS), gastrocnemius (GAS), soleus (SOL), dorsiflexor (DOR) (included tibialis anterior, extensor hallucis longus, and extensor digitorum longus) (Figure 2.1-b). Details about the model may be found in the appendix A.

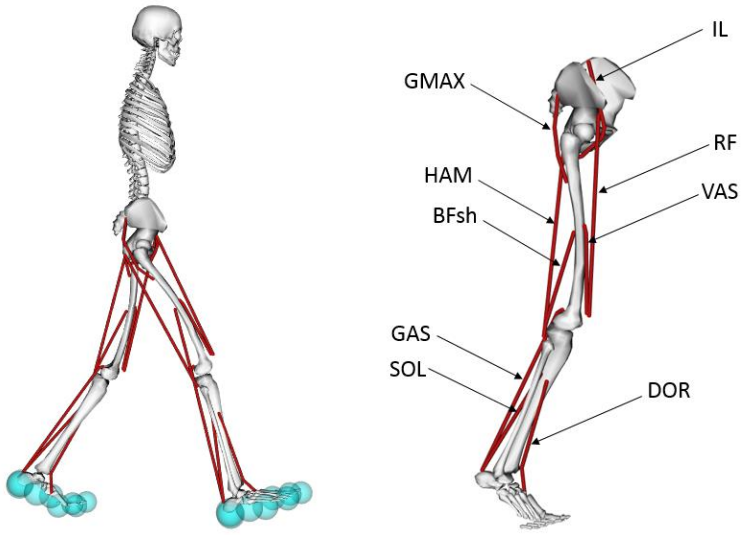

(a) (b)

Figure 2.1: OpenSim musculoskeletal model. The model consists of 12 rigid bodies connected through 11 degrees of freedom (a). The foot-ground contact was modeled by eight OpenSim HuntCrossleyContact spheres under each foot (Porsa et al. 2016) (a). The model is actuated by 18 muscle tendon units (nine on each lower limb) which are represented with Hill-type muscle model (Millard et al. 2013), namely: biarticular hamstring (HAM), biceps femoris short head (BFsh), gluteus maximus (GMAX), iliopsoas (IL), rectus femoris (RF), vasti (VAS), gastrocnemius (GAS), soleus (SOL), dorsiflexor (DOR) (included tibialis anterior, extensor hallucis longus, and extensor digitorum longus) (b). (See the appendix A1 for more details)

To reduce computation time, simulations of a single step of walking were used for the lower level in the optimizations. A full gait cycle was reconstructed with the assumption that the gait is bilaterally symmetric (Ackermann and van den Bogert 2010). The walking speed was fixed at a typical speed of 1.3 m/s (Umberger and Martin 2007). For further computational efficiency in implementing the direct collocation for the lower level, the time axis was discretized to 15 nodes and the Euler method was used due to its simplicity and sparsity properties. We found that 15

nodes/step was the coarsest grid density that adequately represented the dynamics across the gait cycle. The Euler method, while computationally simple, has been used successfully for past simulations of human walking (Ackermann and van den Bogert 2010)(Koelewijn and van den Bogert 2016). The lower level NLP problems were solved using the IPOPT solver (Wächter 2003) with the known sparsity structure of the constraints Jacobian matrix provided, which dramatically reduces the computation cost. The details about interfacing MATLAB with OpenSim and IPOPT can be found in (Lee and Umberger 2016).

2.2.4.1 Problem 2: Inverse problem with synthetic gait

For the case of human walking, we first demonstrate that our algorithm is able to find the optimal weights for the upper level in a case where the true solution is known. To accomplish this, an arbitrary weight vector $\boldsymbol{w}^*$ for the cost function (Eq. 2.7) is chosen. We then generate a synthetic gait pattern, $\bar{\boldsymbol{x}}$, by solving the lower level with the weight vector $\boldsymbol{w}^*$ using the direct collocation method. We now have an inverse problem, which involves recovering the weight vector using our bilevel optimization algorithm (Problem 2). The cost function for the upper level (Eq. 2.6-a) is defined as minimizing the difference between the solution of the lower level ($\boldsymbol{x}^*$) and the synthetic gait $\bar{\boldsymbol{x}}$ in term of the joint kinematics and GRFs (Eq. 2.8).

$$
\begin{aligned}
&e_s \\
&= \frac{1}{t_f}\frac{1}{2}\int_0^{t_f}\left[\frac{1}{3}\left(\frac{\boldsymbol{x}_h^* - \bar{\boldsymbol{x}}_h}{\widehat{SD}_h}\right)^2 + \frac{1}{3}\left(\frac{\boldsymbol{x}_k^* - \bar{\boldsymbol{x}}_k}{\widehat{SD}_k}\right)^2 + \frac{1}{3}\left(\frac{\boldsymbol{x}_a^* - \bar{\boldsymbol{x}}_a}{\widehat{SD}_a}\right)^2\right. \\
&\left. + \frac{1}{2}\left(\frac{\boldsymbol{x}_{VGRF}^* - \bar{\boldsymbol{x}}_{VGRF}}{\widehat{SD}_{VGRF}}\right)^2 + \frac{1}{2}\left(\frac{\boldsymbol{x}_{HGRF}^* - \bar{\boldsymbol{x}}_{HGRF}}{\widehat{SD}_{HGRF}}\right)^2\right] dt
\end{aligned}
\tag{2.8}
$$

where the subscripts h, k, a, indicate variables for hip, knee, and ankle angles which are parts of the state $\boldsymbol{x}$. $VGRF$, $HGRF$ indicate vertical GRF and horizontal GRF, which depend directly upon the state $\boldsymbol{x}$. $\widehat{SD}$ are standard deviations of the gait variables that were obtained from a set of experimental human walking data, which were also used for Problem 3 below. The experimental

data were collected from eight healthy subjects (age = 25.6 ± 1.7 years, height = 1.74 ± 0.09 m, mass = 76.8 ± 14.4 kg, 4 males, 4 females) who walked overground at a speed of 1.3 m/s in a biomechanics laboratory. All subjects provided written informed consent in accordance with local ethics regulations, prior to participation. Kinematic data were recorded (240 Hz) using an 11-camera optical motion capture system (Oqus 300, Qualisys, Gothenburg, Sweden) and GRFs were measured (1200 Hz) using a strain gauge force platform (OR6-5, AMTI, Watertown, MA, USA). Kinematic data were based on a marker set described elsewhere in detail (Neill et al. 2015). Positions of the reflective markers were low-pass filtered using a dual-pass Butterworth digital filter with a cutoff frequency of 6 Hz. Joint angles were calculated using an inverse kinematics approach in OpenSim (Delp et al. 2007). Note that while the average standard deviations for the VGRF and HGRF during the stance phase are 50 N and 17 N, respectively, during the swing phase they are equal to zero. Therefore, in Eq. 2.8, we set $\widehat{SD}_{VGRF} := \max(\widehat{SD}_{VGRF}, 10)$ and $\widehat{SD}_{HGRF} := \max(\widehat{SD}_{HGRF}, 5)$ to avoid dividing by zero.

2.2.4.2 Problem 3: Matching experimental human gait

To further evaluate our approach with human walking, we solved for the weights for the cost function (Eq. 2.7) so that the predictive walking simulation (lower level optimization) resulted in a gait that was as close as possible to the human experimental gait in terms of kinematics and GRFs (Problem 3) (Eq. 2.9).

$$
\begin{aligned}
&e_h \\
&= \frac{1}{t_f}\frac{1}{2}\int_0^{t_f}\left[\frac{1}{3}\left(\frac{\boldsymbol{x}_h^* - \widehat{\boldsymbol{x}}_h}{\widehat{SD}_h}\right)^2 + \frac{1}{3}\left(\frac{\boldsymbol{x}_k^* - \widehat{\boldsymbol{x}}_k}{\widehat{SD}_k}\right)^2 + \frac{1}{3}\left(\frac{\boldsymbol{x}_a^* - \widehat{\boldsymbol{x}}_a}{\widehat{SD}_a}\right)^2\right. \\
&\left. + \frac{1}{2}\left(\frac{\boldsymbol{x}_{VGRF}^* - \widehat{\boldsymbol{x}}_{VGRF}}{\widehat{SD}_{VGRF}}\right)^2 + \frac{1}{2}\left(\frac{\boldsymbol{x}_{HGRF}^* - \widehat{\boldsymbol{x}}_{hGRF}}{\widehat{SD}_{HGRF}}\right)^2\right] dt
\end{aligned}
\tag{2.9}
$$

where $\widehat{\boldsymbol{x}}_h$, $\widehat{\boldsymbol{x}}_k$, $\widehat{\boldsymbol{x}}_a$ are the means of hip, knee, ankle angles from experimental data. $\widehat{\boldsymbol{x}}_{VGRF}$, $\widehat{\boldsymbol{x}}_{HGRF}$ are the means of measured VGRF and HGRF. The main difference between Problem 2

(Eq. 2.8) and Problem 3 (Eq. 2.9) is that Problem 2 uses synthetic target data ($\bar{\boldsymbol{x}}$) that the model should be able to reproduce exactly if the algorithm is robust, while Problem 3 uses experimental target data ($\hat{\boldsymbol{x}}$) that presumably can only be matched to within some threshold. The final predictive gait results obtained with the bilevel approach were compared with: 1) a tracking simulation where the differences with experimental kinematic and GRF data were minimized, together with muscle activation cubed (referred to as "Tracking Sim") (Miller 2014)(Koelewijn and van den Bogert 2016), and 2) a predictive simulation where only muscle activation cubed was minimized (first term in Eq. 2.7) (referred to as "Mus Act cubed"). Note that the "Tracking Sim" and "Mus Act cubed" were generated by solving the optimal control problems of human gait (lower level, Eq. 2.6) with the corresponding cost functions, and not using the bilevel optimization. While both the tracking simulation and the bilevel optimization minimize the gait errors, they are distinctively different. The bilevel optimization solves for the inverse optimal control problem, which results in the cost function or the parameters of the cost function. On the other hand, the tracking simulation is a standard optimal control problem which results in the gait solution. Besides kinematics and GRFs, the quality of predicted muscle activations was evaluated by comparing with on-off time EMG data in the literature (Bonnefoy-Mazure and Armand 2015)(Schmitz et al. 2009).

2.3 Result

2.3.1 Problem 1: Simple example

Table 2.1 shows the solutions found by the nested evolutionary approach for Problem 1. The approach was run three times with randomly generated initial guesses for validating the robustness of the algorithm. The three runs all gave consistent results. The upper level was able to find solutions close to the true solution of $w^* = 1$ after 40 generations with the population size of 14.

Run	Numerical solution (w)	Solution error ($\lvert w - w^* \rvert$)
1	1.0004	4e-4
2	1.0002	2e-4
3	1.0007	7e-4

Table 2.1: Numerical solutions for the simple example. The lower level was solved via the direct collocation method on a 50 node grid using the MATLAB fmincon solver. The upper level was solved with GA that ran for 40 generations with the population size of 14.

2.3.2 Problem 2: Inverse problem with a synthetic gait

In this problem, the goal of the bilevel optimization was to determine the weights in the cost function (Eq. 2.7) so that the final gait patterns closely matched the synthetic gait. To test the robustness of the approach, three different simulations were run. In these simulations, the initial guesses for the upper level were generated randomly and were far from the final solution (Figure 2.2, first generation). The lower level used an initial guess where the model was stepping, but was not close to the final solution. All three runs consistently found weights that were close to the actual solution $\boldsymbol{w}^*$(Table 2.2). The upper level cost (Eq. 2.8) gradually decreased with the number of generations (Figure 2.2). The solution errors, which were defined as the Euclidean distance between $\boldsymbol{w}$ and $\boldsymbol{w}^*$ ($\|\boldsymbol{w} - \boldsymbol{w}^*\|$), also reduced over generation numbers. The resulting gait using the cost function with the optimal weights from run 1 is plotted in Figure 2.3 together with the synthetic gait. Both kinematics and GRFs closely matched the synthetic gait ($e_s = 5.8e - 4$).

Run	Numerical solution ($\boldsymbol{w}$)	Solution error $\|\boldsymbol{w} - \boldsymbol{w}^*\|$
1	[10.8498, 4.6192, 31.9312, 2.1851]	0.7476
2	[10.2942, 4.3404, 31.1364, 2.3032]	0.3792
3	[9.8127, 4.5316, 31.3676, 2.1782]	0.4962
Actual Solution ($\boldsymbol{w}^*$)	[10.2804, 4.4200, 31.4896, 2.1915]	

Table 2.2: The numerical solutions of Problem 2 – Inverse problem with a synthetic gait. All three different runs consistently gave solutions which were close to the actual solution.

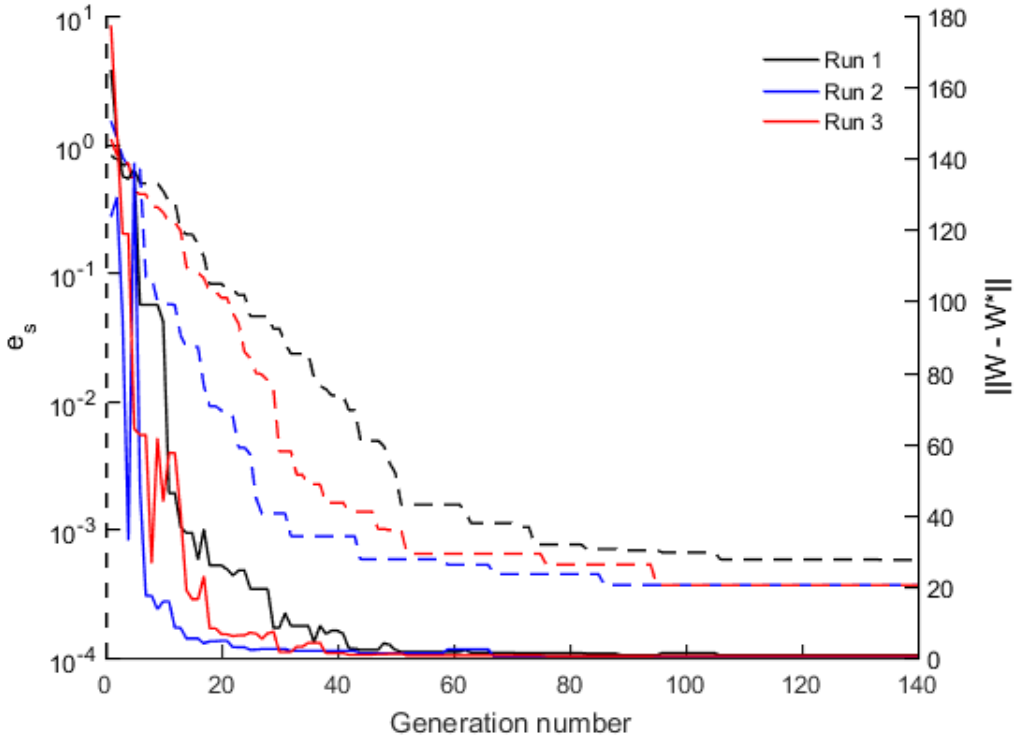

Figure 2.2: The simulation results of Problem 2 – Inverse problem with a synthetic gait from three different runs. The lines with the same color describe the result from the same run. Dashed lines represent upper level cost e_s (Eq. 2.8) which describes how close the predicted gait to the synthetic gait, plotted with the left y-axis. Solid lines represent the solution errors of the weights ($\|\boldsymbol{w} - \boldsymbol{w}^*\|$) plotted with the right y-axis. In all three runs, the bilevel approach was consistently able to find the weights close to the actual solution (solid lines).

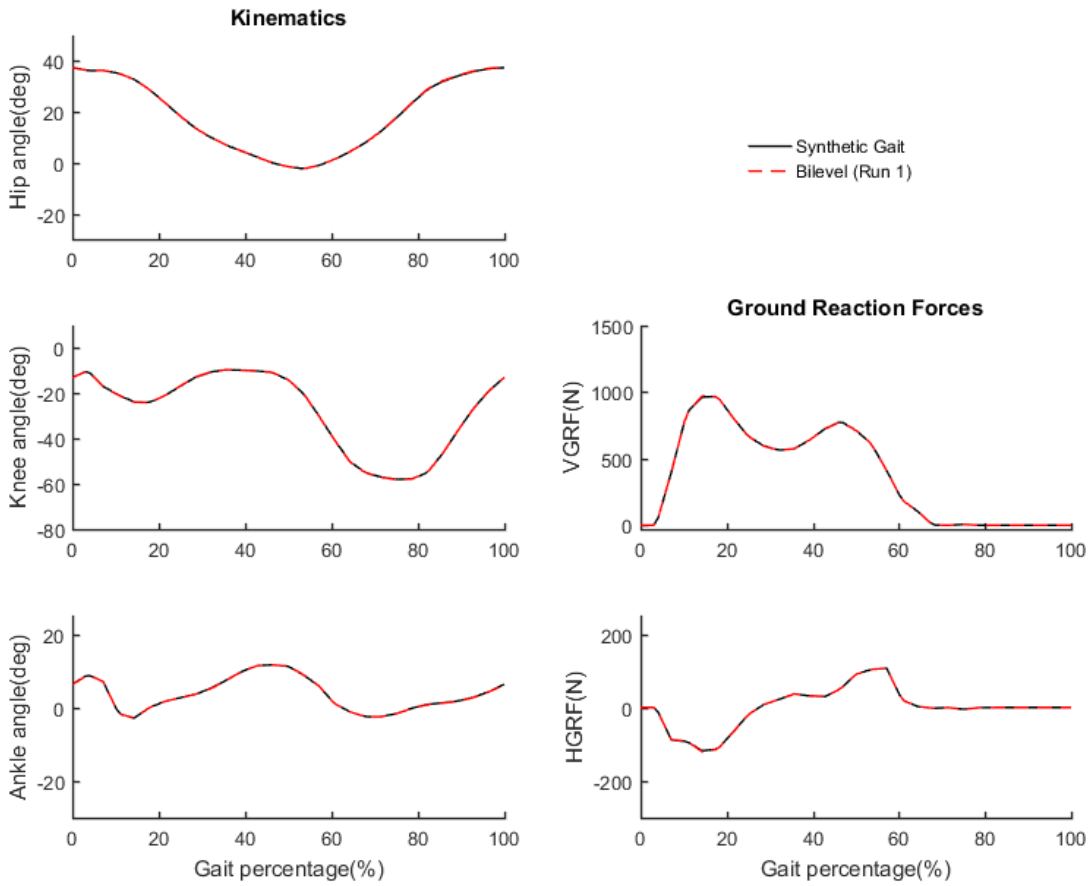

Figure 2.3: Gait kinematics and GRFs with the optimal weights found at run 1 ("Bilevel (Run 1)"). Both kinematics and GRFs match closely the synthetic gait ($e_s = 0.00057690$)

2.3.3 Problem 3: Matching experimental human gait

For Problem 3, the goal was to determine optimal weights for the cost function (Eq. 2.7) so that the predicted gait was close to the experimental human data. The upper level cost e_h (Eq. 2.9), which describes how close the predicted gait is to the human gait, reduced over the generations. The optimal upper level cost value was $e_h = 1.8058$ (Figure 2.4), and the optimal weights are $\boldsymbol{w} = [93.7199, 21.0332, 5.1279, 41.0280]$.

The gait result obtained with the optimal weights ("Bilevel opt") was compared with a tracking simulation, and a predictive simulation where only muscle activation cubed was minimized (Figure 2.5 and Figure 2.6). The gait solution using the cost function with optimal weights found through the bilevel approach ("Bilevel opt", $e_h = 1.8058$) was closer to human

gait than minimizing muscle activation cubed ("Mus Act cubed", $e_h = 5.3924$), but not as close to human gait as the tracking simulation ("Tracking Sim", $e_h = 0.3566$) (Figure 2.4 and Figure 2.5). For the tracking gait solution, the mean absolute errors are 0.36 SD for kinematics and 0.38 SD for GRFs. The "Bilevel opt" has the mean absolute errors of 0.90 SD and 0.94 SD for kinematics and GRFs, respectively. The "Mus Act cubed" has the mean absolute errors of 1.55 SD and 1.65 SD for kinematics and GRFs, respectively. The muscles activation in "Bilevel opt" were in good agreement with on-off EMG data in the literature (Bonnefoy-Mazure and Armand 2015)(Schmitz et al. 2009).

In Problem 2 and Problem 3 that require solving optimal control gaits, each lower level simulation took about 12 minutes running serially on a single core on the i9 3.5GHz computer

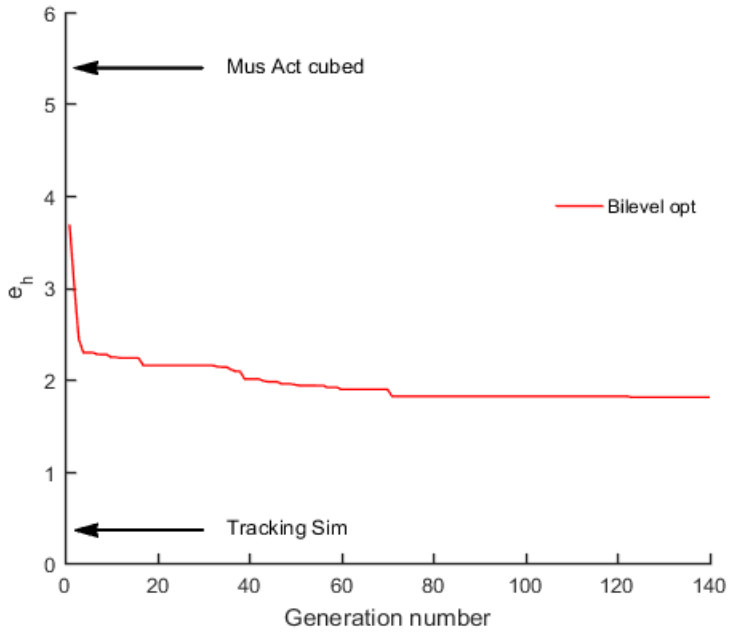

Figure 2.4: The upper level cost e_h (Eq. 2.9) of Problem 3 – Matching experimental human gait. The upper level cost which describes how close the predicted gait compared to the human gait gradually reduced over generations. Eq. 2.9 was also used to calculate e_h for the simulated gait of tracking simulation ("Tracking Sim", $e_h = 0.35655547$) and predictive gait with cost function of minimizing muscle activation cubed ("Mus Act Cubed", $e_h = 5.39248514$). The cost function with optimal weights found by the bilevel approach predicted gait closer to human gait than minimizing muscle activation cubed, but not as close to human gait as the tracking simulation.

with 10 cores. The upper level GA with population size of 40 was run in parallel across the 10 cores, and took about 139 hours to complete 140 generations. To evaluate the effectiveness of the parallel computing on the upper level, we ran one generation of the upper level with normal serial computing, parallel computing on 6 cores, and parallel computing on 10 cores. The computation times were 480 minutes, 98 minutes and 61 minutes, respectively. Thus, parallel execution on 10 cores led to a nearly 8-fold speed-up compared with serial execution.

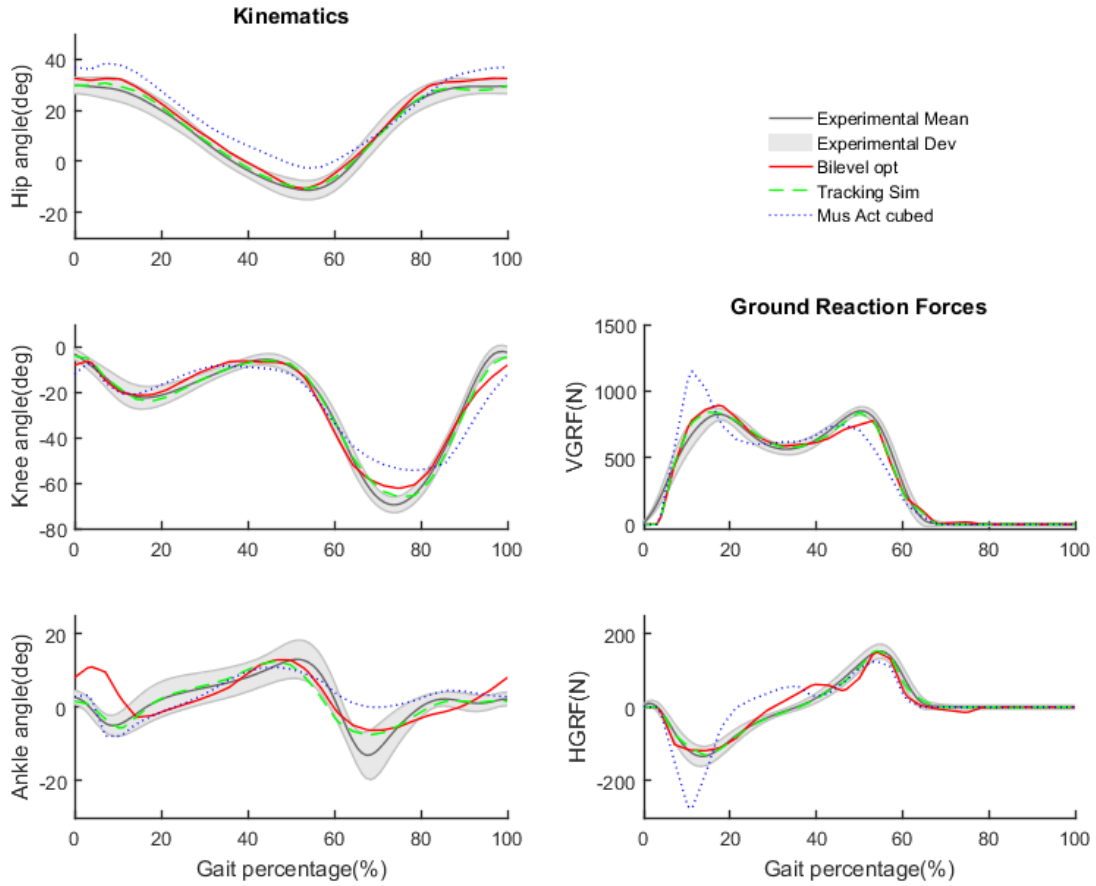

Figure 2.5: Predicted gait kinematics and GRFs using the cost function (Eq. 2.7) with optimal weights found through the bilevel approach ("Bilevel opt", red lines). The black lines and gray areas represent the means and one standard deviation of experimental human gaits from all subjects. The kinematics and GRFs for tracking simulation ("Tracking Sim", green lines), and predictive gait with cost function of minimizing muscle activation cubed ("Mus Act cubed") were also plotted for comparison.

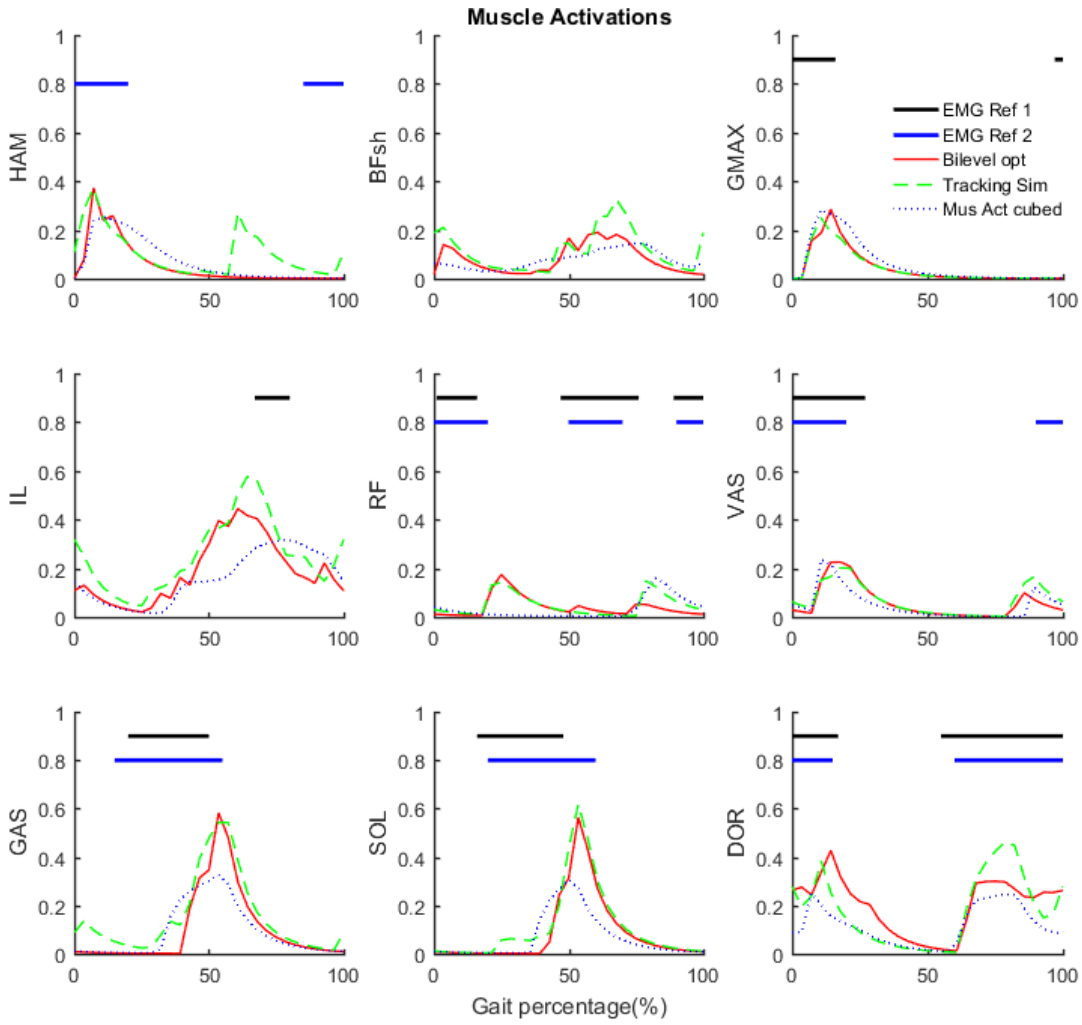

Figure 2.6: Predicted muscle activations using the cost function (Eq. 2.7) with optimal weights found through the bilevel approach ("Bilevel opt", red lines). Muscle activations in tracking simulation ("Tracking Sim", green lines), and predictive simulation with cost function of minimizing muscle activation cubed ("Mus Act cubed", blue lines) were also plotted for comparison. The horizontal bars indicate on-off timing of EMG data; black bars are based on data in (Bonnefoy-Mazure and Armand 2015); blue bars are based on data in (Schmitz et al. 2009).

2.4 Discussion

In this study, we implemented a bilevel optimization approach to determine the cost function for predicting normal human walking. A nested evolutionary approach was used to solve the bilevel optimization problems. The approach was tested on different cases consisting of a simple, standard optimization problem, a test case for finding weights in a cost function that

reproduces a synthetic gait, and the general case of finding weights in a cost function for predicting experimental human gait data. The results showed that the proposed approach was effective and robust for these bilevel optimization problems.

First, a simple and known solution bilevel example in Problem 1 is used to test the nested approach. The approach solved the problem effectively from different, randomly selected initial guesses. Because the lower level is a simple problem with one-dimensional variable, the upper level did not need to run in parallel, and the population size in the GA could be small ($m = 14$). The numerical solutions for all three runs were close to the actual solution with errors smaller than 10^{-3}. The results for Problem 1 indicate that the approach is implemented correctly and is effective at solving bilevel optimization problems.

In Problem 2, which used a synthetic gait pattern as the target, the nested approach converged to similar results from different initial guesses. In Problem 2, a successful run should reproduce the synthetic gait closely, and that was the case for all three runs. This reproducibility demonstrates that the proposed nested evolutionary approach is robust not only for simple bilevel optimization problems, but also for large and complex problems, such as human walking. A lower level simulation solving for optimal control of human gait took about 12 minutes on a single core of an Intel i9 3.5GHz 10-core computer. The fast lower level simulations were obtained by solving the walking problem with the direct collocation method using a relatively coarse grid density (15 nodes) and exploiting the sparsity of the resulting NLP problem. We confirmed that our results obtained using 15 nodes/step generalized to walking simulations generated using a more typical grid density of 50 nodes/step (Ackermann and van den Bogert 2010) (see results in the appendix A). We also evaluated the computation times with different degrees of parallelization for the upper level optimization, including normal serial computing, parallel computing on 6 cores, and parallel computing on 10 cores. The results showed that the computation time reduces almost linearly with the number of cores. Using a computing system with more cores or CPUs (e.g., up to the population size of the GA) should further speed up the

process. In addition, after about 80 generations, although there were some improvements at the upper level cost, the weight solution errors did not improve significantly (Figure 2.2). Therefore, for this particular problem, one may stop after 80 generations to reduce computation time.

For Problem 3, the bilevel optimization approach was used to find the weights for performance criteria in the cost function of human walking. The approach was able to improve the gait by adjusting the weights at the upper level. The gait solution using the cost function with the optimal weights ("Bilevel opt") was considerably closer to the human gait compared to a randomly chosen weights (Figure 2.4). The muscle activations are in good agreement with on-off EMG data (Figure 2.6). In addition, "Bilevel opt" is significantly better than the predictive gait obtained with the commonly used cost function that only minimizes muscle activation cubed ("Mus Act cubed"), in term of kinematics and GRFs (Figure 2.5 and Figure 2.6). "Bilevel opt" has better knee and hip angles compared to "Mus Act cubed". The hip angle of "Mus Act cubed" has an offset compared to the human gait due to the musculoskeletal model leaning the torso forward, presumably to reduce muscle activation cost required for moving forward. However, leaning forward may also reduce the stability of the gait. This problem was solved in "Bilevel opt" because the stability was added to the cost function (Eq. 2.7). Furthermore, the GRFs in "Mus Act cubed" were not as smooth as observed in human subjects (Figure 2.5). The first peak of VGRF following heel strike was substantially greater compared with the experimental VGRF. The HGRF also had larger changes following heel strike for minimum muscle activation than the bilevel optimal result. These changes in GRFs may correlate to jerk cost for the CoM during walking. The "Bilevel opt" penalized the CoM jerk cost, therefore had smoother GRFs. These results suggest that humans walk in a way that does not minimize muscle fatigue (i.e., maximize muscle endurance) in an absolute sense, but also prioritizes smoothness and stability. The performance-based cost function with optimized weights, however, did not result in simulations that match the experimental data as closely as the tracking solution, which suggests that there may still be additional features of human gait that are not captured by the cost function such as

minimizing joint contact forces (Fey et al. 2012), rate of change of GRF (Rebula and Kuo 2015), or metabolic cost (Anderson and Pandy 2001). Moreover, the performance criteria in the cost function could be parameterized in ways other than was done here, which may affect the results. For example, muscular demand can be parameterized using different exponents and with or without muscle volume weighing (Ackermann and van den Bogert 2010), while movement smoothness can be described through the derivative of ground reaction forces (Rebula and Kuo 2015) or muscle forces (Gidley et al. 2019).

An important outcome of the bilevel optimization is that none of the terms were removed from the final cost function by the weight being close to zero. Having all the terms in the final solution indicates that avoiding fatigue, maintaining stability and moving smoothly are likely all-important criteria for human walking. However, from the optimal weights of Problem 3 it is difficult to interpret which of these performance criteria are more important determinants of the way humans walk. The main reason is that these performance criteria have different dimensions, and the meaning of the relative weights are not easy to interpret. In addition, a term that dominates the others in the cost function may not necessarily be the most important factor (Srinivasan 2010). An approach to evaluate the importance of a performance criterion may be comparing the qualities of predictive gaits with and without that criterion included in the cost function. Identifying the criteria and their contribution is an area that is ripe for further investigation into the control of human walking.

In the nested evolutionary approach, the upper level is solved by GA which is a global and derivative-free method. Therefore, the upper level can handle cost functions with complex and non-convex form. Although in this study the nested approach was used to find the optimal weights for different performance criteria in the cost function, the approach could also be used to optimize other parameters in the cost function, such as the exponents for the muscle activations (Ackermann and van den Bogert 2010). Furthermore, our approach could have applications in predicting optimal designs for assistive devices, such as lower limb prostheses (Fey et al.

2012)(Handford and Srinivasan 2016). Finding the optimal design parameters for an assistive device could be formulated as a bilevel optimization problem. The upper level would solve for the design parameters, while the lower level with direct collocation approach would solve for the gait patterns given the device design parameters from the upper level (Koelewijn and van den Bogert 2016). The proposed nested evolutionary approach can be easily adapted to solve these sorts of design problems with only minor changes. A potential challenge is the optimal weightings in the cost function could be different for some clinical populations, which could be addressed through the use of multi-objective methods and sensitivity analyses.

Other past studies focused on identifying cost functions for human movement usually involved relatively simple models (Bottasso et al. 2006)(Albrecht et al. 2011). In those cases, the single-level reduction approach may be used. Using the single-level reduction approach, the lower level was converted to a system of algebra equations using the necessary KKT conditions (Bottasso et al. 2006)(Albrecht et al. 2011). The bilevel was then solved as a standard optimization problem. However, with a more complex musculoskeletal model like in this study, using the single-level reduction approach may lead to a very large-scale optimization problem which may be difficult to solve (Suryan et al. 2016). Furthermore, the single-level reduction approach requires re-formulating the structure of the bilevel problem, which is not the case with the nested approach. Therefore, the nested approach may be easily adapted for different problems such as when the underlying model changes. One specific area that we anticipate great benefits is in optimizing the design of devices for assisting and augmenting human performance.

In the literature, the nested approach was used to solve for the cost functions of human locomotion. Clever and Mombaur (2016) solved for the cost functions of human locomotion with a simple dynamic walking model (three body segments, actuated by the hip torques). The lower level was solved with a multiple-shooting method, while the upper level was solved with a quadratic approximation based method BOBYQA (Powell 2009). Though we do not know of any direct comparisons of computational efficiency between the multiple shooting method and direct

collocation for solving optimal control walking problems, the direct collocation approach may hold a considerable performance advantage (Rao 2009)(Lee and Umberger 2016)(Ackermann and van den Bogert 2010). This is due to the sparsity of the NLP in the direct collocation method, and no integration of the dynamic equation required like in (multiple) shooting methods. Furthermore, in our study, the upper level is solved with GA. GA is ideal for parallel computation, which helps to solve the complex optimization problems in this study within reasonable times.

Although the proposed nested evolutionary approach has been shown to be effective for solving the bilevel optimization problem for human walking, the computational cost remains one of the main challenges. This is because the lower level is expensive to solve. In this study, the computation time was addressed by solving the GA in parallel on a multiple core computer. The computation cost challenge may also be overcome by reducing the numbers of times the lower level needs to be solved. Other algorithms for solving the upper level that requires fewer samples, such as Bayesian optimization (Vaerenbergh et al. 2013), can be examined in further study.

2.5 Conclusion

In this study, we formulated the problem of determining the cost function for human walking as a bilevel optimization problem that was solved effectively using a nested evolutionary approach. The bilevel approach was found to be effective and robust at identifying cost functions that predict normal human walking. The proposed approach should be useful for further investigating the cost functions underlying a range of human movements, and for other purposes such as predicting optimal designs for assistive devices for sports equipment.

CHAPTER 3

PERFORMANCE CRITERIA FOR PREDICTIVE OPTIMAL CONTROL SIMULATIONS OF HUMAN WALKING

Predictive simulation based on optimal control has been widely used for studying the biomechanics of human gaits. However, a remaining challenge in formulating the optimal control problem for walking is that the cost function, which represents the underlying performance criteria humans optimize in walking is generally unknown. Prior studies often made assumptions about the cost function. Different studies used different cost function forms, but the quantitative qualities of the simulations with those cost functions were often not provided, which makes it unclear which cost functions should be used. Therefore, this study aims to evaluate some commonly implemented cost functions in the literature, and examine different cost function forms for predictive walking simulation. The objective is to determine the cost function form which can be used for the predictive walking simulation. We hypothesize that the walking cost function can be described through a set of some performance criteria such as metabolic cost, muscle activation, gait stability, and gait smoothness. Parameters associated with these criteria such as the exponent value or the weights among different criteria were optimized using a bilevel optimization approach to find the best performance of the cost function forms. The results showed the cost functions combined muscle-based performance criteria, gait stability, and smoothness resulted in better gait solutions than any other cost functions only based on muscle performance criteria alone. Such cost function forms which combined some different terms may be used to predict walking at different conditions.

3.1 Introduction

Predictive simulations of human walking were often formulated as an optimal control problem (Anderson and Pandy 2001)(Ackermann and van den Bogert 2010). However, one of the

challenges in formulating the optimal control problem is that the walking cost function is generally unknown. Prior studies commonly made assumptions about the cost function, even though it is known that different cost functions can lead to different simulation results (Ackermann and van den Bogert 2010)(Miller et al. 2011)(Koelewijn et al. 2018)(Gidley et al. 2019). The cost functions were often parameterized based on some performance criteria such as minimizing muscle excitation squared (Van den Bogert et al. 2012) or the cost of transport (Lin et al. 2018). However, the qualities of the gait solutions compared to actual human gait data (e.g., joint angles, GRFs), using these cost functions were typically not evaluated. Therefore, there is a need to evaluate and examine the cost function forms for predictive optimal control of human walking.

It has been observed that the energy cost per unit distance traveled (i.e., cost of transport) in human walking is minimized at the preferred walking speed (Ralston 1976). Therefore, studies often used the cost function based on the metabolic energy cost for the walking simulations (Anderson and Pandy 2001)(Brian R Umberger 2010)(Miller 2014)(Lin et al. 2018). Other performance criteria that should be related to metabolic energy such as sum of muscle activations or excitations (Kaplan and H. Heegaard 2001)(Van den Bogert et al. 2012)(Koelewijn and van den Bogert 2016)(Ackermann and van den Bogert 2010), or sum of muscle stresses (Miller et al. 2011) were also implemented. These performance criteria, from now on referred as muscle-based performance criteria, often allow predicting gait solutions, which are generally similar to human gait, but do not match measured variables (e.g., joint angles, GRFs) within the standard deviation of the data. In addition, the gait solutions with these muscle-based criteria can be significantly different (Koelewijn et al. 2018) (Ackermann and van den Bogert 2010).

Some studies suggested that humans walk to optimize multiple objectives instead of just muscle efforts in an absolute sense (Dorn et al. 2015). Therefore, additional performance criteria have been evaluated as part of the cost functions such as minimizing the joint contact forces (Fey et al. 2012), differences in velocity of the body center of mass (CoM) with targeted velocity

(Dorn et al. 2015), torque applied by reserve actuator (Uchida et al. 2016), passive moments applied at joints (Umberger 2010), vertical center of mass oscillations (Clever and Mombaur 2016), rates of changes of ground reaction forces (GRFs) (Rebula and Kuo 2015), and gait stability (Nguyen, Johnson, et al. 2019). While combining some performance criteria may lead to more realistic gait solutions (Rebula and Kuo 2015), it is unclear which criteria are important to include in the cost function. Furthermore, the quality of such cost functions may depend on the weights among these criteria (Ackermann and van den Bogert 2010)(Rebula and Kuo 2015). The weights among different criteria can be determined through a bilevel optimization approach (Nguyen, Johnson, et al. 2019) to ensure that the best performances of the cost function forms are achieved.

In this chapter, we evaluate different cost function forms for the predictive walking simulation. These cost functions are based on a set of some common performance criteria, namely: muscle fatigue, muscle stress, metabolic energy cost, gait smoothness, and gait stability. To evaluate the best performance of some cost functions, these cost functions' parameters such as the exponent of muscle activation (Ackermann and van den Bogert 2010), or the weights among different performance terms, were optimized using a bilevel optimization approach to allow the gait solutions as close as possible to human gait data (Nguyen, Johnson, et al. 2019). The qualities of the gaits generated with these cost functions are then quantified and compared.

3.2. Method

3.2.1 Musculoskeletal model

Walking simulations were generated with a planar OpenSim (Seth et al. 2011) musculoskeletal model, which was described in (Nguyen, Johnson, et al. 2019) (Figure 3.1). The model has 11 degrees of freedoms: three at the pelvis respective to the ground, one rotation for each hip, knee, ankle, and metatarsophalangeal joint. The lower limbs are driven by 18 muscle-tendon units which are represented with the Hill-type muscle model (Millard et al. 2013) namely:

biarticular hamstring (HAM), biceps femoris short head (BFsh), gluteus maximus (GMAX), iliopsoas (IL), rectus femoris (RF), vasti (VAS), gastrocnemius (GAS), soleus (SOL), dorsiflexor (DOR) (included tibialis anterior, extensor hallucis longus, and extensor digitorum longus) (Figure 3.1). More details about the model can be found in the appendix A.

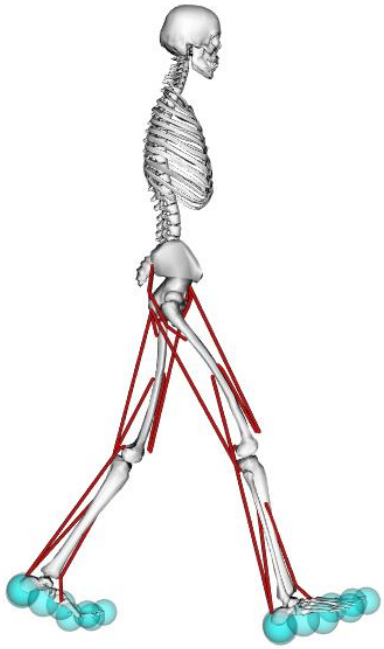

Figure 3.1: The OpenSim musculoskeletal model consists of 12 rigid bodies (torso, pelvis, right and left femur, tibia, talus, calcaneus and toes) which are connected through 11 degrees of freedoms. The foot-ground contact was modeled by eight OpenSim HuntCrossleyContact spheres under each foot (Porsa et al. 2016). The model is actuated by 18 muscle-tendon units which are represented with Hill-type muscle model (Millard et al. 2013). More details about the model can be found in the appendix A1.

3.2.2 Optimal control problem

The walking simulation is formulated as an optimal control problem (Eq. 3.1) (Ackermann and van den Bogert 2010).

$$\min_{\boldsymbol{x},\boldsymbol{u}} J(\boldsymbol{w},\boldsymbol{x},\boldsymbol{u},t) \tag{3.1-a}$$

$$\text{Subject to: } \dot{\boldsymbol{x}} = f(\boldsymbol{x},\boldsymbol{u},t) \tag{3.1-b}$$

$$C_{lb} \leq C(\boldsymbol{x},\boldsymbol{u},t) \leq C_{ub} \tag{3.1-c}$$

where J is the cost function of the human walking, $\boldsymbol{x} \in R^l$ is the state (e.g., joint angles, joint velocities, muscle fiber lengths and activations) with l representing the dimension of the state, $\boldsymbol{u} \in R^m$ is the muscle control (muscle excitation) with m representing the dimension of the control, $\boldsymbol{w}$ represents the unknown parameters in the cost function such as the weights among different performance criteria, t is the time, C represents the constraints, and C_{lb} and C_{ub} are lower and upper bounds on the constraints, respectively. Eq. 3.1-b is the dynamic equation of the musculoskeletal model.

The optimal control problem (Eq. 3.1) is solved using direct collocation approach (Rao 2009). The direct collocation transforms the optimal control problem to a non-linear programming problem, which is later solved with IPOPT solver (Wächter 2003). To reduce the computation cost, a step of walking was simulated with a 15 node grid (Chapter 2). The full stride was reconstructed with the assumption that the gait was symmetric (Ackermann and van den Bogert 2010). The walking time was allowed to vary in a suitable range so that the model can choose the stride rate when the walking speed was fixed at 1.3 m/s (Umberger and Martin 2007).

Some cost functions contain some unknown parameters, $\boldsymbol{w}$, such as the exponent value or weights among different performance criteria. These parameters were optimized using a bilevel optimization approach (Nguyen, Johnson, et al. 2019)(Chapter 2). The bilevel optimization consists of two coupled optimization problems: the lower level problem and the upper level problem. The lower level optimization problem is a predictive simulation of human walking (Eq. 3.2– c, d, e). The upper level optimization solves for the cost function's parameters, $\boldsymbol{w}$, so that the cost function results in the gait that matches as close as possible the human gait (Eq. 3.2). The human gait data are the same data set published in our previous study (Nguyen, Johnson, et al. 2019) that were collected from eight healthy subjects.

$$\min_{\boldsymbol{w}} e \tag{3.2-a}$$

$$\text{Subject to: } \boldsymbol{w}_{lb} \leq \boldsymbol{w} \leq \boldsymbol{w}_{ub} \tag{3.2-b}$$

$$\min_{\boldsymbol{x},\boldsymbol{u}} J(\boldsymbol{w},\boldsymbol{x},\boldsymbol{u},t) \tag{3.2-c}$$

$$\text{Subject to: } \dot{\boldsymbol{x}} = f(\boldsymbol{x},\boldsymbol{u},t) \tag{3.2-d}$$

$$C_{lb} \le C(\boldsymbol{x},\boldsymbol{u},t) \le C_{ub} \tag{3.2-e}$$

where $\boldsymbol{w}_{lb}$ and $\boldsymbol{w}_{ub}$ are lower and upper bounds of $\boldsymbol{w}$, e represents the error between the solution of lower level $\boldsymbol{x}^*$ and the human gait data $\widehat{\boldsymbol{x}}$ (Eq. 3.3).

$$\begin{aligned} & e \\ & = \frac{1}{t_f}\frac{1}{2}\int_0^{t_f}\left[\frac{1}{3}\left(\frac{\boldsymbol{x}_h^* - \widehat{\boldsymbol{x}}_h}{\widehat{SD}_h}\right)^2 + \frac{1}{3}\left(\frac{\boldsymbol{x}_k^* - \widehat{\boldsymbol{x}}_k}{\widehat{SD}_k}\right)^2 + \frac{1}{3}\left(\frac{\boldsymbol{x}_a^* - \widehat{\boldsymbol{x}}_a}{\widehat{SD}_a}\right)^2\right. \\ & \left. + \frac{1}{2}\left(\frac{\boldsymbol{x}_{VGRF}^* - \widehat{\boldsymbol{x}}_{VGRF}}{\widehat{SD}_{VGRF}}\right)^2 + \frac{1}{2}\left(\frac{\boldsymbol{x}_{HGRF}^* - \widehat{\boldsymbol{x}}_{hGRF}}{\widehat{SD}_{HGRF}}\right)^2\right] dt \end{aligned} \tag{3.3}$$

In Eq. 3.3, the lower subscripts h, k, a, indicate variables for hip, knee, and ankle angles. $VGRF$ and $HGRF$ indicate vertical GRF and horizontal GRF, respectively. $\widehat{SD}$ are standard deviations of the experimental human gait data. t_f is the final time. The bilevel optimization (Eq. 3.2) was solved through a nested evolutionary approach where the lower level was solved with the direct collocation method, and the upper level was solved with a genetic algorithm (Nguyen, Johnson, et al. 2019).

3.3.3 Cost functions

First, to show the model's ability to perform walking simulation, a tracking cost function J_T (Eq. 3.4) is used to simulate (Neptune et al. 2001). The tracking cost function consists of a muscle fatigue term and a tracking term. The muscle fatigue term is described as the sum of total muscle activation cubed (Ackermann and van den Bogert 2010)(Nguyen, Johnson, et al. 2019). The tracking term represents the error between the simulated gait and the human gait in term of

kinematic and GRFs. The weight w associated with the tracking term was chosen so that muscle fatigue term and the tracking term are closely equal.

$$
\begin{aligned}
&J_T \\
&= \frac{1}{t_f}\sum_{i=1}^{m}\int_0^{t_f} a_i^3(t)dt \\
&+ w\frac{1}{t_f}\frac{1}{2}\int_0^{t_f}\left[\frac{1}{3}\left(\frac{\boldsymbol{x}_h - \widehat{\boldsymbol{x}}_h}{\widehat{SD}_h}\right)^2 + \frac{1}{3}\left(\frac{\boldsymbol{x}_k - \widehat{\boldsymbol{x}}_k}{\widehat{SD}_k}\right)^2 + \frac{1}{3}\left(\frac{\boldsymbol{x}_a - \widehat{\boldsymbol{x}}_a}{\widehat{SD}_a}\right)^2\right. \\
&\left.+ \frac{1}{2}\left(\frac{\boldsymbol{x}_{VGRF} - \widehat{\boldsymbol{x}}_{VGRF}}{\widehat{SD}_{VGRF}}\right)^2 + \frac{1}{2}\left(\frac{\boldsymbol{x}_{HGRF} - \widehat{\boldsymbol{x}}_{HGRF}}{\widehat{SD}_{HGRF}}\right)^2\right]dt
\end{aligned}
\tag{3.4}
$$

where a_i is muscle activation of the muscle i^{th} in total $m = 18$ muscles.

Next, cost functions that do not consist of the tracking term were examined. These cost functions (now referred to as performance-based cost functions) can be used in predictive walking simulations. The first performance-based cost function was based on minimizing the cost of transport (CoT) (Eq. 3.5) (Anderson and Pandy 2001).

$$J_1 = \frac{1}{M}\frac{\int_0^{t_f}\dot{E}_{total}dt}{X(t_f) - X(0)} \tag{3.5}$$

where M is the body weight, $\dot{E}_{total}$ is the rate of metabolic expenditure; $X(0)$ and $X(t_f)$ are the model positions in the fore-aft direction at the beginning and final times, respectively. The muscle metabolic cost was calculated based on an energy expenditure model described in (Umberger, Gerritsen, and Martin 2003).

The following cost functions were minimizing the total muscle fatigue (sum of muscle activations cubed) (Eq. 3.6) and muscle stress (Eq. 3.7), respectively.

$$J_2 = \frac{1}{t_f}\sum_{i=1}^{m}\int_0^{t_f} a_i^3(t)dt \tag{3.6}$$

$$J_3 = \frac{1}{t_f}\sum_{i=1}^{m}\int_0^{t_f}\left(\frac{F_i}{PCSA_i}\right)^3 dt \tag{3.7}$$

where F_i is the contraction force of muscle i^{th}, and $PCSA_i$ is the physiological cross-sectional area of muscle i^{th}.

Ackermann et al., 2010, (Ackermann and van den Bogert 2010) examined the cost function based on sum of muscle activations with different exponents (Eq. 3.8) ($w_{s1} = 1, 2, 3, 10$). Inspired by this idea, we used the bilevel optimization approach to find the optimal value of the exponent w_{s1} in the range $1 \leq w_{s1} \leq 20$.

$$J_4 = \frac{1}{t_f}\sum_{i=1}^{m}\int_0^{t_f} a_i^{w_{s1}}(t)dt \tag{3.8}$$

In the literature, it is a common approach that all muscle-based performance criteria (e.g., metabolic cost, muscle fatigue, muscle stress) were weighted equally for all muscles. Some studies weighted each muscle-based cost differently such as by their volumes (Ackermann and van den Bogert 2010) or based on the joint at which the muscles act (Serrancolí, Font-Llagunes, and Barjau 2014). In this chapter, some cost functions where the muscle-based performance criteria were weighted differently for each muscle were evaluated (Eq. 3.9, 3.10, 3.11). We assumed the weights for muscles on the left leg are equal to weights for corresponding muscles on the right leg. Without loss of generality, the weights for HAMs (left and right legs) are fixed to be equal to 10. The other muscle weights can vary in a suitable range, $0.1 \leq w_i \leq 300$.

$$J_5 = \frac{1}{M}\frac{\sum_{i=1}^{m} w_i \int_0^{t_f} \dot{E}_i dt}{X_{cm}(t_f) - X_{cm}(t_0)} \tag{3.9}$$

$$J_6 = \frac{1}{t_f}\sum_{i=1}^{m} w_i \int_0^{t_f} a_i^3(t)dt \tag{3.10}$$

$$J_7 = \frac{1}{t_f}\sum_{i=1}^{m} w_i \int_0^{t_f}\left(\frac{F_i}{PCSA_i}\right)^3 dt \tag{3.11}$$

It has been proposed that the central nervous system controls to produce smooth movements (Flash and Hogan 1985). Therefore, gait smoothness may be important in walking and should be included in the cost function. In this study, the gait smoothness was described as the center of mass (CoM) jerk cost. The CoM jerk cost was defined through third derivatives of CoM positions in fore-aft (CoM_x) and vertical directions (CoM_y) (Eq. 3.12). Due to the different dimensions of the qualities in Eq. 3.12, these terms were scaled to yield reasonable magnitudes (Nguyen, Johnson, et al. 2019).

$$J_8 = \frac{10}{m}\frac{1}{t_f}\sum_{i=1}^{m}\int_0^{t_f} a_i^3(t)dt + w_{s1}\frac{10^{-6}}{t_f}\int_0^{t_f}\left(\frac{d^3CoM_x}{dt^3}\right)^2 dt + w_{s2}\frac{10^{-6}}{t_f}\int_0^{t_f}\left(\frac{d^3CoM_y}{dt^3}\right)^2 dt \quad (3.12)$$

The gait smoothness may also be described through the rates of changes of GRFs (Rebula and Kuo 2015). Therefore, the cost functions J_9 and J_{10} (Eq. 3.13 and Eq. 3.14) added the rates of changes of the GRFs to the cost functions. Different exponents (two in J_9 and four in J_{10}) penalize the rates of changes differently. The higher the exponent, the more penalty on the peaks of rates of changes.

$$J_9 = \frac{10}{m}\frac{1}{t_f}\sum_{i=1}^{m}\int_0^{t_f} a_i^3(t)dt + w_{s1}\frac{10^{-7}}{t_f}\int_0^{t_f}\left(\frac{d}{dt}\left(\frac{VGRF}{Mg}\right)\right)^2 dt + w_{s2}\frac{10^{-3}}{t_f}\int_0^{t_f}\left(\frac{d}{dt}\left(\frac{HGRF}{Mg}\right)\right)^2 dt \quad (3.13)$$

$$J_{10}$$

$$= \frac{10}{m}\frac{1}{t_f}\sum_{i=1}^{m}\int_0^{t_f} a_i^3(t)dt + w_{s1}\frac{10^{-9}}{Mg}\frac{1}{t_f}\int_0^{t_f}\left(\frac{dVGRF}{dt}\right)^4 dt \quad (3.14)$$

$$+ w_{s2}\frac{10^{-4}}{Mg}\frac{1}{t_f}\int_0^{t_f}\left(\frac{dHGRF}{dt}\right)^4 dt$$

Besides smoothness, stability may be also an essential factor in walking (Hak et al. 2013). In this study, we used a stability measure based on the total difference between the position of the CoM in the horizontal direction (CoM_x) and the middle of the extended base of support ($midBoS_x$), and the total difference between the position of the head in the horizontal direction ($head_x$) and the $midBoS_x$ (Nguyen, Johnson, et al. 2019). The extended base of support is defined as the convex area containing the projections of two feet on the ground. The next two cost functions (J_{11} and J_{12}) combine gait stability and smoothness terms, with the sum of the muscle fatigue term (Eq. 3.15), or with CoT (Eq. 3.16).

$$J_{11}$$

$$= \frac{10}{t_f}\sum_{i=1}^{m}\int_0^{t_f} a_i^3(t)dt + w_{s1}\frac{10^{-1}}{t_f}\int_0^{t_f}(CoM_x - midBoS_x)^2 dt$$

$$+ w_{s2}\frac{10^{-1}}{t_f}\int_0^{t_f}(head_x - midBoS_x)^2 dt + w_{s3}\frac{10^{-6}}{t_f}\int_0^{t_f}\left(\frac{d^3CoM_x}{dt^3}\right)^2 dt \quad (3.15)$$

$$+ w_{s4}\frac{10^{-6}}{t_f}\int_0^{t_f}\left(\frac{d^3CoM_y}{dt^3}\right)^2 dt$$

$$J_{12}$$

$$= \frac{10^{-3}}{M}\frac{\sum_{i=1}^{m}\int_0^{t_f}\dot{E}_i dt}{X_{cm}(t_f) - X_{cm}(t_0)} + w_{s1}\frac{10^{-1}}{t_f}\int_0^{t_f}(CoM_x - midBoS_x)^2 dt$$

$$+ w_{s2}\frac{10^{-1}}{t_f}\int_0^{t_f}(head_x - midBoS_x)^2 dt + w_{s3}\frac{10^{-6}}{t_f}\int_0^{t_f}\left(\frac{d^3CoM_x}{dt^3}\right)^2 dt \quad (3.16)$$

$$+ w_{s4}\frac{10^{-6}}{t_f}\int_0^{t_f}\left(\frac{d^3CoM_y}{dt^3}\right)^2 dt$$

The next cost function (J_{13}) combines muscle fatigue with the muscles weighted differently, gait smoothness, and stability terms (Eq. 3.17). In the cost functions from J_4 to J_{13}, the unknown parameters ($\boldsymbol{w}$) were solved through the bilevel optimization (Nguyen, Johnson, et al. 2019). Although the gait results from the bilevel optimization are not predictive because the bilevel optimization requires experimental gait data, the results can show the best gait solutions in cases the cost functions are used in predictive walking simulations. The cost functions from J_4 to J_{13} contains unknown parameters ($\boldsymbol{w}$) which were solved through the bilevel optimization.

$$
\begin{aligned}
&J_{13} \\
&= \frac{1}{t_f}\sum_{i=1}^{m} w_i \int_0^{t_f} a_i^3(t)dt + w_{s1}\frac{10^{-1}}{t_f}\int_0^{t_f}(CoM_x - midBoS_x)^2 dt \\
&+ w_{s2}\frac{10^{-1}}{t_f}\int_0^{t_f}(head_x - midBoS_x)^2 dt + w_{s3}\frac{10^{-6}}{t_f}\int_0^{t_f}\left(\frac{d^3CoM_x}{dt^3}\right)^2 dt \\
&+ w_{s4}\frac{10^{-6}}{t_f}\int_0^{t_f}\left(\frac{d^3CoM_y}{dt^3}\right)^2 dt
\end{aligned}
\tag{3.17}
$$

3.3.4 Evaluation

To quantify the qualities of the cost functions, the mean absolute error normalized by the SD between the predicted gaits and the human gait was calculated for hip, knee, and ankle angles, and GRFs (Eq. 3.18). With the expectation that the predicted gait lies within $\pm$ 1 SD of the experimental means, E is expected to be smaller than one. Besides kinematics and kinetics, the predicted muscle activation pattern, CoT, and walking stride frequency were evaluated with the measured data or the experimental data in the literature.

$$
E = \frac{1}{t_f}\int_0^{t_f}\frac{|\boldsymbol{x} - \widehat{\boldsymbol{x}}|}{\widehat{SD}}dt \tag{3.18}
$$

3.3 Results

The tracking cost function J_T resulted in the kinematics and GRFs within half of SD of the experimental means (0.36 SD for kinematics and 0.38 SD for GRFs) (Figure 3.2, Figure 3.6). The CoT is 3.79 J/m/kg, which is within the human mean $\pm$ 1 SD (3.4 $\pm$ 0.4 J/m/kg) (Das Gupta, Bobbert, and Kistemaker 2019)(Figure 3.3). The simulated stride frequency (0.89 Hz) is within 1 SD of measured data (0.92 $\pm$ 0.04 Hz) (Figure 3.3). The muscle activation patterns are in good agreement with the on-off timing of EMG data in the literature (Bonnefoy-Mazure and Armand 2015)(Schmitz et al. 2009) (Figure 3.4).

All the performance-based cost functions were able to generate human-like gaits. However, the qualities of the gait solutions are considerably different (Figure 3.2 and Figure 3.3)(also see Table S-2 in the appendix B). The kinematic errors range from 0.85 SD (J_{13}) to 3.67 SD (J_3) of the experimental means. The GRFs errors range from 0.71 SD (J_5) to 2.24 SD (J_3) of the experimental means. Seven of the 13 performance-based cost functions predicted gait stride frequencies within the experimental mean $\pm$ 1 SD ($J_2, J_4, J_6, J_7, J_9, J_{10}, J_{12}$). Nine of the 13 performance-based cost functions predicted CoT within 1 SD of the experimental mean ($J_3, J_4, J_5, J_6, J_7, J_8, J_{11}, J_{12}, J_{13}$).

Minimizing the muscle fatigue (sum of muscle activation cubed) (J_2) predicted better kinematics and GRFs (1.55 SD and 1.65 SD, respectively) compared to minimizing CoT (J_1) (2.06 SD and 2.1 SD respectively) and minimizing muscle stress (J_3) (3.67 SD and 2.24 SD respectively) (Figure 3.2 and Figure 3.7). In addition, the muscle activations in J_2 are overall in better agreement with the experimental data (Figure 3.4). In J_1 and J_3, some muscles such as VAS did not activate over the gait cycle. The optimal value of the exponent w_{s1} in J_4 is 13.59. Quantitatively, this optimal exponent gave better GRFs compared to the exponent of three in J_2 (Figure 3.2 and Figure 3.7). However, the kinematics was slightly worse compared to J_2. The

muscle activations in J_4 were overall flatter than in J_2 (Figure 3.4). The CoT with J_4 was higher than with J_2 (Figure 3.3).

J_5, J_6, and J_7, representing metabolic energy, muscle fatigue, and muscle stress, have each muscle-based performance weighted differently, which resulted in better kinematics and GRFs compared to equally weighted all muscle-based costs as in J_1, J_2, and J_3 respectively (Figure 3.2, Figure 3.7, Figure 3.8). All three cost functions J_5, J_6, and J_7 resulted in significantly high GAS activations (Figure 3.4). J_6 and J_7 also predicted high DOR activations. Meanwhile, GMAX did not activate over the gait cycle in J_5 and J_6, and activated small amount in J_7 (Figure 3.4).

Adding smoothness terms in the cost functions (J_8, J_9, and J_{10}) led to smoother GRFs patterns. The first peaks of GRFs at heel strike are lower compared to in J_2 (Figure 3.7 and Figure 3.9). In addition, the knee at the beginning of the stance phase (around 20% of the gait cycle) flexed more than in J_2 (Figure 3.9). Penalizing the GRFs rates of changes with exponent two and four resulted in similar gait solutions (Figure 3.2 and Figure 3.9). Muscle activations in J_8, J_9, and J_{10} are generally in good agreement with EMG data (Figure 3.5). To evaluate the gait smoothness with these cost functions, we quantified the CoM jerk cost and GRF rates of changes in the gait solutions with J_2, J_8, J_9, J_{10} (Table 3.1).

Cost functions	**VGRF rate of change**	**HGRF rate of change**	$\boldsymbol{CoM_x}$ **jerk cost**	$\boldsymbol{CoM_y}$ **jerk cost**
J_2	73.6009	6.8881	2537.3331	8033.4621
J_8	27.3326	2.1245	193.0484	377.0615
J_9	50.3645	1.1708	1025.4145	32359.9898
J_{10}	48.6341	1.3182	919.9706	25869.7566

Table 3.1: Quantifying the GRFs rates of changes, CoM jerk costs in fore-aft and vertical directions. The GRFs rates of changes was calculated as second and third terms of J_9 (Eq. 3.13) without the scaling factors and weights. CoM jerk costs were calculated as second and third terms of J_8 (Eq. 3.12) without the scaling factors and weights.

J_{11} and J_{12} which includes the stability and smoothness term resulted in the kinematics and GRFs within and close to 1 SD of the experimental means (0.91 SD and 0.94 SD for J_{11}, 1.07 SD and 1.06 SD for J_{12}) (Figure 3.2). Note that the gait result with the cost function J_{11} was already published in (Nguyen, Johnson, et al. 2019). The predicted muscle activations are in good agreement with the on-off timing of EMG data (Figure 3.5). J_{13} improved further the kinematics and GRFs (0.85 SD and 0.84 SD respectively) (Figure 3.10) by weighting the muscle-based costs differently across mucles.

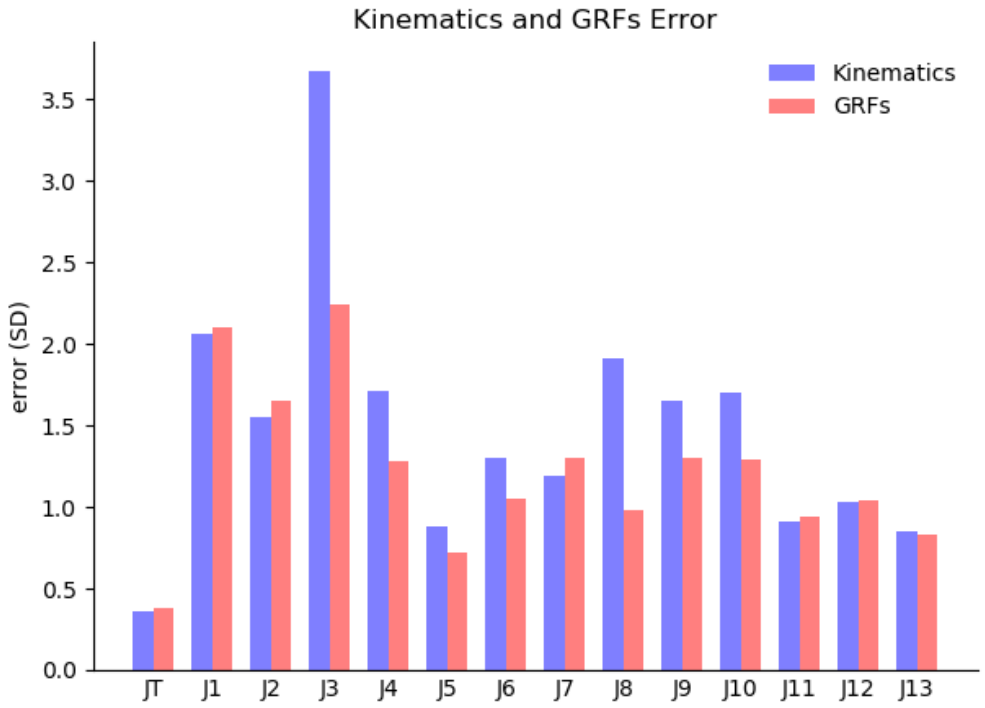

Figure 3.2: Kinematics and GRFs errors with different cost functions. The tracking cost function (J_T) resulted in the kinematics and GRFs within 0.5 SD. J_5, J_{11}, J_{12} and J_{13} resulted in the kinematics and GRFs within 1 SD.

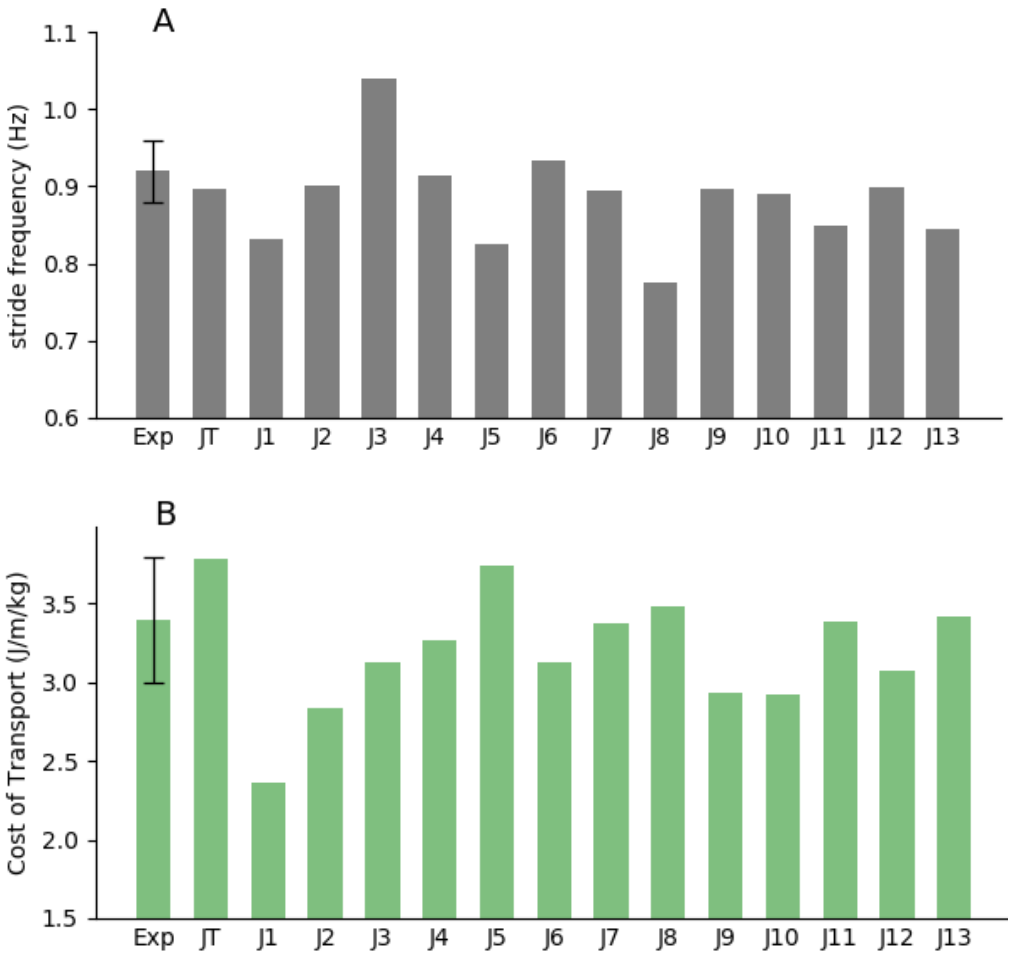

Figure 3.3: Stride frequencies (A) and costs of transport (B) results. The experimental stride frequency was measured through eight subjects (Nguyen, Johnson, et al. 2019), the experimental CoT was based on (Das Gupta et al. 2019). The error bars represent $\pm$ 1 SD. Tracking cost function and seven of 13 performance-based cost functions predicted stride frequencies within mean $\pm$ SD of experimental data. Nine of 13 performance-based cost functions predicted CoT within 1 SD of the experimental mean.

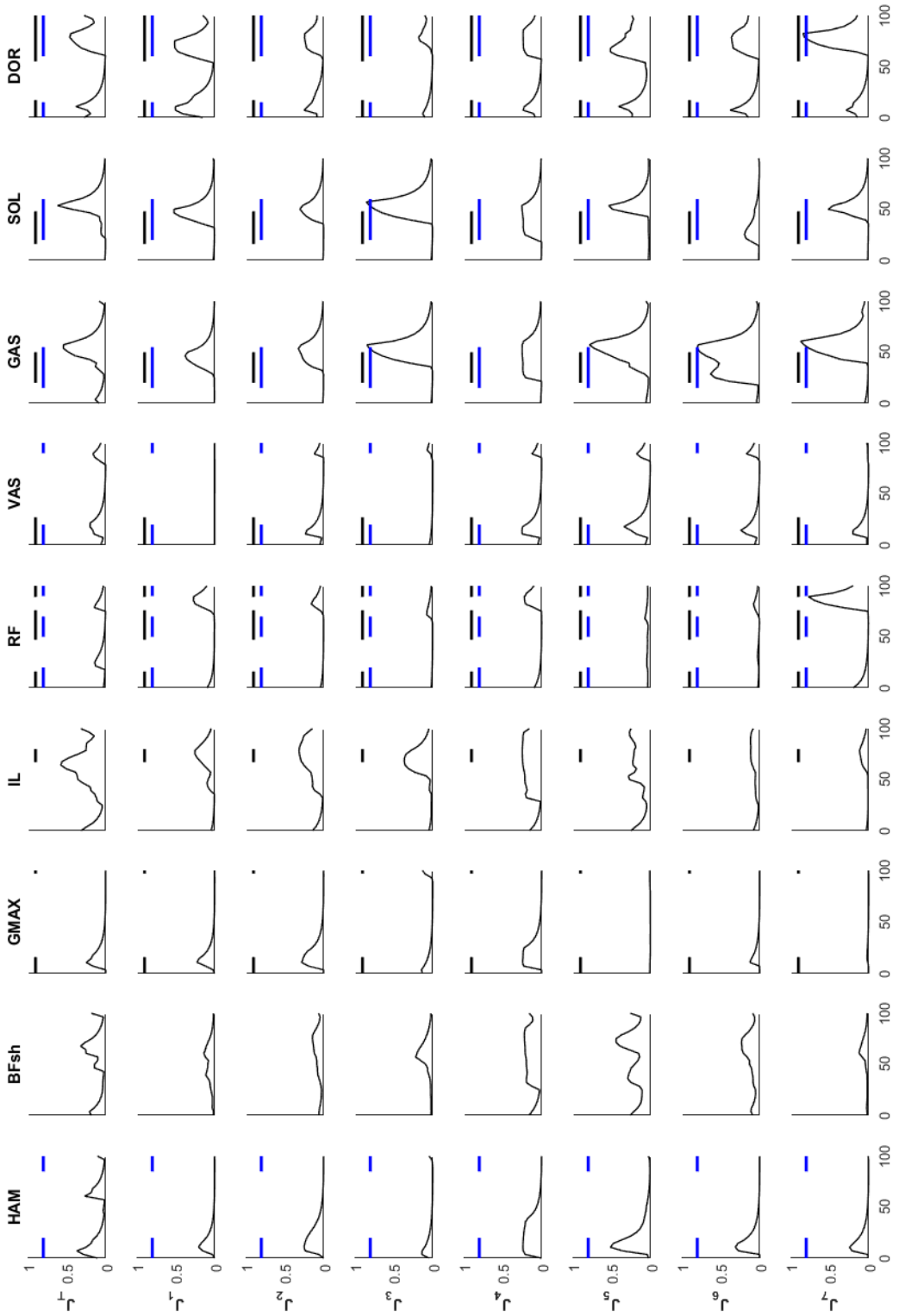

Figure 3.4: Predicted muscle activations (black thin lines) using the tracking cost function J_T and the cost functions J_1- J_7 . The horizontal bars indicate on-off timing of EMG data; black bars are based on data in (Bonnefoy-Mazure and Armand 2015); green bars are based on data in (Schmitz et al. 2009)

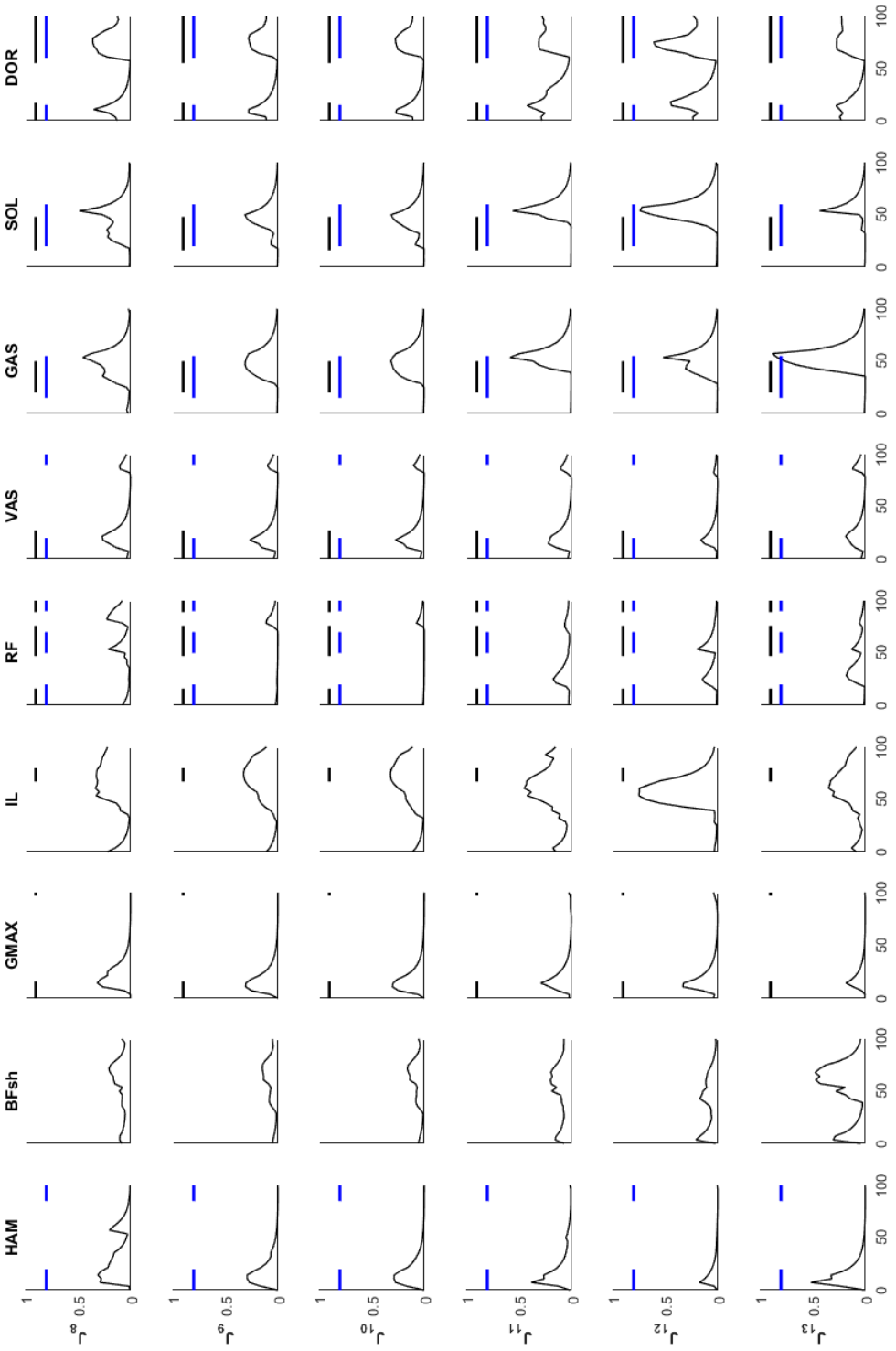

Figure 3.5: Predicted muscle activations (black thin lines) using the cost functions J_8- J_{13}. The horizontal bars indicate on-off timing of EMG data; black bars are based on data in (Bonnefoy-Mazure and Armand 2015); green bars are based on data in (Schmitz et al. 2009).

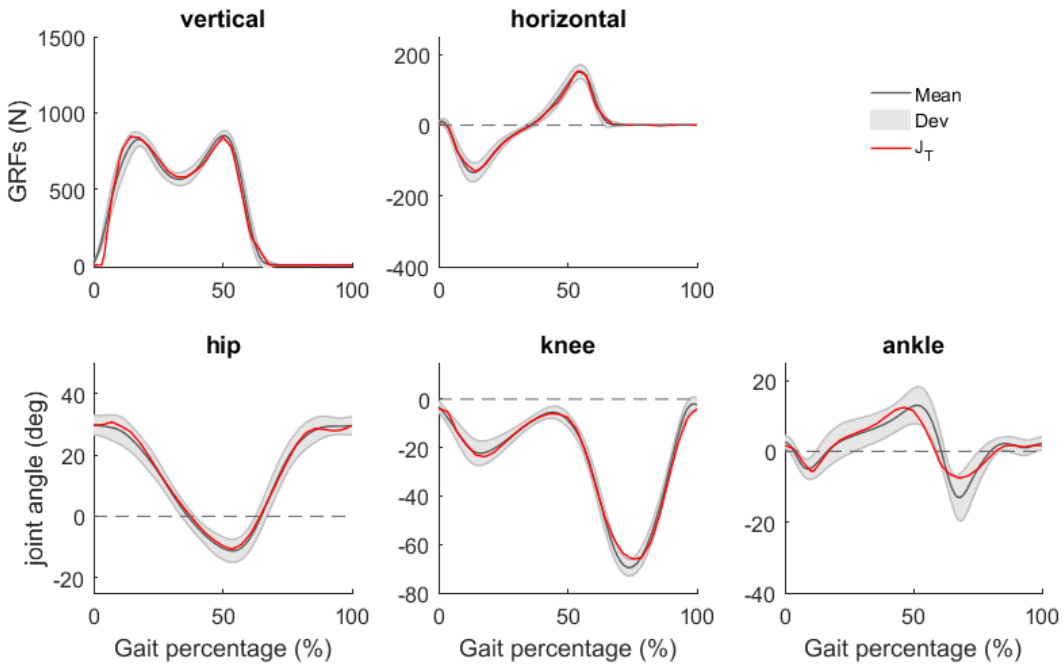

Figure 3.6: Kinematics and GRFs using the tracking cost function (J_T). Both kinematics and GRFs are under 0.4 SD of the experimental data.

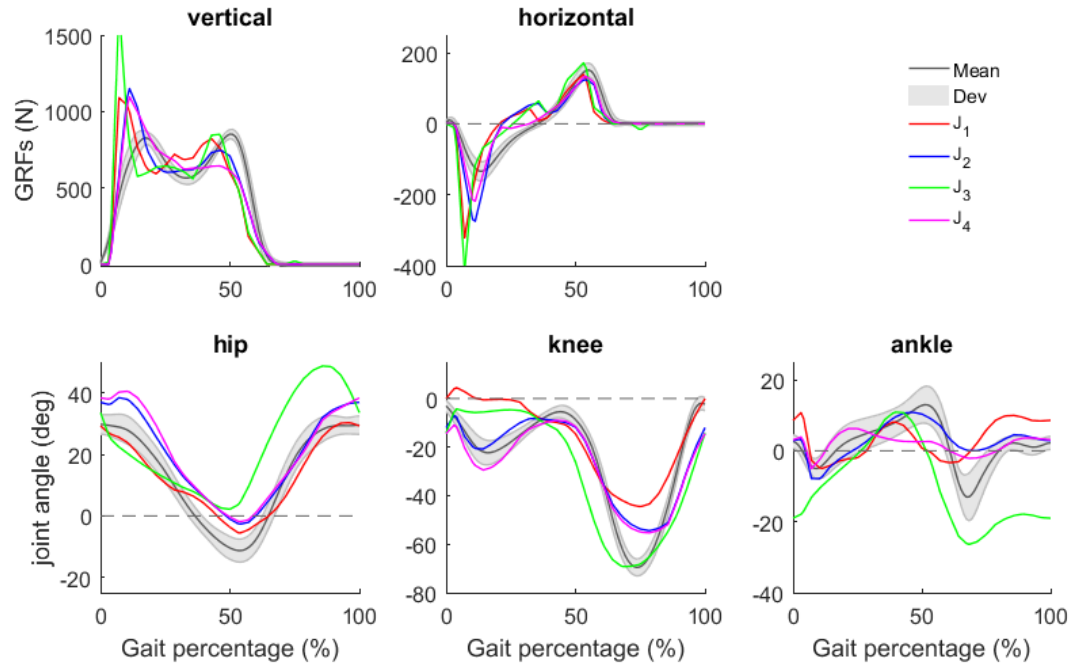

Figure 3.7: Kinematics and GRFs using the cost functions J_1- J_4. Minimizing muscle activation cubed (J_2) predicted more realistic kinematics and GRFs compared to minimizing CoT (J_1) and minimizing muscle stress (J_3). Exponent w_{s1} in J_4 was optimized, which did not substantially improve the kinematics and GRFs compared to J_2 with the exponent of three.

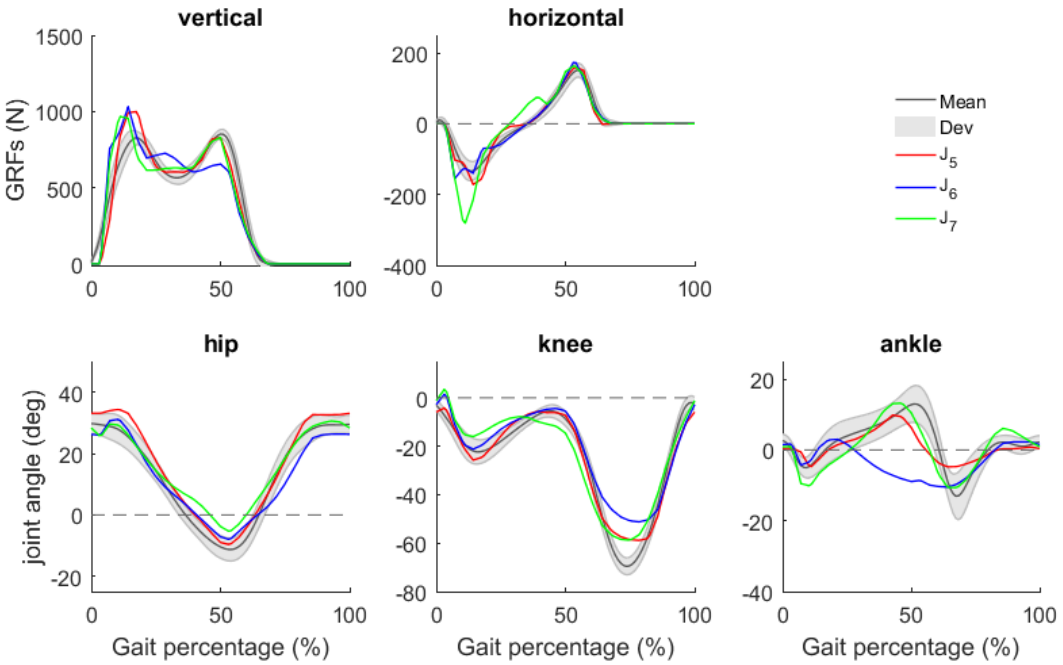

Figure 3.8: Kinematics and GRFs using the cost functions J_5, J_6, and J_7, which weights each muscle-based criterion individually. These cost functions significantly improved the gait solutions compared to J_1, J_2, J_3 in term of kinematics and GRFs.

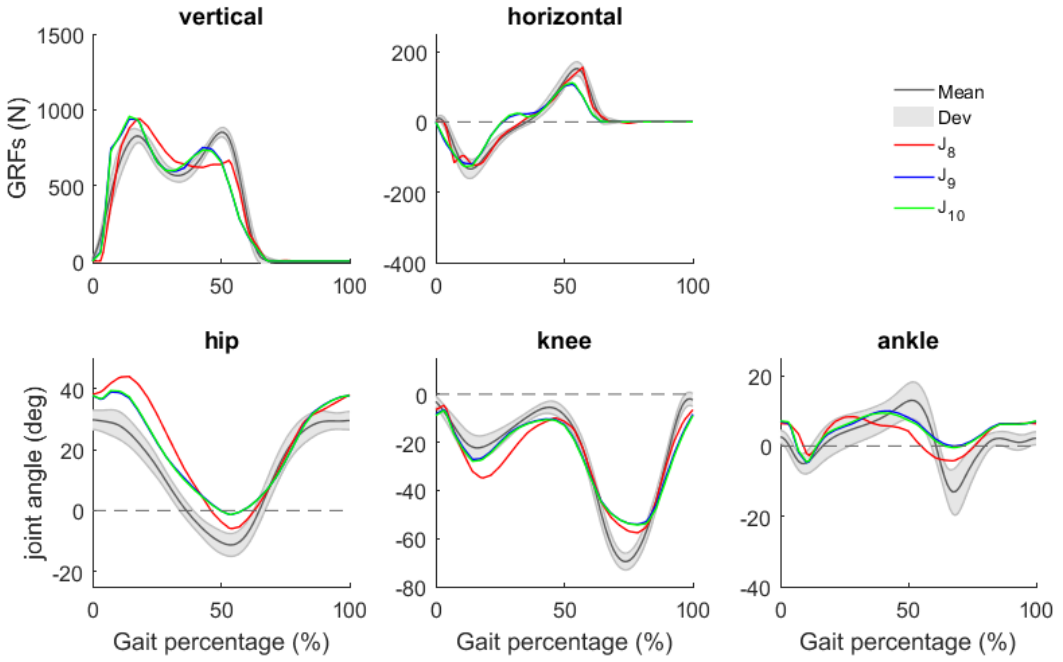

Figure 3.9: Kinematics and GRFs using the cost functions J_8, J_9 and J_{10}, which consist of muscle fatigue term and smoothness terms. The first peaks of GRFs with these cost functions were more realistic compared to J_2 which only consists of muscle fatigue term. J_9 and J_{10} have similar kinematics and GRFs.

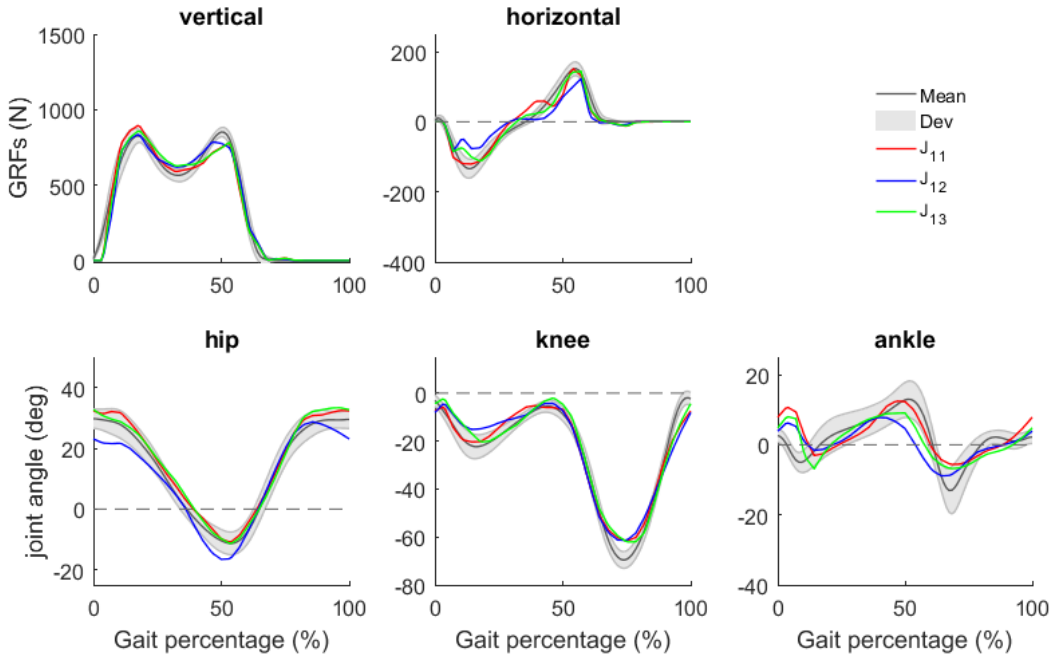

Figure 3.10: Kinematics and GRFs using the cost functions J_{11}, $J_{12}$and J_{13}, which consist of muscle fatigue term, smoothness, and stability terms. Both kinematics and GRFs using these cost functions are about 1 SD of the experimental means.

3.4 Discussion

In this study, we examined a tracking cost function and a variety of performance-based cost function forms for optimal control of human walking. The unknown parameters (e.g., exponent value, weights) in some cost functions were optimized using the bilevel optimization approach to evaluate the best outcomes with the cost functions. The tracking cost function resulted in a good tracking solution, which demonstrates the ability of the musculoskeletal model to produce human-like walking. All performance-based cost functions were able to generate walking solutions, but with different qualities compared to actual human gait data in term of kinematics, kinetics, stride frequency, CoT, and muscle activation pattern.

J_1, J_2, and J_3 based on CoT, muscle fatigue, and muscle stress, respectively, have been commonly used in the literature (Anderson and Pandy 2001)(Ackermann and van den Bogert 2010)(Miller et al. 2011)(Dorn et al. 2015)(Lin et al. 2018). In this study, J_2 predicted more realistic gait kinematics, GRFs, and muscle activations compared to J_1 and J_3 (Figure 3.7). This

result is similar to the result in (Miller et al. 2011) which compared the three cost functions for running simulations. J_1, minimizing CoT, naturally predicted the lowest CoT in all cost functions (Figure 3.3). In J_1, the VAS, a major knee extensor, did not activate over the gait cycle, which causes the knee to not flex at the early stance (Figure 3.4). Similarly, the knee straight at the early stance in J_3 may be explained by the fact that the VAS did not activate (Figure 3.4). Since VAS muscle is one of the largest muscle groups (Nguyen, Johnson, et al. 2019)(appendix A), adopting the straight knee walking strategy that does not require to activate VAS; therefore may help save the cost in J_1 and J_3. However, this walking strategy is not in the case of actual human gait, which has the knee flexs about 20 degrees and VAS activated (Figure 3.7 and Figure 3.4).

In J_4, we allowed w_{s1} to be in the range of $[1, 20]$. The optimal value of the exponent $w_{s1} = 13.59$ did not significantly improve the gait kinematics and GRFs compared to the cubed exponent in J_2 (Figure 3.2 and Figure 3.7). While the GRFs were slightly better than in J_2, the kinematics was not as good as in J_2. With the high exponent ($w_{s1} = 13.59$), only the high peaks in muscle activations matter. Therefore, the muscle activations in J_4 became flatter than in J_2. Similar flat muscle activation patterns were also seen in (Ackermann and van den Bogert 2010) that examined the exponent of ten. The muscle activations compared with EMG on-off time are generally similar for J_4 and J_2 (Figure 3.4). However, the flat muscle activation patterns in J_4 is unlikely to be realistic as seen in actual human EMG data (Schmitz et al. 2009). While the upper bound of w_{s1} is 20, the optimal exponent is $w_{s1} = 13.59$, which suggests that using a higher exponent may not lead to better kinematics and GRFs. Therefore, it is unlikely that the *minmax* criteria, as proposed in (Rasmussen, Damsgaard, and Voigt 2001), which is equivalent to a very large exponent will result in a better gait.

J_5, J_6, and J_7, representing metabolic cost, muscle fatigue, muscle stress, but having each muscle-based criterion weighted differently, improved the kinematics and GRFs compared to equally weighting all muscle-based performance criteria. However, the muscle activation patterns

may be compromised. Some muscles with large weights were turned off during the gait cycle, while some muscles with low weights activated with significantly high magnitudes (Figure 3.4). For example, in J_7 GMAX with the weight of 286.18 did not activate (see table S-3 in the appendix B for the optimized weight results), DOR with the weight of 0.31 activated with very high magnitude (Figure 3.4). This issue of muscle activation patterns may be improved by narrowing down the range of the muscle weights. However, doing this will likely decrease the quality of kinematics and GRFs. To demonstrate this, we limited the range of muscle weights as [5, 50], the cost function J_6 with the optimal weights resulted in the kinematics and GRFs error of 1.28 SD and 1.14 SD, respectively, which are not as good as when using the weight range of [0.1, 300]. A challenge in determining the muscle weights is that the relationship between the weight and the predicted activation magnitude is highly non-linear. For instance, in J_7, VAS has the weight of 1.76 which is smaller than GAS weight (6.86) (Table S-3, appendix B), but the activation magnitude of GAS is still higher than VAS (Figure 3.4). Because of this non-linear relationship, manually adjusting the muscle weights may be very difficult. Therefore, using the bilevel optimization approach like in this study can help determine the optimal muscle weights in the cost functions. Nevertheless, the optimized muscle weights may lead to unrealistic muscle activation patterns like in J_5, J_6, and J_7.

With the cost functions only based on muscle-based performance criteria (metabolic cost, muscle fatigue, muscle stress in J_1, J_2, J_3, and J_4), the first peaks of VGRF and HGRF are considerably high compared to the human GRFs (Figure 3.7). This problem was addressed by adding the smoothness terms into the cost functions (J_8, J_9, J_{10}) (Figure 3.9). To better compare the smoothness of the gait solutions with these cost functions, we quantified the CoM jerk cost and GRF rates of changes in the gait solutions with J_2, J_8, J_9, J_{10} (Table 3.1). The GRFs rates of changes were calculated as the second and third terms of J_9 (Eq. 3.13) without the scaling factors and weights. CoM jerk costs were calculated as the second and third terms of J_8 (Eq. 3.12)

without the scaling factors and weights. The results showed that minimizing the CoM jerk cost (J_8) also resulted in smooth GRFs. In addition, minimizing rates of the changes of the GRFs (J_9, J_{10}) decreased the CoM jerk cost in the fore-aft direction (Table 3.1). This suggests the propositional relationship between the CoM smoothness and the observed smooth GRFs in human gait. Furthermore, in J_8, J_9, J_{10}, more knee flexions were seen compared to in J_2. It is suggested that the knee flexion at the early stance phase may serve to smooth GRFs or absorb the shock to reduce jerks (Gard and Childress 1999), our results of knee flexions with minimizing the jerk and GRFs rates of changes support this idea.

In cost functions J_{11} and J_{12}, the instability was penalized besides the muscle-based performance criteria and the CoM jerk cost. These cost functions significantly improved the gait kinematics and GRFs (Figure 3.2, Figure 3.10). The predicted muscle activations with these cost functions are also in good agreement with the EMG data (Figure 3.5). The results with these cost functions suggest that minimizing muscle-based performance (e.g., muscle fatigue, metabolic cost), maximizing gait smoothness and stability, are all likely important in human walking. The cost function J_{13} resulted in kinematics and GRFs closest to the human means in all performance-based cost functions. J_{13} improved the simulated gait compared to J_{11} by adjusting the muscle weights. The range of muscle weights in J_{13} was limited in a relatively narrow range [5, 50] to avoid the potential unrealistic muscle activation patterns as seen in J_6. In these cost functions, J_{11}, J_{12}, and J_{13}, the stability term was based on the differences between the projected CoM and the center of extended BoS, the differences between the projected head position and the extended BoS (Nguyen, Johnson, et al. 2019). The extended BoS is used to avoid the discontinuities from normal defined BoS which is typically used in some stability measures in the literature (Nguyen, Johnson, et al. 2019). Although using this stability measure has allowed improving the gait results, future research may also consider other stability measures (Bruijn et al. 2013).

In this study, the CoT was calculated using the metabolic energy expenditure model described in (Umberger et al. 2003). The cost function J_1, minimizing CoT, as expected, predicted the lowest CoT (2.36 J/m/kg) (Figure 3.3). The CoT of the tracking solution is highest and equal to 3.79 J/m/kg. Nine of the performance-based cost functions predicted CoT within 1 SD of the experimental data (Figure 3.3-B). Minimizing muscle fatigue criterion in general predicted more realistic CoT compared to minimizing CoT (J_2, J_{11} in comparison with (J_1, J_{12})). In addition, adding more performance criteria in the cost functions tends to lead to higher CoT (Figure 3.3). This result is understandable in term of mathematical optimization with a multi-objective cost function. In term of biomechanics, the higher CoT when adding smoothness and stability terms in the cost functions suggests that maintaining gait smoothness and stability requires additional effort (Alan Hreljac and Martin 1993).

In this chapter, the results with the cost functions J_4 to J_{13} involved the bilevel optimization, which used the experimental gait data. Therefore, the gait solutions with these cost functions are not considered predictive solutions. The gaits with these cost functions, however, show the best gait results if the cost functions are used in the predictive walking simulation. The cost functions with the optimized weights can potentially be used to predict the gait at different conditions. To demonstrate that, we have used the cost function J_{11} with the optimized weights to simulate human walking at different speeds (Figure S-4, appendix A). The predictive results show some trends in the changes of kinematics and kinetics over the speed range, which are similar to the experimental data in (Edith M Arnold et al. 2013). For example, the hip range increased when the speed increased. The knee flexion at the stance phase increased when the speed increased. First peaks of VGRF and HGRF, which are at heel stride also increased with the speeds. These results suggest the potential uses of the cost function with optimized weights for predictive simulations.

3.5 Conclusion

This study examined a variety of possible cost function forms based on different performance criteria. The best performances of the cost function forms were evaluated by optimizing the parameters in the cost functions using a bilevel optimization approach. The results showed that the gait solutions can be significantly improved by using the cost function based on muscle-based performance (metabolic cost, muscle fatigue), gait smoothness, and gait stability. This type of cost function form may be used to predict walking at different conditions.

CHAPTER 4

PREDICTIVE SIMULATION OF HUMAN WALKING AUGMENTED BY A POWERED ANKLE EXOSKELETON

This chapter is adapted from a paper with the title *Predictive simulation of human walking augmented by a powered ankle exoskeleton* accepted to the IEEE International Conference on Rehabilitation Robotics (Nguyen, Umberger, et al. 2019).

The human ankle provides significant positive power during the stance phase of walking which has resulted in studies focusing on methods to reduce the energetic walking cost by augmenting the ankle with exoskeletons. Recently, a few devices have successfully reduced the metabolic cost of walking by replacing part of the biological ankle plantar flexor torque. Despite of these achievements, development of assistive ankle devices remains challenging, partly because the current practice of design and control of powered exoskeletons is highly time and effort consuming, which prevents quickly exploring different design and control parameters. Predictive simulations using musculoskeletal models coupled with robotic devices may facilitate the process of design and control of assistive devices. In this study, we simulate human walking augmented by a powered ankle exoskeleton. The walking problem was formulated as a predictive dynamic optimization in which both the optimal assistive device torque and the gait were solved simultaneously. Cases with exoskeletons assisting one ankle and both ankles were considered. The results showed the energetic cost of walking could be reduced by 45% with one ankle augmented, and by 52% with both ankles augmented. This study contributes towards the goal of providing optimal assistive torque through external devices and theoretical peak reductions that could be expected from such devices.

4.1 Introduction

Reducing the energetic cost of human walking by assisting ankle torque production is of interest in many studies since the human ankle produces the greatest amount of positive work compared to the hip and knee joints (Neptune et al. 2001)(Farris and Sawicki 2011a). Although many exoskeletons have been developed, relatively few have succeeded in reducing the energetic cost of walking (Malcolm et al. 2013)(Zhang et al. 2017). One possible reason may be that the candidate designs must be built, and then the control profiles are often hand-tuned based on trial-and-error, which can be time-consuming and may not achieve optimal performance (Jackson and Collins 2015)(Malcolm et al. 2013)(Galle et al. 2017)(Caputo, Adamczyk, and Collins 2015). The current practice of build and test cycles is slow, which inhibits systematic optimization of device design and control parameterization. An effective way to address this challenge may be by using predictive simulation based on dynamic optimization of the coupled human-robotic device system (Handford and Srinivasan 2018)(Handford and Srinivasan 2016).

Recently, human-in-the-loop approaches have been used to optimize assistive torque profiles during the locomotion tasks (Kim et al. 2017)(Zhang et al. 2017)(Ding et al. 2018). Although this experimental approach has shown to be promising in finding optimal torque control of the assistive devices, it has been applied only in the cases where relatively simple torque patterns with few parameters were optimized. When complex torque patterns with more parameters are required, the human-in-the-loop approach may be difficult to converge in a reasonable time (Zhang et al. 2017). In addition, the success of the experimental approach may be partly due to the known good generic assistance pattern (Zhang et al. 2017). In these cases, the predictive simulation based on the dynamic optimization approach may allow finding the generic optimal device control. Furthermore, the predictive simulation may allow exploring non-biological assistance profile without the risks to the subject.

Several recent studies have used the simulation approach to study human locomotion augmented by assistive devices. For example, Fey et al. (Fey et al. 2012) used dynamic

optimization with experimental tracking data to optimize the stiffness of a passive prosthesis. A forward integration approach was used to evaluate the performance of a powered ankle prosthesis (Laprè et al. 2014). The computed muscle control algorithm (Thelen et al. 2003) within OpenSim (Seth et al. 2011) was used to simulate human running with assistive devices (Uchida et al. 2016), and human walking with assistive devices while carrying heavy loads (Dembia et al. 2017). Although these simulation studies can provide insights into the design and control of assistive devices, a substantial limitation of these studies is they were each based on a set of experimental data and it was assumed that the gait kinematics and kinetics did not change with the presence of the assistive devices.

The simulation based on dynamic optimization approach, on the other hand, can be formulated independently from experimental data (Anderson and Pandy 2001), and is referred to as predictive simulation. Predictive simulation has been recently used to simulate amputee walking on a prosthetic knee (Zhao, Berns, and Baptista 2013), amputee walking on powered prosthesis ankles to examine different control strategies of the ankle prosthesis (Handford and Srinivasan 2018)(Handford and Srinivasan 2016), simulate pathological gait with ankle-foot orthosis to identify the optimal device stiffness (Sreenivasa et al. 2017). To our knowledge, however, there has not a predictive simulation study for normal human walking with assistive exoskeletons. Therefore, in this study we simulate human walking augmented by a powered ankle exoskeleton using predictive dynamic optimization. The walking problem is formulated as a large-scale optimization that does not rely on tracking a set of experimental gait data. The optimal control of the device is found simultaneously along with the resulting gait solution. To evaluate the performance of the device on human walking, we simulate cases when the exoskeleton assists one ankle, and cases when the exoskeletons assist both ankles.

4.2 Method

4.2.1 Human-exoskeleton model

The human-exoskeleton model was adapted from the musculoskeletal model described in (Nguyen, Johnson, et al. 2019), which was implemented in OpenSim Ver. 3.3 (Seth et al. 2011)(Figure 4.1). The model consists of 12 rigid body segments, which are connected through 11 degrees-of-freedoms (three at the pelvis, one rotation for each hip, knee, ankle, and metatarsophalangeal joint). The musculoskeletal model was assumed to have a mass of 76.8 kg and a height of 1.75 m. The lower limbs are actuated by 18 muscle-tendon units, which are represented with a Hill-type muscle model (Millard et al. 2013). These muscles and muscle groups are: biarticular hamstring, biceps femoris short head, gluteus maximus, iliopsoas, rectus femoris, vasti, gastrocnemius, soleus, dorsiflexor (tibialis anterior, extensor hallucis longus, and extensor digitorum longus). The foot-ground contact was modeled using contact spheres described by OpenSim HuntCrossleyContact model (Porsa et al. 2016). A powered ankle exoskeleton was added in parallel to the biological ankle joint. The exoskeleton parameters were based on a light-weight (0.83 kg), tethered ankle device actuated by an off-board motor (Witte et al. 2015). The exoskeleton can produce about 120 Nm plantarflexion torque, and has a range of motion from 30^0 plantarflexion to 20^0 dorsiflexion as found in an experimental design (Witte et al. 2015). This exoskeleton was chosen because it has some favorable performance advantages such as light-weight and capability of producing high torque, allowing rapid exploration of a wide range of control strategies. In addition, the exoskeleton has been used experimentally to explore the optimal assistive ankle torque profile in walking (Zhang et al. 2017) that provides a basis for comparison with our simulations based on the predictive simulation approach. To model the exoskeleton, we used an ideal torque model and added the device mass to the ankle.

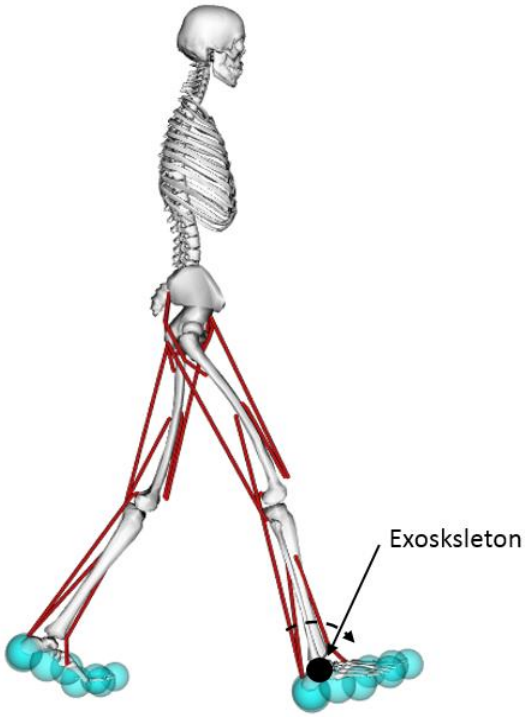

Figure 4.1: Musculoskeletal model with an ankle exoskeleton. The musculoskeletal model consists of 12 rigid segments connected through 11 degrees of freedoms. The model is actuated by 18 muscle tendon units. The exoskeleton is modeled using an ideal torque that provides assistance to the ankle.

4.2.2 Predictive dynamic optimization

In this study, we formulated the walking problem as a predictive dynamic optimization problem (Eq. 4.1) (Ackermann and van den Bogert 2010).

$$\min_{\boldsymbol{x},\boldsymbol{u}} J \tag{4.1-a}$$

$$\text{Subject to: } \dot{\boldsymbol{x}} = f(\boldsymbol{x}, \boldsymbol{u}, t) \tag{4.1-b}$$

$$C_{lb} \leq C(\boldsymbol{x}, \boldsymbol{u}, t) \leq C_{ub} \tag{4.1-c}$$

where $\boldsymbol{x}(t) \in R^l$ is the state (e.g., joint angles, joint velocities, muscle fiber lengths and activations) with l representing the dimension of the state, $\boldsymbol{u}(t) \in R^m$ is the control (muscle excitation, exoskeleton torque control) with q representing the dimension of the control, t is the time, C represents the constraints, and C_{lb} and C_{ub} are lower and upper bounds on the constraints,

respectively. Eq. 4.1-b represents the dynamic equation of the musculoskeletal model and J is the cost function for walking (Nguyen, Johnson, et al. 2019) (Eq. 4.2).

$$
\begin{aligned}
&J \\
&= \frac{10}{t_f}\sum_{i=1}^{m}\int_0^{t_f} a_i^3(t)dt + w_1\frac{10^{-1}}{t_f}\int_0^{t_f}(CoM_x - midBoS_x)^2 dt \\
&+ w_2\frac{10^{-1}}{t_f}\int_0^{t_f}(head_x - midBoS_x)^2 dt + w_3\frac{10^{-6}}{t_f}\int_0^{t_f}\left(\frac{d^3CoM_x}{dt^3}\right)^2 dt \\
&+ w_4\frac{10^{-6}}{t_f}\int_0^{t_f}\left(\frac{d^3CoM_y}{dt^3}\right)^2 dt
\end{aligned}
\tag{4.2}
$$

where a_i is the muscle activation of muscle i^{th} out of m muscles. CoM_x and CoM_y are positions of center of mass (CoM) in horizontal and vertical directions, respectively. $head_x$ is the position of the head in the horizontal direction. $midBoS_x$ is the center of the extended base of support which is defined as the convex area that contains the vertical projections of the two feet on the ground. t_f is the final time. The cost function J consists of several performance terms which are weighted by w_1, w_2, w_3 and w_4. The first term, representing muscle endurance, was the sum of muscle activation cubed. The second and third terms, representing the gait stability, were defined as the total difference between the CoM position and the center of the extended base of support, and the total difference between the head position and the center of the extended base of support. The fourth and fifth terms, representing CoM smoothness, are defined as third derivatives of CoM position in horizontal and vertical directions. The weights among different terms are chosen to be $[w_1,\ w_2,\ w_3,\ w_4]$ = [93.72, 21.03, 5.13, 41.03], which were optimized through an bilevel optimization approach to allow the predictive walking simulation results that closely replicate human gait (Nguyen, Johnson, et al. 2019) (Chapter 2).

The simulation of a full stride walking was generated. The walking speed was fixed at a typical speed of 1.3 m/s (Umberger and Martin 2007). The walking time t_f was allowed to vary in a reasonable range so that the model can choose different walking stride frequencies. The

direct collocation approach was used to solve the dynamic optimization problem (Eq. 4.1)(Ackermann and van den Bogert 2010)(Lee and Umberger 2016). The time axis was discretized to 51 nodes, and the Euler method was used to convert the differential dynamic equation (Eq. 4.1-b) into a set of equality constraints (Ackermann and van den Bogert 2010)(Wächter and Biegler 2006). The optimization problem was transformed to a non-linear programming problem that was latter solved with the IPOPT solver (Wächter 2003).

First, we simulated walking with the exoskeleton added on one ankle (right side) that could produce a maximum 2 Nm/kg torque ("Uni torque 2" simulation) (equivalent to about 150 Nm of peak torque) which is slightly higher than the actual device torque (120 Nm), but equal to the peak torque of a similar ankle device in the same study (Witte et al. 2015). To compare with the result in a similar experimental study, we generated a simulation where we limited the maximum assistive torque to 1 Nm/kg (Zhang et al. 2017) ("Uni torque 1"). We also simulated walking when the exoskeletons were worn on both ankles. Similarly, the maximum device torques were limited to 2 Nm/kg ("Bi torque 2") and 1 Nm/kg ("Bi torque 1"). In addition, a predictive walking simulation without the exoskeleton the was generated ("No Exo") for a baseline to evaluate the performance of the exoskeleton. The energetic walking cost reductions were calculated using an energy expenditure model as described in (Umberger et al. 2003).

4.3 Result

Figure 4.2 shows the predicted net energetic cost reductions in the cases of walking with the exoskeleton. The cost reductions with the exoskeleton worn on one leg were 16% and 45% for "Uni torque 1" and "Uni torque 2" cases, respectively (Figure 4.2). When both legs were augmented by the exoskeletons, the cost reductions were 21% and 52% for "Bi torque 1" and "Bi torque 2" cases, respectively.

The optimal assistive torques in all four cases have similar patterns (Figure 4.3). All have one small peak near the heel stride and one main peak. The main peak started from about 30% of

the gait cycle and lasts until about 65% of the gait cycle. The maximum peak torques were achieved at around 52% of the gait cycle. The rising time is longer than the falling time. In "Uni torque 2" and "Bi torque 2", although the maximum assistive torque can be 2 Nm/kg, the peak torques for the optimal solutions are less than the maximum (Figure 4.3).

In terms of gait kinematics, the ankle with the assistance increased the range of motion, especially the plantarflexion, compared to normal walking without the exoskeleton. In addition, there was greater knee flexion during the stance phase (Figure 4.4). In cases of walking with the device, the ground reaction forces (GRFs) in the horizontal direction (HGRF) of the assisted leg have higher peaks at the push-off phase (Figure 4.5).

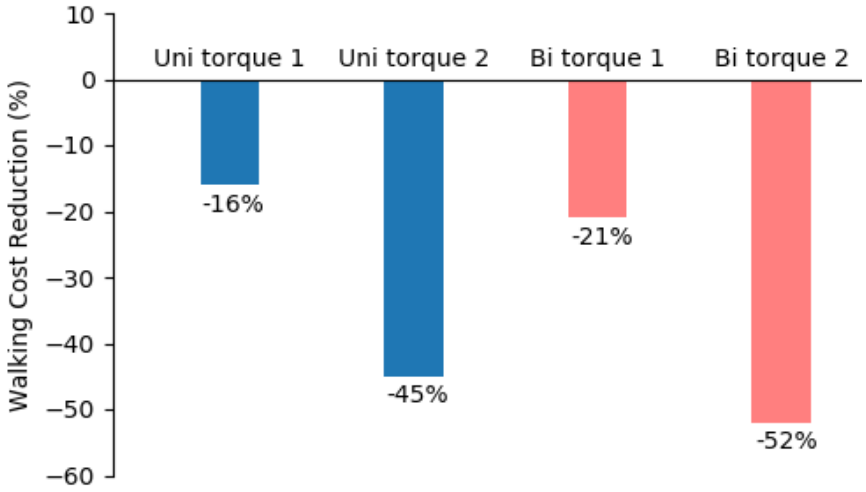

Figure 4.2: Predicted energetic cost reductions. In "Exo torque 1", the maximum torque the device can produce is limited to 1 Nm/kg. In "Exo torque 2", the maximum torque the device can produce is 2 Nm/kg. The walking costs were calculated using the model of energy expenditure described in (Umberger et al. 2003).

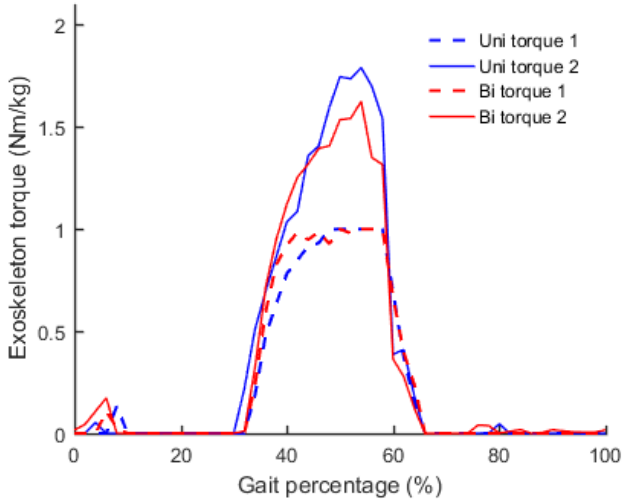

Figure 4.3: The predicted optimal exoskeleton torque as percentage of the gait cycle.

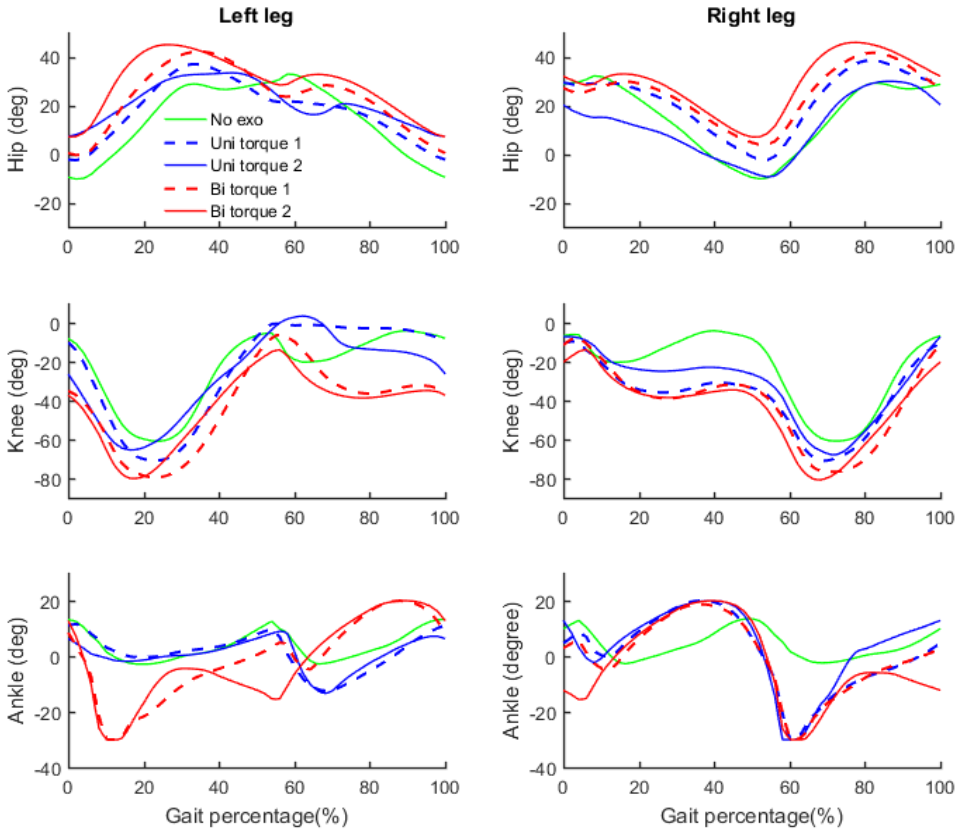

Figure 4.4: Gait kinematics with and without the ankle exoskeleton. The green lines represent the joint angles in normal walking without exoskeleton. The blue lines represent the joint angles in cases of "Uni torque 1" and "Uni torque 2" where the exoskeleton was worn on only the right leg. The red lines represent the joint angles in cases of "Bi torque 1" and "Bi torque 2" where the exoskeletons were worn on both legs. The ankles with the assistive devices increased the range of motions compared to walking without the device.

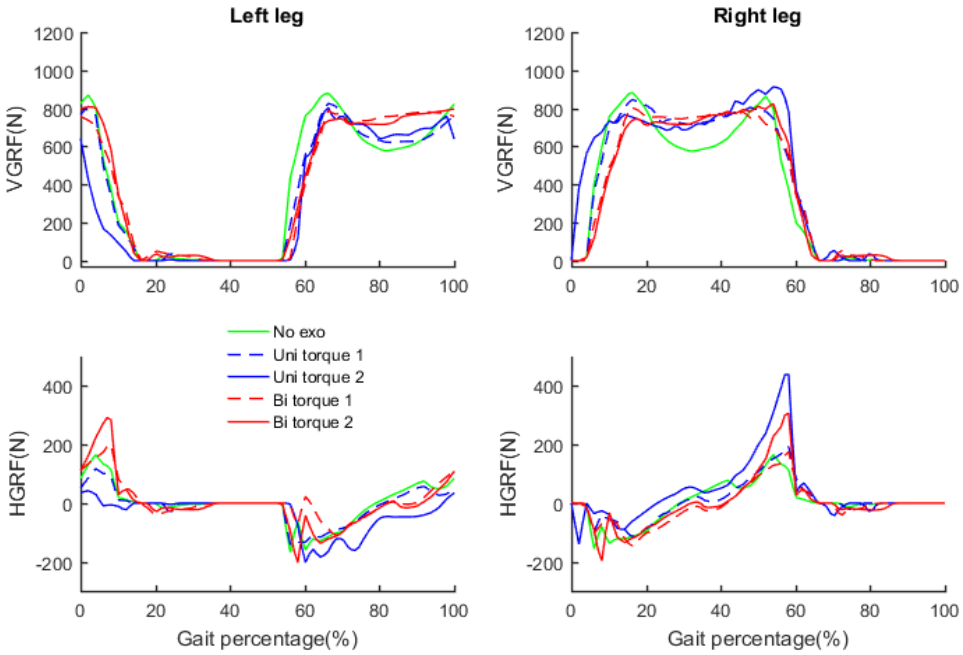

Figure 4.5: Predicted ground reaction forces in vertical direction (VGRF) and horizontal direction (HGRF) with and without wearing the exoskeleton. The green lines represent the GRFs in normal walking without exoskeleton. The blue lines represent the GRFs in cases of "Uni torque 1" and "Uni torque 2" where the exoskeleton was worn on only right leg. The red lines represent the GRFs in cases of "Bi torque 1" and "Bi torque 2" where the exoskeletons were worn on both legs. The HGRF peaks at push-off increased for the assisted leg.

4.4 Discussion

In this study, we simulated human walking augmented by a powered ankle exoskeleton using a predictive dynamic optimization approach. Different configurations of the exoskeleton were simulated to evaluate the performance of the device. Compared to normal walking without the device, walking exoskeleton assistance on one leg reduced energy cost by up to 45%, and walking with assistance on both legs reduced energy cost by up to 52%.

In the "Uni torque 1" case, the predicted net metabolic cost reduction of 16% is similar to the experimental result found in (Zhang et al. 2017) (average of 14 %), which had a similar set-up. The cost of walking in "Uni torque 2" reduced 45% compared to normal walking. This is due to more assistive torque being provided during late stance (Figure 4.3). Experimental study found

the ankles provide up to 46% of positive power in walking (Farris and Sawicki 2011b). In the case “Uni torque 2”, the assisted ankle produced significant push-off torque (Figure 4.3) that resulted in substantially high HGRF (Figure 4.5) compared to un-assisted ankle. The assisted ankle potentially contributed most of the total power produced by both ankles. Therefore, 45% cost reduction in this case may be possible. With the same torque limits, augmenting ankle torques for both legs further reduce the cost of walking. The reduction in “Bi torque 1” is 21% which is also comparable to 25% reduction found in (Zhang et al. 2017) for a single subject walking with bilateral ankle exoskeletons. In a similar experimental study, a reduction of 12% was found (Galle et al. 2017) with subjects having assistance on both legs. The lesser reduction in cost was likely due to smaller assistive torque magnitudes used in (Galle et al. 2017) (< 0.6 Nm/kg) than in our simulation.

The optimal torque patterns found in our simulations have two peaks (Figure 4.3). However, the first peak near heel strike is small and may be insignificant. The second peak pattern closely matches the experimental results (Zhang et al. 2017) in term of timing and shape. In our current study, the exoskeletal torque was allowed to choose any arbitrary patterns. The fact that the optimal torque patterns have one main peak (seen in Figure 4.3) suggests that the one peak pattern with four parameters chosen in (Zhang et al. 2017) may be sufficient to capture the optimal assistive torque. In the “Uni torque 2” and “Bi torque 2” cases, although the maximum torque allowed is 2 Nm/kg, the optimal magnitudes are smaller. This represents a limit as to how much assisting torque at the ankle is beneficial for reducing walking cost (Quesada, Caputo, and Collins 2016).

In all simulation cases of wearing the exoskeleton, the assisted ankle ranges of motions, especially plantarflexion increased (Figure 4.4), which was also found in some experimental studies (Galle et al. 2013)(Koller et al. 2015)(Quinlivan et al. 2017)(Galle et al. 2017). Potentially, increasing plantarflexion helps produce more forward acceleration with the external assistive torque at late stance phase, as seen in HGRF profiles (Figure 4.5). The ranges of assisted

ankle motions were close to the device limits of 30^0 plantarflexion to 20^0 dorsiflexion. This range of motion was set based on the actual exoskeleton design (Witte et al. 2015) and covers most of the range of ankle angle in human walking (Murray et al. 1984)(Umberger and Martin 2007) and human walking with assistive devices (Koller et al. 2015)(Quinlivan et al. 2017)(Panizzolo et al. 2016)(Gordon and Ferris 2007). However, a wider range of ankle plantarflexion in walking with an exoskeleton was also found in the literature (Galle et al. 2013)(Galle et al. 2017). Therefore, future simulation study may potentially expand this limited range of the ankle to further evaluate the performance of the device design.

Here, the exoskeleton was modeled as an ideal torque actuator that does not have internal dynamics and is capable of changing instantaneously torque magnitude. However, in the current study, the predicted assistive torques changed in a realistic manner (Figure 4.3), similar to experimental devices (Witte et al. 2015)(Zhang et al. 2017). In addition, the actual exoskeleton we based our model on is a light-weight, off-board actuated device with the capability of producing high torque and power, and relatively high bandwidths (> 17 Hz) (Witte et al. 2015). Therefore, the ideal torque actuator model may be sufficient to use in this study.

4.5 Conclusion

In this study, we simulated human walking augmented by the exoskeleton via dynamic optimization that is independent from the experimental data. The predicted optimal assistive torques and walking energetic cost reductions are similar to the experimental results obtained with the same device. This suggests the potential use of the predictive dynamic optimization approach for addressing problems of finding assistive device design and control.

CHAPTER 5

PERFORMANCE CRITERIA FOR PREDICTIVE OPTIMAL CONTROL SIMULATIONS OF AMPUTEE WALKING

This chapter addresses the question of the cost function in predictive simulation of amputee walking. Using similar approach presented in chapter 3, different cost function forms were examined for simulations of an unilateral transtibial amputee walking. The results showed the cost function based on muscle fatigue, gait smoothness, and gait stability led to the best gait result compared to cost functions only based on muscle performance criteria.

5.1 Introduction

Predictive simulation based on optimal control approach has been used for amputee gait simulations (Handford and Srinivasan 2016)(Handford and Srinivasan 2018). The results can potentially give valuable insights in assistive device design and control. However, one of the main challenges in formulating the predictive simulation amputee gait is that the walking cost function is generally unknown. Furthermore, with the part of the limb loss and biological changes from subject to subject, it may be challenging to determine the performance criteria in amputee walking. Studies often made assumptions about the cost function even though it is known that different cost functions can lead to different results (Ackermann and van den Bogert 2010)(Koelewijn et al. 2018). Therefore, in this study, we evaluate different cost function forms for predictive simulation of amputee gait.

It has been observed that walking metabolic cost per distance traveled (cost of transport) is minimized at the preferred walking speed in able-bodied (Ralston 1976). Therefore, studies often used the cost of transport as an performance criterion in the simulation of able-bodied walking (Anderson and Pandy 2001)(Brian R Umberger 2010)(Miller 2014)(Lin et al. 2018). Similarly, the cost of transport (CoT) in amputee walking was found to be minimal at the preferred walking speed (Gardiner et al. 2017)(Genin et al. 2008). Therefore, in amputee

simulations, prior studies also used minimizing the cost of transport in the cost function. For example, Fey et al. 2012 used minimizing metabolic cost and joint contact forces as criteria in the cost function in transtibial amputee walking simulation (Fey et al. 2012). (Handford and Srinivasan 2016) minimized both metabolic cost and prosthesis power cost in simulations of transtibial amputee walking on a powered prosthesis. (Esposito and Miller 2018) minimized metabolic cost in a tracking simulation of transtibial amputee walking. While minimizing metabolic cost was usually used in amputee walking simulation, it is unclear if other performance criteria should be used in the cost function.

Besides cost of transport, some other performance criteria were used in predictive able-bodied walking, such as minimizing sum of muscle activations or excitations (Kaplan and H. Heegaard 2001)(Van den Bogert et al. 2012)(Koelewijn and van den Bogert 2016)(Ackermann and van den Bogert 2010), sum of muscle stresses (Miller et al. 2011), minimizing joint contact forces (Fey et al. 2012), differences in velocity of the body center of mass (CoM) with targeted velocity (Dorn et al. 2015)(more details about performance criteria used in normal able-bodied walking was discussed in chapter 3). The cost functions based on these criteria have been used to generate the able-bodied walking. In chapter 3, adding gait smoothness and gait stability in the cost function resulted to better gait solutions in able-bodied. Therefore, using these performance criteria potentially may improve the amputee walking simulations.

In this chapter, we evaluate some potential cost function forms in the predictive simulation of unilateral transtibial amputee gaits. These cost functions are based on some performance criteria namely: muscle activation, muscle stress, cost of transport, gait smoothness, and gait stability. To evaluate the best combination of these criteria, a bilevel optimization approach was used to optimize the weights among different criteria in the cost functions. The qualities of the resulting gaits with these cost functions were quantified and compared.

5.2 Method

5.2.1 Transtibial amputee model

The unilateral transtibial amputee musculoskeletal model was adapted from the model in chapter 2 which was a planar musculoskeletal model implemented in OpenSim Ver 3.3 (Seth et al. 2011) (Figure 5.1) (Nguyen, Johnson, et al. 2019). The amputee model was fitted with a passive prosthesis (Laprè et al. 2014) on the amputated limb (right side). The model has 10 degrees of freedoms: three at the pelvis respective to the ground, one rotation for each hip and knee, one rotation for ankle of the intact limb (left side), one rotation for foot flexion of the prosthesis, and metatarsophalangeal joint for the intact limb. The lower limbs are driven by 15 muscle tendon units (nine on the intact limb, six on the amputated limb) which are represented with a Hill-type muscle model (Millard et al. 2013). The muscles on the intact limb are biarticular hamstring (HAM), biceps femoris short head (BFsh), gluteus maximus (GMAX), iliopsoas (IL), rectus femoris (RF), vasti (VAS), gastrocnemius (GAS), soleus (SOL), dorsiflexor (DOR) (included tibialis anterior, extensor hallucis longus, and extensor digitorum longus) (Figure 5.1). On the amputated side, three muscles (GAS, SOL, and DOR) were taken out. The connection between the socket and the residual limb was assumed to be rigid by setting high translational and rotational stiffnesses. The musculoskeletal model was scaled to the average height and mass of the three unilateral amputee subject data found in (LaPrè et al. 2018).

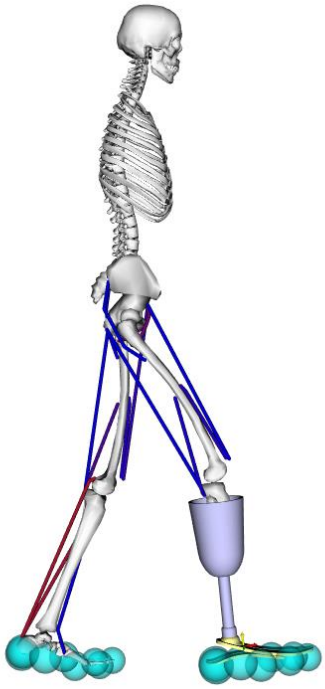

Figure 5.1: The transtibial amputee musculoskeletal model consists of 10 degrees of freedom. The amputated limb (right leg) was worn a passive prosthesis. The foot-ground contact was modeled by eight OpenSim HuntCrossleyContact spheres under each foot (Porsa et al. 2016). The model is actuated by 15 muscle tendon units which are represented with Hill-type muscle model (nine muscles on the intact limb and six muscles on the amputated limb).

5.2.2 Cost functions

To show the capability of the musculoskeletal model to perform walking simulation, a tracking cost function J_{AT} (Eq. 5.1) is used (Neptune et al. 2001)(Koelewijn and van den Bogert 2016). The tracking cost function consists of the fatigue term (sum of muscle activation cubed) and the tracking term (Eq. 5.1). The tracking term represents the error between the simulated gait and the human gait in term of kinematic and GRFs. The weight w_1 was chosen so that muscle fatigue term and the tracking term are closely equal.

$$
\begin{aligned}
&J_{AT} \\
&= \frac{1}{t_f}\sum_{i=1}^{m}\int_0^{t_f} a_i^3(t)dt \\
&+ w_1\frac{1}{t_f}\frac{1}{2}\int_0^{t_f}\left[\frac{1}{3}\left(\frac{\boldsymbol{x}_h - \widehat{\boldsymbol{x}}_h}{\widehat{SD}_h}\right)^2 + \frac{1}{3}\left(\frac{\boldsymbol{x}_k - \widehat{\boldsymbol{x}}_k}{\widehat{SD}_k}\right)^2 + \frac{1}{3}\left(\frac{\boldsymbol{x}_a - \widehat{\boldsymbol{x}}_a}{\widehat{SD}_a}\right)^2\right. \\
&\left.+ \frac{1}{2}\left(\frac{\boldsymbol{x}_{VGRF} - \widehat{\boldsymbol{x}}_{VGRF}}{\widehat{SD}_{VGRF}}\right)^2 + \frac{1}{2}\left(\frac{\boldsymbol{x}_{HGRF} - \widehat{\boldsymbol{x}}_{HGRF}}{\widehat{SD}_{HGRF}}\right)^2\right]dt
\end{aligned}
\tag{5.1}
$$

where a_i is muscle activation of the muscle i^{th} in total m muscles. $\widehat{\boldsymbol{x}}$ indicates the experimental means found in (LaPrè et al. 2018). $\widehat{SD}$ indicates standard deviation. The lower subscripts h, k, a, indicate variables for hip, knee, and ankle angles. $VGRF$, $HGRF$ indicate vertical GRF and horizontal GRF.

Five different performance-based cost functions that do not include the tracking term were examined. The first cost function was minimizing the cost of transport (Eq. 5.2) (Fey et al. 2012)(Handford and Srinivasan 2016).

$$J_{A1} = \frac{1}{M}\frac{\int_0^{t_f}\dot{E}_{total}dt}{X(t_f) - X(0)} \tag{5.2}$$

where M is the body weight, $\dot{E}_{total}$ is the rate of metabolic expenditure; $X(0)$ and $X(t_f)$ are the model horizontal positions at the beginning and final times, respectively. The muscle metabolic cost was calculated based on the energy expenditure model described in (Umberger et al. 2003).

The second and third performance-based cost functions were minimizing the total muscle fatigue (sum of muscle activations cubed) (Eq. 5.3) and muscle stress (Eq. 5.4), respectively.

$$J_{A2} = \frac{1}{t_f}\sum_{i=1}^{m}\int_0^{t_f} a_i^3(t)dt \tag{5.3}$$

$$J_{A3} = \frac{1}{t_f}\sum_{i=1}^{m}\int_0^{t_f}\left(\frac{F_i}{PCSA_i}\right)^3 dt \tag{5.4}$$

where F_i is the contraction force of muscle i^{th}, and $PCSA_i$ is the physiological cross-sectional area of muscle i^{th}.

Based on the results from chapter 3 about the performance criteria in able-bodied walking simulations, the cost function that includes muscle activation, gait smoothness, and stability was able to predict good able-bodied gait. Therefore, this cost function form will be evaluated in simulation of amputee walking (Eq. 5.5).

$$\begin{aligned} & J_{A4} \\ & = \frac{10}{t_f}\sum_{i=1}^{m}\int_0^{t_f} a_i^3(t)dt + w_1\frac{10^{-1}}{t_f}\int_0^{t_f}(CoM_x - midBoS_x)^2 dt \\ & + w_2\frac{10^{-1}}{t_f}\int_0^{t_f}(head_x - midBoS_x)^2 dt + w_3\frac{10^{-6}}{t_f}\int_0^{t_f}\left(\frac{d^3CoM_x}{dt^3}\right)^2 dt \\ & + w_4\frac{10^{-6}}{t_f}\int_0^{t_f}\left(\frac{d^3CoM_y}{dt^3}\right)^2 dt \end{aligned} \quad (5.5)$$

With the limb loss, the amputees potentially walked to minimize the load at the socket interface. Therefore, here we tested that hypothesis by adding the socket load criterion into the cost function (Eq. 5.6).

$$J_{A5} = \frac{10}{t_f}\sum_{i=1}^{m}\int_0^{t_f} a_i^3(t)dt + w_1\frac{10^{-5}}{t_f}\int_0^{t_f} F_{pis}^2 dt + w_2\frac{10^{-2}}{t_f}\int_0^{t_f} T_{fle}^2 dt \quad (5.6)$$

where F_{pis} represents the vertical pistoning force at the socket, T_{fle} represents the flexion moment at the socket.

5.2.3 Predictive dynamic optimization

The predictive dynamic optimization is described in detail in chapter 3 (Eq. 3.1). Here, the full stride cycle is generated with a 31-node grid. The walking speed was fixed at 1.25 m/s. The final time was allowed to change in a reasonable range so that the model can choose different stride frequencies. With the cost functions that contains the weighting term $\boldsymbol{w}$, the weights are optimized through the bilevel optimization approach as presented in chapter 2. The evaluation of the simulated gaits was done by evaluating the kinematic and GRF errors (Eq. 3.18), CoT, stride frequency, and muscle activation, which is similar as the evaluation process described in chapter 3 for the able-bodied simulations.

5.3 Results

All cost functions were able to generate human-like gait solutions (Figure 5.2)(Figure 5.3). However, the gait qualities were different in term of kinematic and GRF errors (Figure 5.6) (Table S-4 in the appendix C). The tracking cost function J_{AT} has the smallest errors (under 1 SD). The best results using performance-based cost functions is with J_{A4} with the kinematics and GRFs errors of 1.86 SD and 1.27 SD, respectively. The hip angles for most of the performance-based cost functions are higher than the experimental means (Figure 5.2). The knee at prosthetic side flexed more during the stance phase. The VGRFs at heel stride are considerably high with $J_{A1}, J_{A2}, J_{A3}, J_{A5}$.

Over the gait cycle, most of the cost functions predicted consistent patterns of intact GAS, SOL, and DOR, and amputated side HAM, IL. Some muscles such as prosthetic side RF and VAS did not activate or activated relatively less compared to other muscles (Figure 5.5). J_{A1} predicted almost no activation in BFsh, RF, VAS (intact side), and BFsh, GMAX, VAS (prosthetic side) (Figure 5.4). J_{A1} predicted lowest CoT (2.162 J/kg/m) (Figure 5.7). Tracking cost function J_{AT} predicted the highest CoT (3.515 J/kg/m), and the lowest stride frequency (0.77 sec) (Figure 5.7).

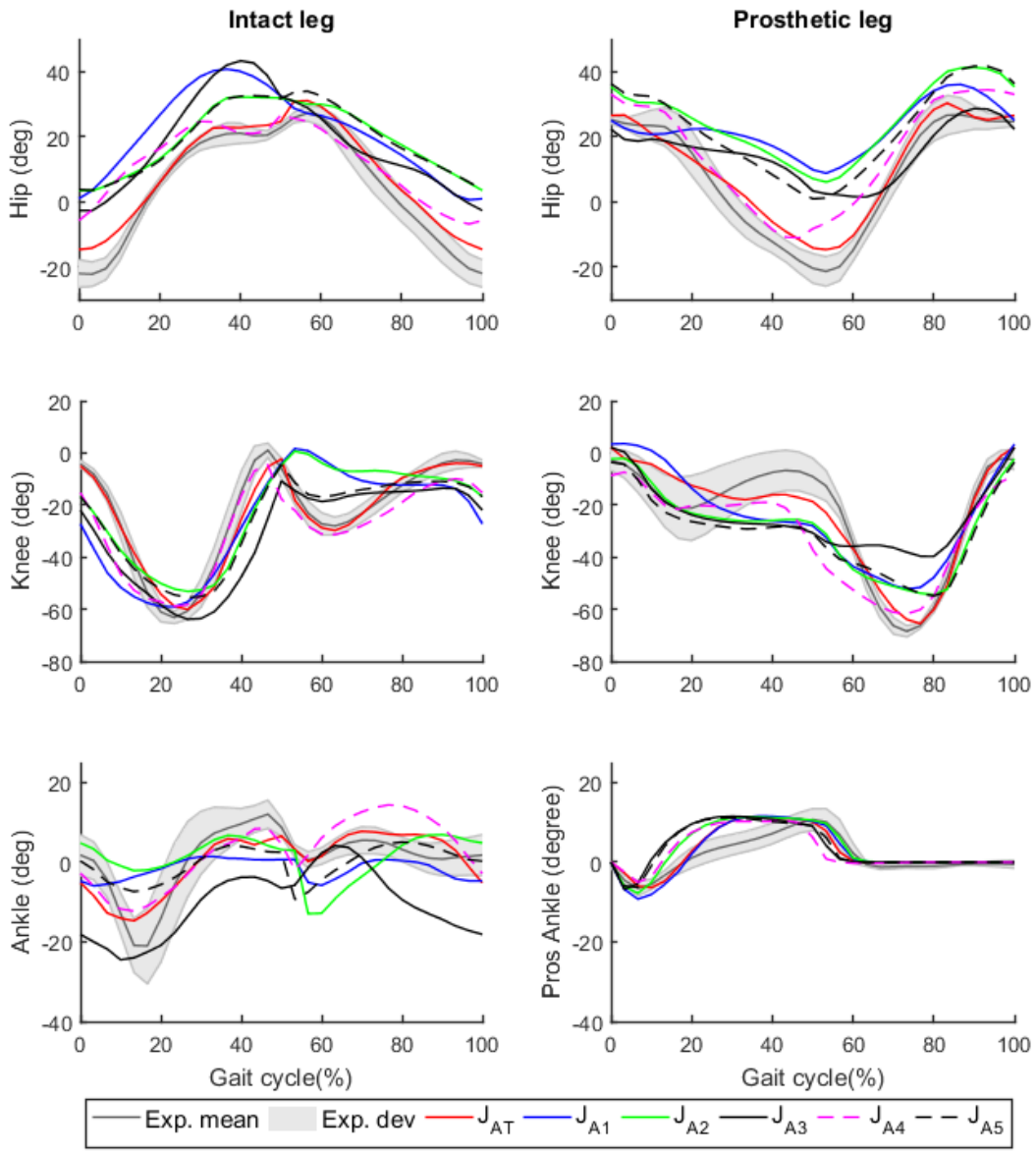

Figure 5.2: Gait kinematics with different cost functions. All cost functions was able to produce human-like kinematic gaits.

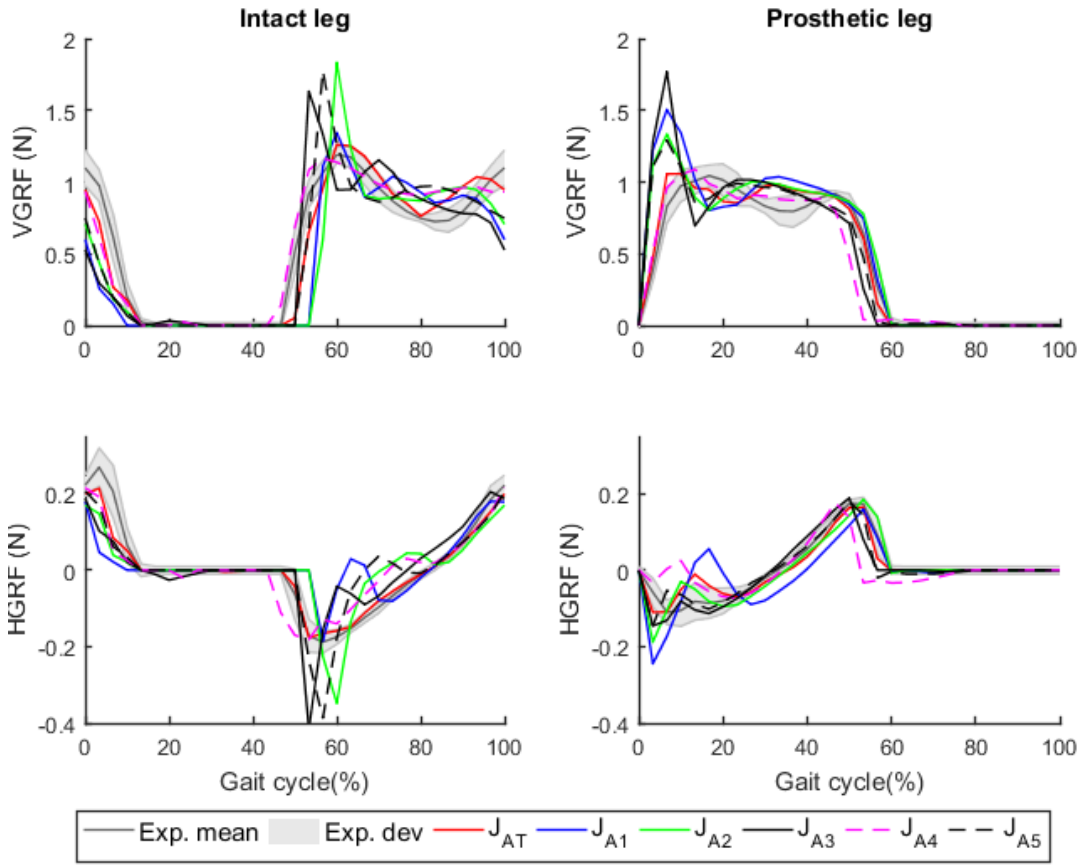

Figure 5.3: GRFs with different cost functions.

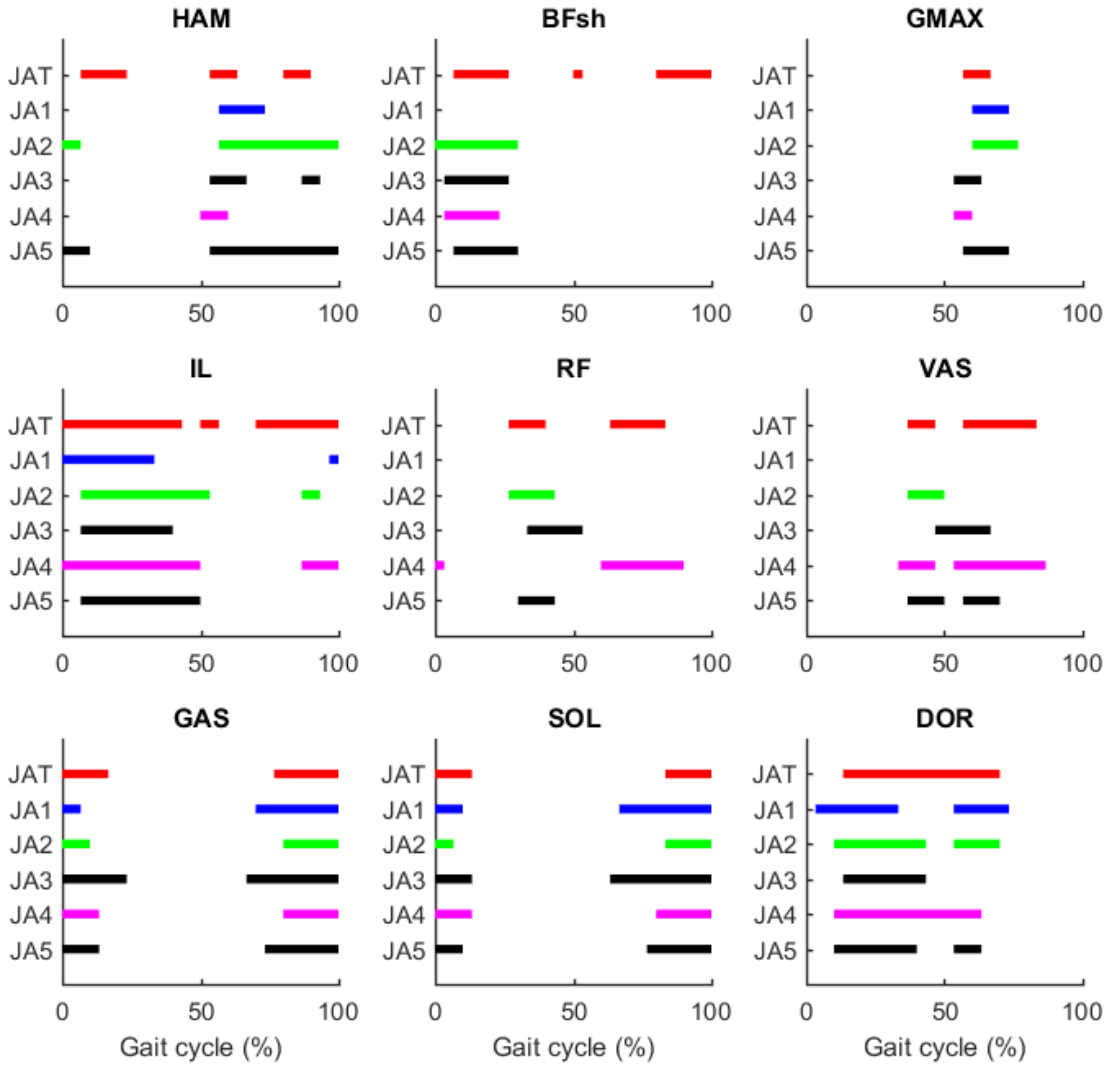

Figure 5.4: Muscle activation on-off timings for the intact limb with different cost functions.

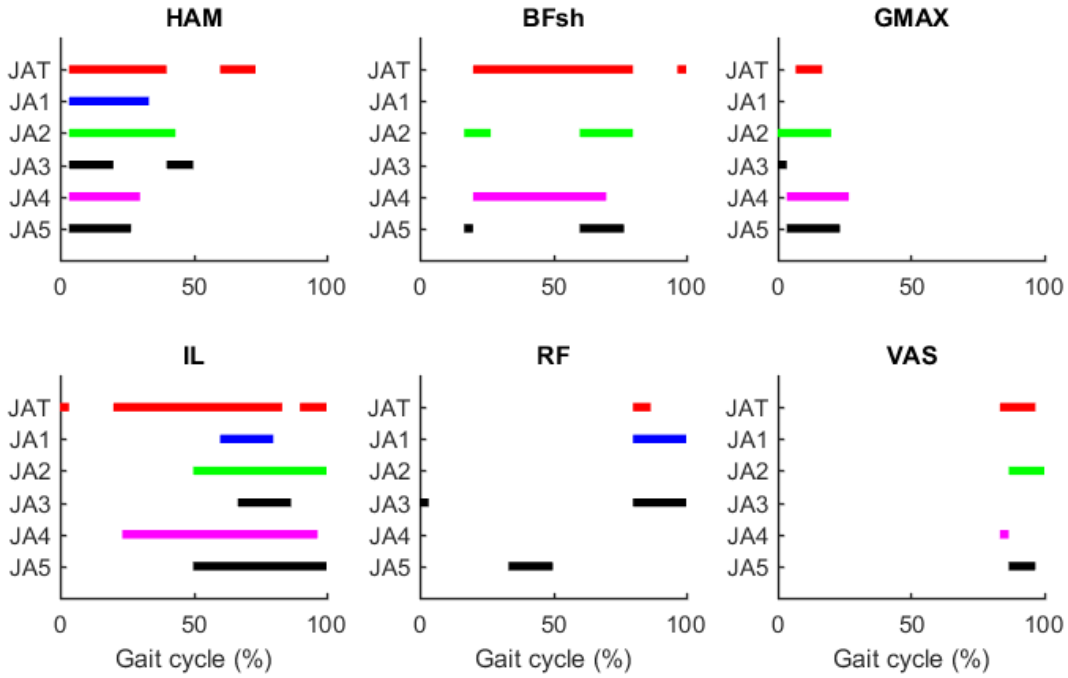

Figure 5.5: Muscle activation on-off timings for the prosthetic limb with different cost functions.

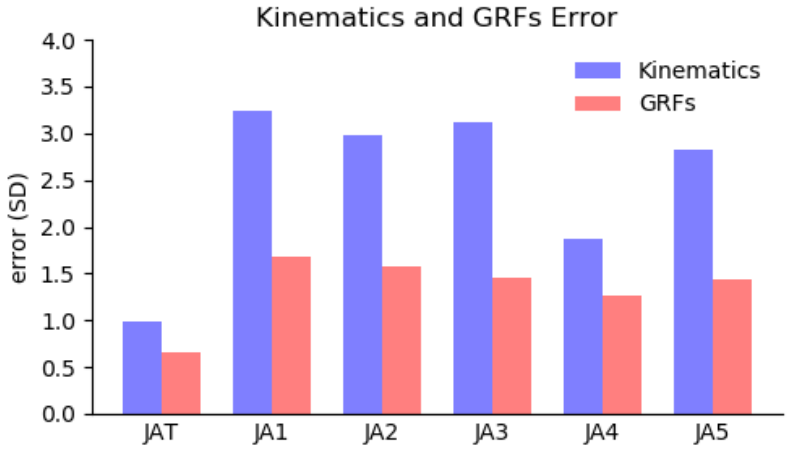

Figure 5.6: Gait kinematics and GRFs errors with different cost functions. The errors were calculated based on the absolute error which was then normalized to the SD (Eq. 3.18)

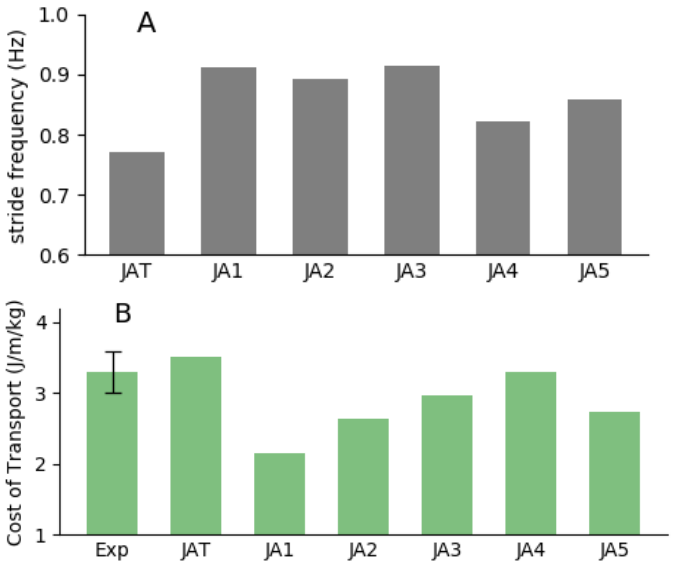

Figure 5.7: Cost of transports and stride frequencies with different cost functions. The experimental CoT with 1 SD mean bar were based on the data in (Esposito et al. 2014)

5.4 Discussion

In this chapter, we have examined different cost functions for optimal control of amputee gait. The tracking cost function resulted in good walking solution with both kinematics and kinetics within 1 SD of experimental means. This demonstrates the musculoskeletal model is capable of producing reasonable walking solutions. All performance-based cost functions were able to generate human-like gait solutions. However, the qualities of the gait solutions in comparison to human gait among these cost functions were different.

Minimizing muscle activation (J_{A2}) produced slightly better kinematics and kinetics compared to minimizing metabolic cost (J_{A1}) and minimizing muscle stresses (J_{A3}) (Figure 5.6). These results are similar in the case of able-bodied simulations of walking (Chapter 3) and running (Miller et al. 2011). As expected, minimizing metabolic cost (J_{A1}) led to the lowest CoT (2.162 J/m/kg)(appendix C) in all performance-based cost functions. Using J_{A1}, BFsh, RF, VAS on the intact side, BFsh, GMAX, VAS on the prosthetic side did not activate. These results are not in good agreement with the measured EMG in amputee walking (Fey et al. 2012)(Huang and Ferris 2012) where most of the muscle found to be activated over the gait cycle.

Adding the socket load into the cost function (J_{A5}) did not improve much the gait in term of kinematic and kinetics compared to just using minimizing muscle activation (J_{A2}). In addition, the muscle activation patterns in J_{A5} and J_{A2} are relatively similar (Figure 5.5). This result suggests that it may be unlikely the amputees walked to minimize socket load. However, it is also possible that we have not accurately captured the load in the way the represents what amputees try to minimize, such as peak pressure on a specific part of the resisual limb instead of overall load during the gait cycle as in this chapter.

The cost function J_{A4}, which includes muscle activation term, gait smoothness, and stability was able to significantly improve the gait solution (Figure 5.2)(Figure 5.3)(Figure 5.6). The GRF peak at the heel stride was lower and smoother compared to other performance-based cost functions, and was closer to the experimental mean. The GRFs may correlate to jerk cost for CoM during walking as described in chapter 3. Therefore, the smoother GRFs pattern may be due to the penalty of jerk cost in J_{A4}. Penalizing the jerk cost may give smooth GRFs (chapter 3); however, it also requires more walking energy cost. As a result, the CoT with J_{A4} (3.3 J/kg/m) was higher compared to other performance-based cost functions. However, the CoT with J_{A4} is within the SD of experimental data found in the literature (3.0 – 3.6 J/kg/m, (Esposito et al. 2014)).

In this chapter, the walking solutions are not as close to the experimental data as able-bodied walking solutions in chapter 3. For example, the tracking amputee solution has the errors under 1 SD, while the able-bodied tracking solution has the errors under 0.5 SD. Also, the best performance-based cost function yielded solutions within 1 SD for able-bodied (Figure 3.2), where the best performance-based amputee solution was 1.5 SD (Figure 5.6). There are some factors may account for these. First, the prosthesis model may not represent accurately the dynamic of the actual prostheses. The prosthesis model was modeled with a revolute joint which represents the “ankle” joint. However, the actual prostheses, rather than having a joint, allow

bending with flexible material over the foot. Therefore, future studies may consider model the prostheses with multiple stiffness points over the foot, as seen in (Fey et al. 2012). Second, the residual limb – socket interface in this study was assumed to be rigid. On the other hand, experimental studies showed some pistoning and flexion movements of the residual limb within the socket during walking (LaPrè et al. 2018)(Sanders et al. 2006)(Eshraghi et al. 2012). Modeling the residual limb – socket interface, however, is challenging because of the patient specific residual limb structure, highly non-linear bone and soft tissue, and a lack of a technology to quantify residual limb movement within the prosthetic socket over the gait cycle. For the last issue, there are some recent attempts to develop devices for measuring the bone movement within the socket (Laprè et al. 2017) which may be promising to use for modeling the residual limb-socket interface.

5.5 Conclusion

In this study, we have evaluated different cost function forms for simulation of amputee walking. The results showed that using cost functions with muscle fatigue, gait smoothness, and gait stability resulted in better gait solution compared to typical cost functions in the literature which were only based on muscle-based performance criteria. Future studies simulating amputee walking may consider this cost function form for formulating the optimization problem.

CHAPTER 6

INCLUSION OF ACTUATOR DYNAMICS IN SIMULATIONS OF ASSISTED HUMAN MOVEMENT

This chapter is adapted from a paper with the same title, which is submitted to the International Journal for Numerical Methods in Biomedical Engineering.

Simulation of musculoskeletal systems using dynamic optimization is a powerful approach for studying the biomechanics of human movements and can be applied to human-robot interactions. The simulation results of human movements augmented by robotic devices may be used to evaluate and optimize the device design and controller. However, simulations are limited by the accuracy of the models which are usually simplified for computation efficiency. Typically, the powered robotic devices are often modeled as massless, ideal torque actuators that is without mass and internal dynamics, which may have significant impacts on the simulation results. This chapter investigates the effects of including the mass and internal dynamics of the device in simulations of assisted human movement. The device actuator was modeled in various ways with different detail levels. Dynamic optimization was used to find the muscle activations and actuator commands in motion tracking and predictive simulations. The results showed that the effects of device mass and inertia can be small. However, the electrical dynamics of the motor can significantly impact the results. This outcome suggests the importance of using an accurate actuator model in simulations of human movement augmented by assistive devices.

6.1 Introduction

Simulation of musculoskeletal systems using dynamic optimization is a powerful approach for studying the biomechanics of human movements. Recently, it has been used to simulate human-robot interactions (Handford and Srinivasan 2016)(Uchida et al. 2016). The simulation results of human movements augmented by robotic devices may be used to evaluate and optimize device designs and controllers (Zhou, Li, and Bai 2017). However, simulations are

limited by the accuracy of the models which are usually simplified for computation efficiency. Often, the robotic actuators are modeled as massless and ideal force or torque inputs which means the mass and the internal dynamics (e.g., electromechanical dynamics of the electrical motor) of the devices are excluded. This oversimplification may potentially lead to errors in the results and incorrectly guide the design process. Therefore, adding the actuator mass and dynamics may increase the accuracy of the simulation results, which could facilitate the design and evaluation process with a stronger correlation between simulation and the physical device.

A common approach used to simulate human movements is forward dynamics. Given the control inputs such as muscle excitations or actuator commands, forward dynamics calculates the resulting motion of the system through forward integration of the dynamic model (Lee and Umberger 2016)(Mansouri and Reinbolt 2012)(Sartori et al. 2012). A major challenge of forward dynamics is that the control inputs are usually unknown. Since many of the joints in the human musculoskeletal system are actuated by redundant sets of muscles, optimization is often used to estimate the actual muscle excitation patterns. Optimization has been extensively used to study human movement (Anderson and Pandy 2001)(Ackermann and van den Bogert 2010)(Xiang et al. 2011)(Fey et al. 2012). More recently, optimization has been applied to simulate human movement augmented by powered assistive devices (Handford and Srinivasan 2016)(Uchida et al. 2016). Design of assistive devices and associated controllers may be possible through simulation of the combined human-device system, leveraging optimization to solve for the coupled system dynamics.

Many of these simulation studies have modeled actuators of assistive devices acting on the human body as ideal, massless, generalized torques that can produce unrealistically large torques capable of changing magnitude instantaneously, potentially impacting the accuracy of the simulation results. For example, Handford & Srinivasan, (2016) simulated the gait of persons with an amputation using a powered prosthesis modeled as an ideal, massless torque ankle

actuator (Handford and Srinivasan 2016). The group used dynamic optimization to find the muscle and powered prosthesis controls required to minimize both the person's and prosthesis' energetic costs. The simulation results showed that optimal assistance from a prosthesis could reduce the human's metabolic cost by more than 70% below that of an able-bodied human's walking. To date, an experimental study found that a powered foot-ankle prosthesis was not able to reduce the metabolic cost below non-amputee levels (Herr and Grabowski 2012). A similar experimental result was found in (Quesada et al. 2016), where an experimental powered foot-ankle prosthesis emulator was not capable of approaching the metabolic cost of a person without amputation, despite being able to achieve higher than normal anatomical levels of ankle work. Although many elements likely contributed to differences between modeled and observed results, one cause may be that the device in the Handford & Srinivasan (2016) study produced large ankle torque impulses during late stance where most current prostheses are not capable of such high torques (Herr and Grabowski 2012)(Lawson et al. 2014). Uchida et al. (2016) used the OpenSim (Delp et al. 2007) computed muscle control algorithm (Thelen et al. 2003) to simulate human running with an assistive device modeled as ideal, massless torque actuator. The simulations found up to a 30% reduction in metabolic cost (Uchida et al. 2016). This reduction far exceeded the results reported in the accompanying experimental studies that found only 8 - 10% reductions (Sugar et al. 2015) or even increases in metabolic cost (Cherry et al. 2016). Higher actual energy expenditure could have been caused by assistive device dynamics being excluded in silico.

In general, using simplified torque actuators that is lack of mass and dynamics, and capable of producing instantaneous torque proportional to a reference control input, can potentially affect simulation results. This chapter investigates the effects of including the electromechanical dynamics of a DC motor and transmission in simulations of power-assisted upper limb movements. Here, we use a simple arm model coupled with an powered exoskeleton as shown in Figure 6.1 for demonstrations. The methods section details the dynamic optimization

process used to find the optimal muscle and assistive device state and control. The results present data from a case study implementing the detailed actuator model, and the discussion highlights the effects including actuator dynamics on the simulation.

6.2 Method

The dynamics of a DC motor actuator was included in the simulations of an upper limb exoskeleton augmenting the elbow joint. The upper limb musculoskeletal model is based on the OpenSim (Seth et al. 2011) simplified upper limb model 'Arm26'. This arm model has two joints (shoulder and elbow joints) and six muscles based on Hill-type muscle model described by Thelen (Thelen 2003). These muscles are Triceps long head (TRIlong), Triceps lateral head (TRIlat), Triceps medial head (TRImed), Biceps long head (BIClong), Biceps short head (BICshort), and Brachialis (BRA). An object with a mass of 1.0 kg was added to the hand (NA model). A powered assistive device was added at the elbow of the NA model to produce an assistive torque about the elbow joint. In this chapter, the assistive device is modeled in three ways (Figure 6.1). First, the device is modeled as a massless, ideal torque (IT model). That means the mass of the device is ignored and the device can change the output torque magnitude instantaneously. The IT model is commonly used in the literature (Handford and Srinivasan 2016)(Uchida et al. 2016)(Ong, Hicks, and Delp 2015). Second, the device is modeled as an ideal torque with mass (ITM model). Third, the dynamics of a DC motor with a gearbox and the mass of the actuator are included (DCM model). The mass of the assistive device, DC motor, gearbox, and linkages are shown in Table 6.1. The mass of ITM model is set to be equal to DCM, 300 g (as shown in Table 6.1).

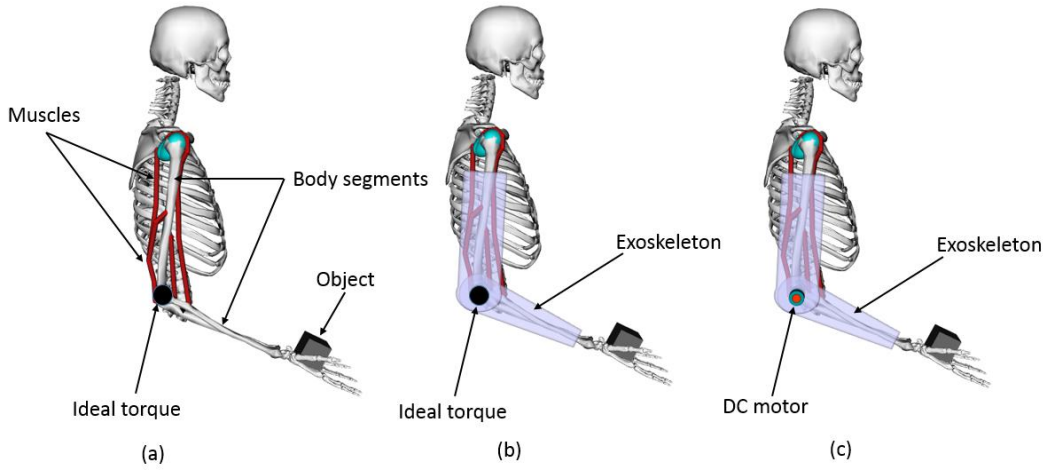

Figure 6.1. The 'Arm26' OpenSim model is shown with different assistive device models. (a) Massless ideal torque (IT): the assistive device was modeled as an ideal torque without mass and internal dynamics; (b) Ideal torque with mass added (ITM): the assistive device was modeled as an ideal torque and the mass of the device was added to the arm, (c) DC motor actuator (DCM): the assistive device was modeled as a DC motor with gear box and the mass of the device was included.

Variables	DC motor 15W model	DC motor 30W model	DC motor 70W model	Unit
Nominal voltage (*V*)	48	36	48	V
Stall torque	84.1	369	915	mNm
Resistance (*R*)	53	6.89	6.89	Ω
Inductance (*L*)	27.8	4.29	5.85	mH
Torque constant (*K*)	92.8	70.6	131	mNm/A
Rotor inertia	35	93	181	gcm^2
Motor mass	46	75	141	g
Assistive device mass	271	300	366	g
Gear box ratio	1:59.45	1:13.57	1:5.46	
Viscous friction coefficient (*b*)	3.68e-6	7.84e-6	17.50e-6	Nms

Table 6.1: DC motor arm model parameters. The parameters of the DC motors are based on the actual parameters found in the datasheet. The viscous friction coefficients are estimated based on the no-load condition. The gear box ratios are chosen so that the devices can provide 5Nm torque output. The total assistive device includes the motor and other components such as gear box and supporting bars.

6.2.1 DC motor model

The DCM model included a DC motor that is governed by the following equations (Electro-Craft Corporation 1977).

$$L\frac{di}{dt} = V - K\frac{d\theta}{dt} - Ri \tag{6.1}$$

$$T = Ki \tag{6.2}$$

$$T_{load} = T - J_m\frac{d^2\theta}{dt^2} - b\frac{d\theta}{dt} \tag{6.3}$$

The electrical terms are the voltage input (V), current (i), inductance (L), and resistance (R). The mechanical terms are the rotor moment of inertia (J_m), coefficient of viscous friction of the motor (b), motor torque constant (K), rotor angle (θ), motor output torque (T), and load torque (T_{load}). The inputs of the model are voltage and initial states of current and rotor angle. The output of the model is the resultant torque, T. The model parameters can be specified to match a DC motor being used in a design, or be optimized to help choose a suitable DC motor actuator for an application.

The DC motor actuator is implemented in OpenSim 3.3 as a plug-in. The electrical dynamics of the DC motor as described in (Eq. 6.1) and (Eq. 6.2) are implemented directly in a new DC motor class derived from the parent actuator class of OpenSim (Seth et al. 2011). The mechanical dynamics of the motor are described in (Eq. 6.3), which accounts for the stator and rotor of the DC motor as separate body segments in the OpenSim model. The mass and inertia are defined for these bodies along with electrical parameters when creating the model. The DC motor model can be used within the OpenSim GUI or the MATLAB/Python scripting interface by importing the class into the system (Anon 2018).

The DC motor parameters used in this study are based on a 30 W brushless DC motor (EC 45-Flat, Maxon Motors, Sachseln, Switzerland) because Maxon DC motors have been used in some assistive devices (Cempini, Hargrove, and Lenzi 2017)(LaPre, Umberger, and Sup IV 2016). The parameters of the motor based on (Anon 2019) is shown in Table 6.1. This motor has

a nominal voltage of 36 V and a stall torque of 0.369 Nm. The motor is connected to a gearbox with a gear ratio of 1:13.57. This motor gearbox combination allows the assistive device to produce 5 Nm in the stalled condition. As a result, the models with ideal torque actuators are limited to a maximum output torque of 5 Nm.

6.2.2 Simulation configurations

The simulations were done using a dynamic optimization approach (Anderson and Pandy 2001)(Ackermann and van den Bogert 2010). The dynamic optimization is a powerful approach that can be used to formulate predictive simulations, and has been used extensively to simulate human movements (Anderson and Pandy 2001)(Ackermann and van den Bogert 2010)(Porsa et al. 2016)(Gidley et al. 2019)(Nguyen, Johnson, et al. 2019). The dynamic optimization problem used in this work is constructed as: searching for a state vector $\boldsymbol{x}(t)$ and a control vector $\boldsymbol{u}(t)$ that minimize the objective function (Eq. 6.4-a), which is subjected to constraints of the dynamic equation of the system (Eq. 6.4-b) and is bound to constraints on the states and controls, (Eq. 6.4-c) and (Eq. 6.4-d), and any additional problem-specific task constraints such as final or initial states (Davy and Audu 1987)(Lee and Umberger 2016). The state $\boldsymbol{x}$ consists of joint positions, joint velocities, muscle lengths and activations, and DC motor current in the case of the DCM simulations. The control $\boldsymbol{u}$ consists of muscle excitations and ideal torque control input with ITM and IT models, and DC motor voltage with DCM model. The form of the objective function (Eq. 6.4-a), dictates whether the problem is either motion tracking or a predictive simulation.

$$\min_{\boldsymbol{x},\boldsymbol{u}} J(\boldsymbol{x},\boldsymbol{u},t) \tag{6.4-a}$$

$$\text{Subject to: } \dot{\boldsymbol{x}} = f(\boldsymbol{x},\boldsymbol{u},t) \tag{6.4-b}$$

$$\boldsymbol{x}_{lb} \leq \boldsymbol{x} \leq \boldsymbol{x}_{ub} \tag{6.4-c}$$

$$\boldsymbol{u}_{lb} \leq \boldsymbol{u} \leq \boldsymbol{u}_{ub} \tag{6.4-d}$$

where $\boldsymbol{x}_{lb}$ and $\boldsymbol{x}_{ub}$ represent the lower bound and upper bound of the state. These bounds are defined based on the biological limits. Similarly, $\boldsymbol{u}_{lb}$ and $\boldsymbol{u}_{ub}$ represent the lower bound and

upper bound of the control. The muscle excitations are normalized to the same range of [0, 1]. The controls of the actuator are normalized to the same range of [-1, 1].

6.2.3 Motion tracking

In the motion tracking problem, the objective function minimizes a sum of the squared muscle activations (muscle effort term) and the squared errors in desired motion over time (tracking term). The desired motion was created synthetically.

$$J = \frac{1}{m}\sum_{i=1}^{m}\int_{t_0}^{t_f} a_i^2 dt + \frac{1}{C}\sum_{k=1}^{C}\int_{t_0}^{t_f} e_k^2 dt \tag{6.5}$$

In Eq. 6.5, m is the number of muscles, a_i is muscle activation of the i^{th} muscle, C is the number of tracked coordinates, and e_k is the tracking error of k^{th} coordinate (elbow and shoulder angles (rad)). In this study, sagittal plane shoulder and elbow joint positions are tracked ($C = 2$). The assistive device power is not optimized.

6.2.4 Predictive simulation

In the predictive simulation, the problem is defined as finding the muscle excitations and assistive device control to drive the arm from an initial position with initial joint velocities equal to zero, to a final position without constraints on the motion path or final joint velocities, and minimize an objective function. In this study, the objective is minimizing the sum of squared muscle activations over time (Eq. 6.6). The requirements of initial and final joint angles and the initial joint velocities were imposed as the constraints.

$$J = \sum_{i=1}^{m}\int_{t_0}^{t_f} a_i^2 dt \tag{6.6}$$

Both motion-tracking and predictive problems are solved with the direct collocation method (Kaplan and H. Heegaard 2001) which has been used in biomechanics research because of its advantage in speed over traditional direct shooting methods (Lee and Umberger

2016)(Porsa et al. 2016)(Ackermann and van den Bogert 2010). In the direct collocation method, all state and control variables are parameterized. The original optimization problem is transformed into a non-linear dynamic programming problem and then solved by an optimization solver. In this study, the time duration for the motion (0.5 s) is discretized into 50 nodes. An open-source optimization solver – IPOPT (Wächter and Biegler 2006) – is used for solving the non-linear dynamic programming problem, and is implemented in OpenSim through the MATLAB interface (Lee and Umberger 2016). The simulations with different actuator models were evaluated by comparing the assistive torque, muscle activations and kinematics (joint positions and velocities).

6.3 Results

6.3.1 Motion tracking

The results of the motion tracking simulations using three models of assistive elbow devices (IT, ITM, DCM) and one model without an assistive device (NA) are presented in Figure 6.2 - Figure 6.4. All four models were able to track the reference kinematic motion data with the root-mean-squared error (RMS) lower than 0.5 degrees for IT, ITM and DCM, and lower than one degree for NA (Figure 6.2). The peaks of muscle activations in all three cases using an assistive device were lower than without using an assistive device (Figure 6.3). The average muscle activations are 13.3%, 3.3%, 3.5% and 5.9% in NA, IT, ITM, and DCM, respectively (100% indicates full activation over the time period). The IT and ITM models had similar results of muscle activations and torque outputs (Figure 6.3 and Figure 6.4). However, the DCM model resulted in different muscle activation patterns. Greater activations of elbow flexor muscles (BIClong, BRA) were observed at the start (0 to 0.15 seconds), and greater activations of elbow extensor muscles (TRIlat, TRImed) were observed in the latter half of the simulation (from 0.25 – 0.50 seconds) compared to the other augmented models (Figure 6.3). All three assistive models had similar actuator control inputs (Figure 6.4A). The torque output of the two ideal torque

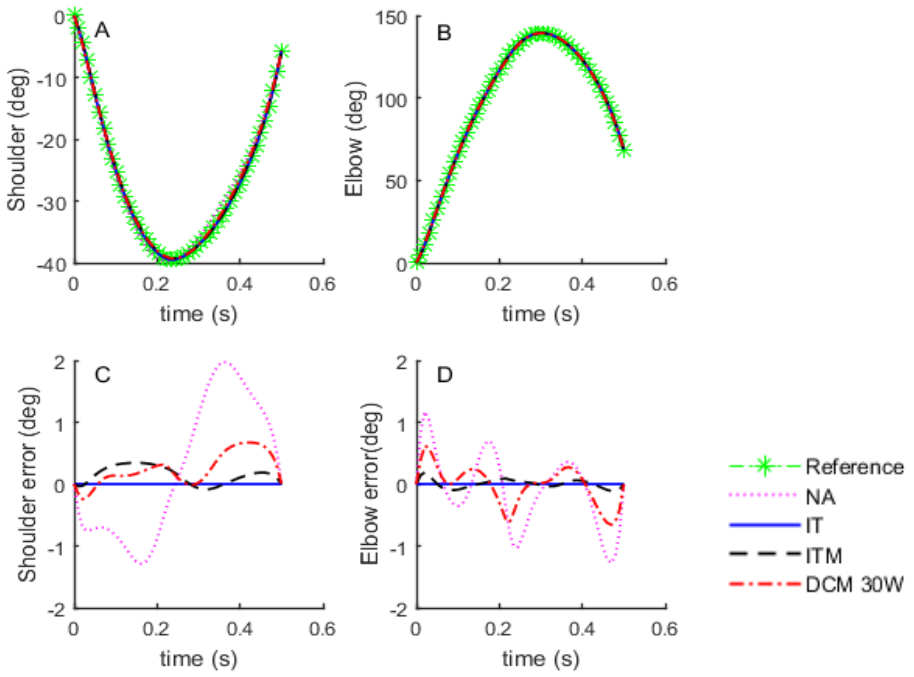

Figure 6.2: Kinematic data from data tracking is shown for each arm model (NA – without assistive device, IT – ideal torque without mass, ITM – ideal torque with mass included, DCM – developed DC motor model and gear box). All models were able to track the reference motion with RMS < 0.5 degrees with IT, ITM, and DCM, and < 1 degree with NA.

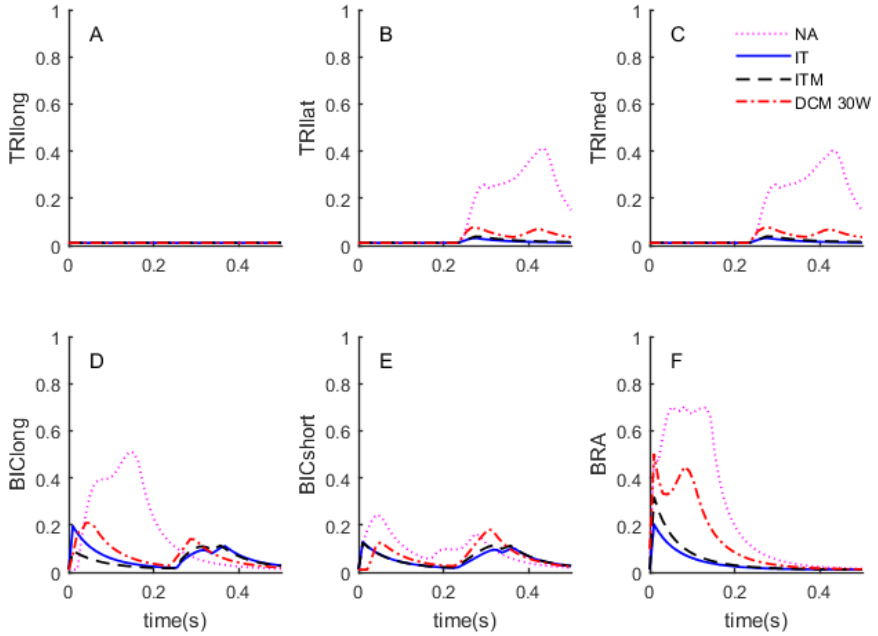

Figure 6.3: Muscle activations of data tracking simulations (NA – without assistive device, IT – ideal torque without mass, ITM – ideal torque with mass, and DCM – developed DC motor model with gear box). Three models with assistive devices had lower peak and average muscle activations on compared to the NA model. DCM activated more elbow flexor muscles (BIClong, BRA) at the beginning (0 to 0.15 seconds), and more elbow extensor muscles at the end of simulation period (0.25 – 0.5 seconds).

produced by the DCM model was less than the other two assistive models during the first half of the simulation (0 - 0.23 s) (average of 3.71 Nm in DCM, 5 Nm in IT and ITM), and towards the end of the simulation (0.35 – 0.50 s) (average of 3.90 Nm in DCM, 5 Nm in IT and ITM) even though the control inputs were nearly the same (Figure 6.4B).

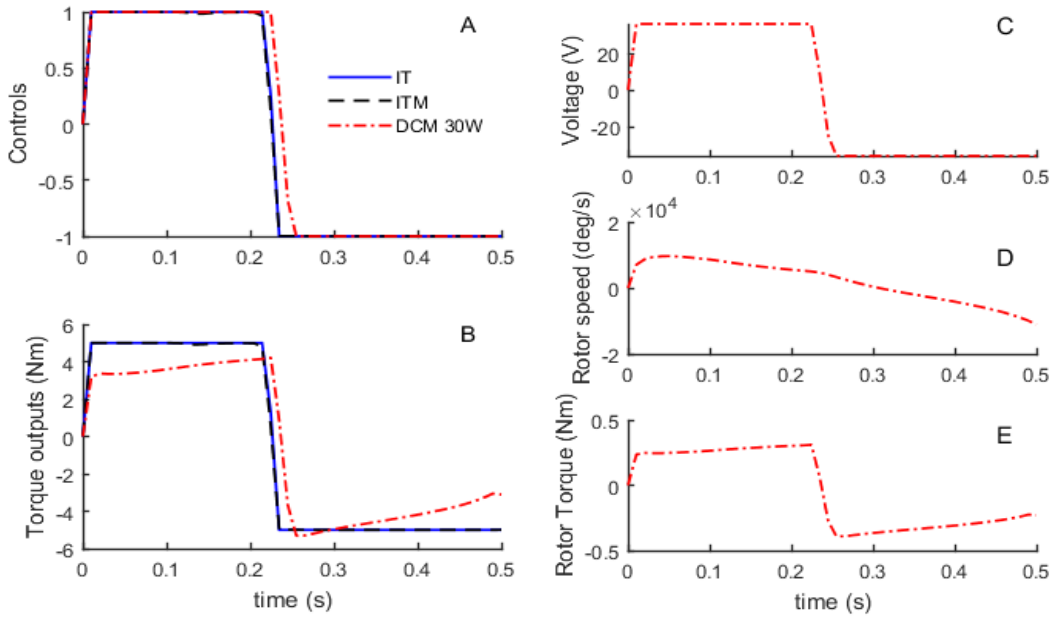

Figure 6.4: A, B - controls and torque outputs of assistive devices (IT – ideal torque without mass, ITM – ideal torque with mass, and DCM – developed DC motor model with gear box); C, D, E – voltage, rotor speed and torque of DC motor. The controls of assistive devices were similar for three models. The absolute torque magnitude output using the DC motor model is lower at the beginning (0 - 0.23 seconds) and the end of simulation period (0.35 – 0.5 seconds).

6.3.2 Predictive simulation

In all four models, the constraints of initial positions and velocities, and final positions were satisfied. The average muscle activations in all the arm models with assistive devices were less than in the model without an assistive device (Figure 6.6) (6.5% in NA, 1.7% in IT, 1.6% in ITM, 2.7% in DCM over the simulated time period). The two ideal torque actuator models (IT and ITM) produced similar kinematics and muscle activation patterns (Figure 6.5 and Figure 6.6). In the case of DCM model, however, the motion trajectory was different from the others. The

elbow and shoulder ranges of motion were less than the ideal torque actuator cases. In addition, the peak velocities of the shoulder and elbow joints were less when the DCM model was used. Activations of the elbow flexor muscles (BIClong, and BRA) were higher during the DCM simulation beginning (0 – 0.20 seconds) and higher for BIClong and BICshort near the DCM simulation end (0.30 – 0.50 seconds) compared to IT and ITM models. The controls for all assistive device models were similar during the first 0.3 seconds (Figure 6.7A). However, the torque produced by the DC motor was less than both ideal torque models (average of 3.7 Nm in DCM, 5 Nm in IT and ITM). At the end of the simulations (0.37 – 0.50 seconds), the DC motor optimal control inputs were different from the controls found for either of the ideal torque models, which resulted in different torque outputs from the DC motor (Figure 6.7B).

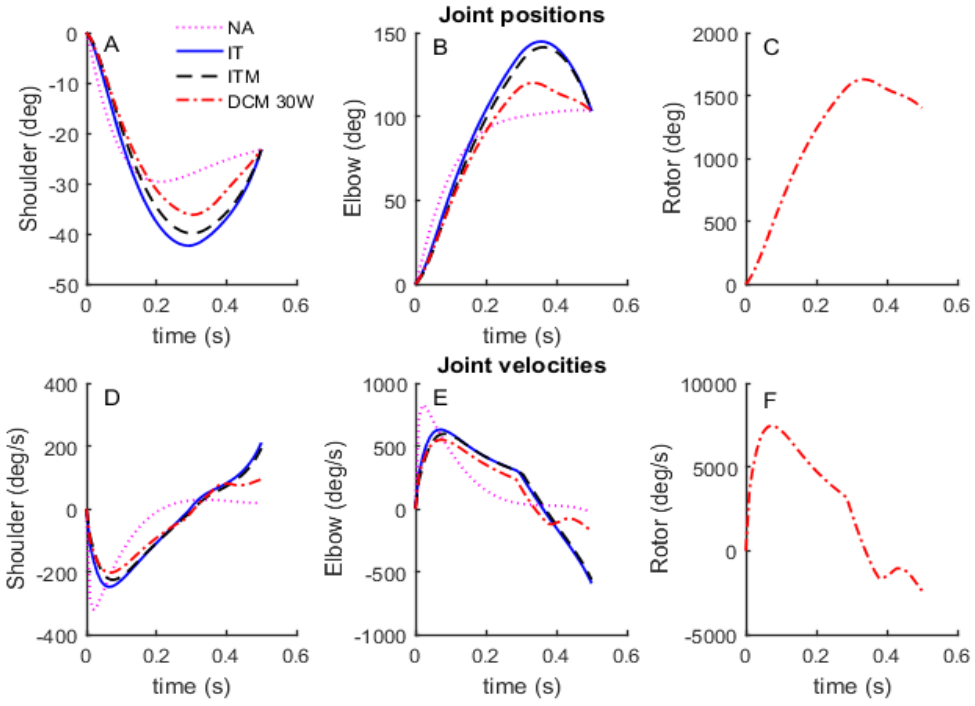

Figure 6.5: Kinematic data in predictive simulation for each arm model (NA – without assistive device, IT – ideal torque without mass, ITM – ideal torque with mass, and DCM – developed DC motor model and gear box). Two arm models with ideal torque actuators (IT and ITM) predict similar motion paths which are different from the DCM predictive motion.

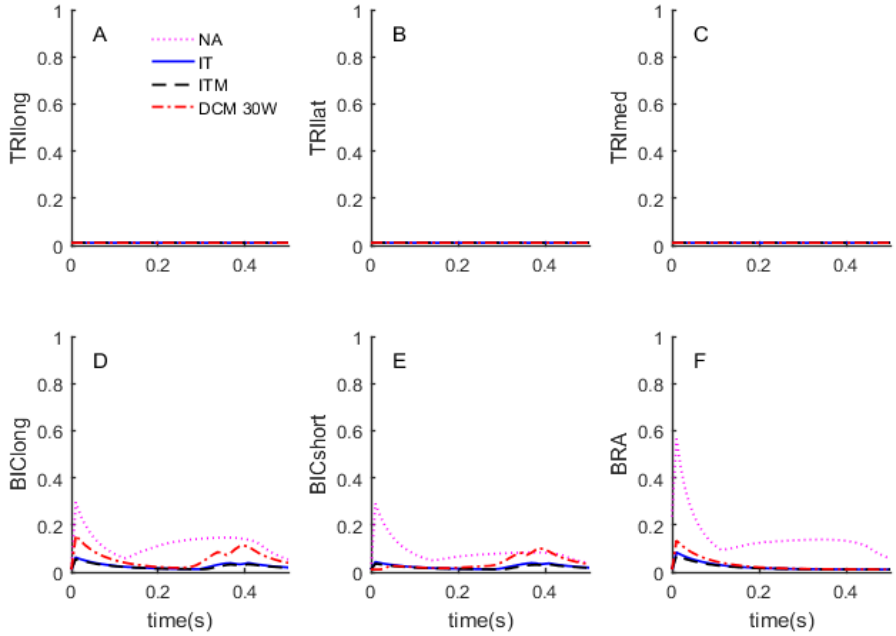

Figure 6.6: Muscle activations in the predictive problem with different arm models (NA – without assistive device, IT – ideal torque without mass, ITM – ideal torque with mass, and DCM – developed DC motor model and gear box). The DCM model required more muscle activations (BIClong, BICshort, BRA) than IT and ITM. All models with assistive devices have lower average muscle activations compared to the NA.

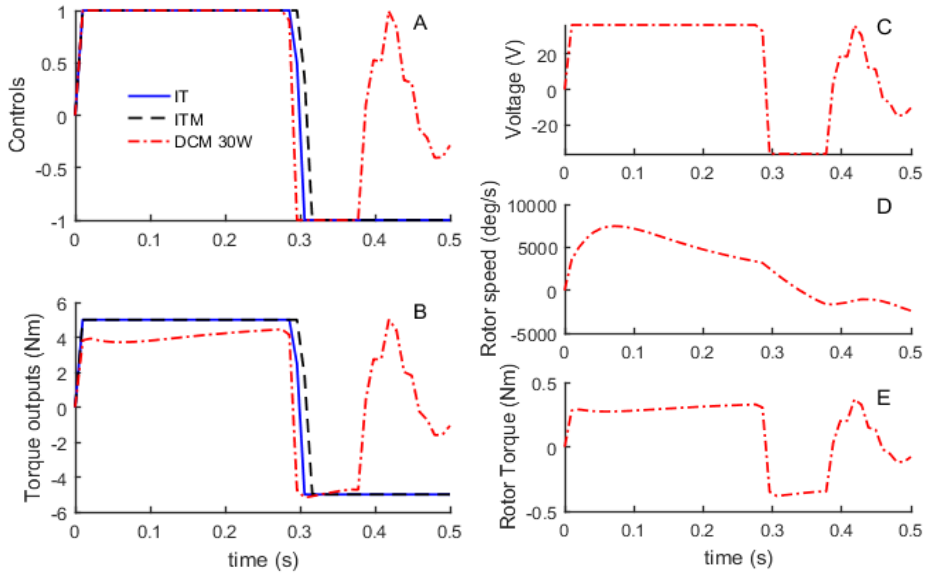

Figure 6.7: A) Controls and B) torque output of the assistive devices and the corresponding C) voltage, D) rotor speed, and E) current of the DC motor in the predictive problem (IT – ideal torque without mass, ITM – ideal torque with mass, and DCM – developed DC motor model with gear box). The controls of assistive devices in IT and ITM model were similar, which resulted in similar torque outputs. The control of assistive device in DCM model was different than the others (0.37 – 0.5 seconds), which resulted in different torque output.

6.4 Discussion

In this study, we simulated a powered assistive elbow device working in parallel with a musculoskeletal model of the arm. The actuators of the devices based on DC motors were modeled in diverse ways in increasing detail levels, namely: ideal torque without mass (IT), ideal torque with mass (ITM), and our developed DC motor model (DCM). The IT model ignores the device mass and internal dynamics of the actuator; the ITM model captures the device mass, but ignores the internal dynamics of the actuator; the DCM model captures the device mass and the internal dynamics of the actuator. Dynamic optimizations were used with these models to solve the muscle and device controls. Due to the electrical and mechanical dynamics of the DC motor, modeling the actuator with different detail levels led to notable differences in simulation results.

In both motion tracking and predictive simulations, the muscle effort is penalized, and the device power is not. To complete the movement, the device tends to produce maximum torques before engaging the muscles. IT and ITM models produced similar output torques and muscle controls. The similar controls and torque outputs suggest that simulation results are insensitive to the mass of the device, although the assistive device modeled is relatively lightweight (0.3 kg), and it does not undergo significant motion due to shoulder movements (Figure 6.2A and Figure 6.5A). In the motion tracking problem, all models were able to track the desired kinematic data. The torque produced by the DC motor is different from the other models due to the electrical and mechanical dynamics which capture the speed-current or speed-torque relationships (Eq. 6.1 and 6.2). The DC motor torque depends both on the voltage input and on the speed of the rotor. With the same voltage input, when the relative speed of the rotor decreases, *di/dt* is positive, so the current will increase, which increases torque output as defined in Eq. 6.2, and vice versa (Figure 6.4C, D, and E). However, the trend is different in the case of the ideal torque actuator which produces output torque proportionally to the control input (Figure 6.4A, B). In addition, the DC motor also captures the moment of inertia of the rotor. However, in this study, the effect is small due to the small rotor inertia (Table 6.1). As shown in Figure 6.8, the maximum difference in

torque output when modeled with and without inertia is less than 6%. Notably, the DC motor produced a greater torque magnitude than the ideal torque actuator models (5 Nm) following the voltage control reversal (0.25-0.29 s) (Figure 6.4B). This phenomenon was caused by the motor speed and voltage having opposite signs (voltage is -36 V, and motor speed is positive) (Figure 6.4C, D).

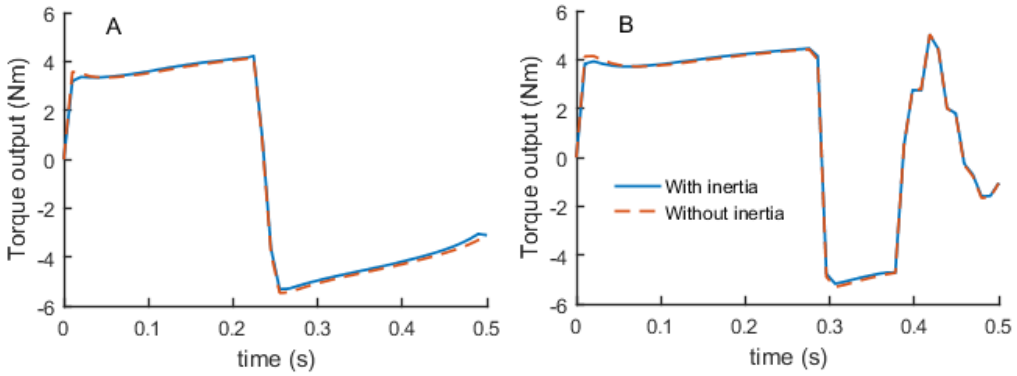

Figure 6.8 : Output torque of DC motor with a gearbox with and without taking rotor inertia into account: A-Data tracking problem and B-Predictive simulation. The torque without rotor inertia were calculated by setting $J_m = 0$ in Eq. 6.3. The maximum difference in torque output when modeled with and without inertia is less than 6%.

The differences in assistive torque outputs make the muscle activations in the DCM model higher than in ideal torque actuator cases. Elbow flexor/extensor co-contraction is also observed between 0.25 and 0.50 seconds (Figure 6.3). This co-contraction is due to the need for a flexion moment at the shoulder (Figure 6.2A) and an extension moment at the elbow (Figure 6.2B) during this period to achieve the desired motion. BICshort and BIClong act as elbow flexors as well as shoulder flexors because they cross both joints. With the DC motor model, the assistive extension torque output at the elbow is not sufficient alone; the motion requires additional torque from other elbow extensors (TRIlat, TRImed) (Figure 6.3). As a result, these muscles are all activated, which causes co-contraction at the elbow which is not seen in IT and ITM simulations.

In the predictive simulation, the task is to move the arm from an initial position with zero velocity to a final position without an imposed final velocity. The optimal strategy was to harness

the device power as much as possible. The elbow extensors did not activate due to the characteristics of the optimal movement path solutions. The optimal movement paths can be divided into two parts (Figure 6.5A, B). During the first part (0 – 0.3 seconds), the arm lifted the object. Flexion torque were required from elbow flexors and the devices. During the second part (0.3 – 0.5 seconds), the arm moved down, and the extension torque required was provided by the assistive devices and the gravity (Figure 6.5B). Therefore, elbow extensors did not activate during the movements. The DCM model used slightly different motion paths compared to other models using the ideal torque actuator. The controls for all assistive device models were similar during the first 0.30 seconds (Figure 6.7A). However, the torque produced by the DC motor was less than the ideal torque models (from 0 – 0.3 seconds, Figure 6.7B) due to the speed-current relationship of DC motor (Eq. 6.1). Therefore, the magnitude of both shoulder and elbow velocities are relatively low at the beginning (0-0.25 seconds) (Figure 6.5D, E). Interestingly, near the end (0.35-0.50 seconds), the DCM model produced different motion and velocity trajectories compared to IT and ITM. This difference may be explained because the DCM would need to produce about -5 Nm of torque as seen in IT and ITM (Figure 6.7B) in order for the DCM to produce the motion trajectory chosen by the ideal torque models. However, the DCM cannot provide such high magnitude torque required when the elbow velocity is in the range between 160-564 deg/s (Figure 6.5E) due to the speed-torque limitations of the DC motor. Therefore, the DCM chose the different trajectory.

In these simulations, a 30 W motor with a gearbox of 1:13.57 is used to provide a maximum assistive torque of 5 Nm. To evaluate the effect of using different DC motors, we also simulated the motion tracking problem with lower and higher power motors which are 15 W with a gear ratio of 1:59.45 (DCM 15W), and 70 W with a gear ratio of 1:5.46 (DCM 70W) (Table 6.1). For all cases, the assistive device controls were similar. However, with a higher power motor, the torque output was closer to the ideal torque (Figure 6.10). As a result, the muscle activations were smaller than compared to the lower power motor cases (Figure 6.9). The average

muscle activations are 13.6% in DCM 15W, 5.9% in DCM 30W, and 4.8% in DCM 70W. The gear ratio in the higher power motor case is low, which allows the motor to work at a lower speed. As a result, the motor torque is less affected by the motor speed. With a smaller motor (15 W), the motor requires a higher gear ratio to have a maximum output torque of 5 Nm and resulting in the motor operating at a higher speed. For this motor, the output speed was higher than the nominal speed of the motor, which makes the output torque negative even when the voltage control is positive (from 0-0.14 seconds, Figure 6.10). The motor provided negative power, which led to high muscle activations (even higher than the NA model) from elbow flexors (Figure 6.9D-F). As expected, the total muscle activations with the low power motor are higher than with the larger motor and can be even higher than without using an assistive device as seen in DCM 15 W. The simulations with different DC motors with scaled gearboxes show the significance of including the electromechanical dynamics of actuators. Furthermore, they can potentially be used to aid in the design of assistive devices. For example, the simulations could be used to determine the optimal motor size for the device. In general, the higher power the motor, the heavier the motor is (Table 6.1). Using a high power motor can produce higher torque at the elbow (Figure 6.10). However, a high power motor is heavy, which may impede the motion of the shoulder. In this study, however, the movements simulated (mainly movements of the elbow, relatively small movement at the shoulder) was not sensitive to the exoskeleton mass. Future study should investigate more movements of the upper limb.

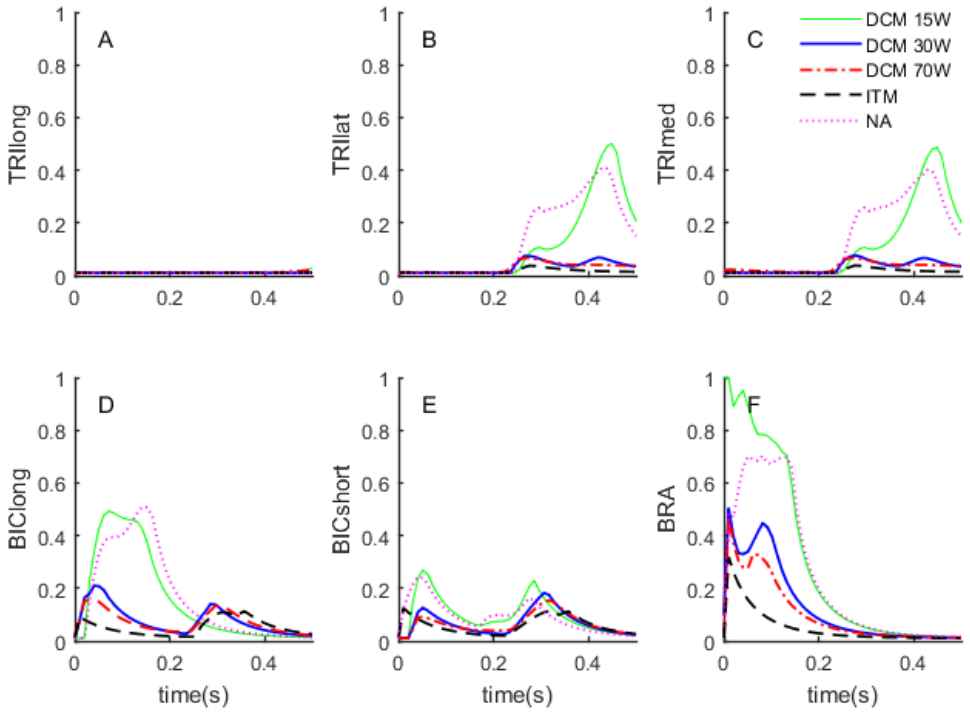

Figure 6.9 : Muscle activations in tracking problem with different DC motors: DCM 15W – model with 15W DC motor, DCM 30W – model with 30W DC motor, DCM 70W – model with 70W DC motor. With smaller power model, the muscle activations are overall higher.

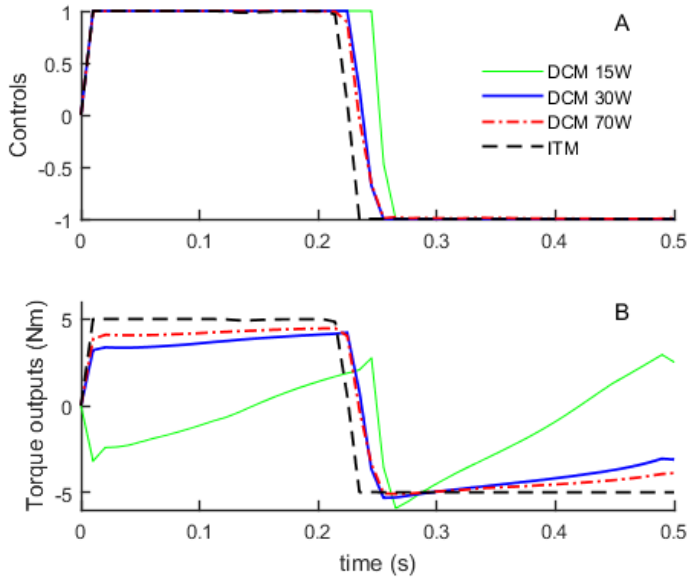

Figure 6.10: Optimal controls and torque outputs of assistive devices with different DC motors and gear boxes: DCM 15W – model with 15W DC motor, DCM 30W – model with 30W DC motor, DCM 70W – model with 70W DC motor. The controls of the assistive devices are similar; however, the torque outputs are different, especially for DCM 15W.

Several limitations of this study are worth discussing. First, the upper limb musculoskeletal model is relatively simple with six muscle-tendon units and a rigid connection between the exoskeleton and the upper limb. Although similar upper limb models have been used in some studies and had successfully shown the ability to replicate actual movements (Mehrabi et al. 2017), a more complicated model may better capture the dynamics of the movements. Second, in the optimization problems, we used the cost function of minimizing muscle activation squared. This cost function represents muscle effort which has been used for generating human movements in the literature (Koelewijn et al. 2018)(Ackermann and van den Bogert 2010). However, other cost functions based on different criteria such as metabolic energy cost (Anderson and Pandy 2001), movement smoothness (Nguyen, Johnson, et al. 2019), and device cost (Handford and Srinivasan 2016) could also be considered. With the challenging of modeling the musculoskeletal model and defining the cost functions, it may be not easy to simulate the arm movement closely matches the reality. Therefore, the simulation results in this study may have some limitations to some extent. Future study should collect experimental data to validate the simulation results.

6.5 Conclusion

In this chapter, a DC motor class is developed for use in the OpenSim environment. This new actuator class increases simulation realism when modeling robotic devices physically assisting a person. The effects of using a DC motor actuator model highlight the impact on coupled system dynamics. In dynamic optimizations for both motion tracking and predictive simulation problems, the results show that integrating the DC motor class into the coupled human-robot model can lead to different results compared to using ideal torque actuator models. While the effect of actuator mass and inertia can be small when it is lightweight and does not undergo significant motion, the electrical dynamics of the motor can considerably impact

simulation results. This outcome suggests the importance of using an accurate actuator model in the simulation of powered assistive devices. In addition, the simulation results with different DC motors can be used as a guideline for assistive device design and control. The developed DC motor class used in this chapter is available in the OpenSim project repository (https://simtk.org/projects/roboticact).

CHAPTER 7

CONCLUSION AND FUTURE WORK

7.1 Summary and conclusion

Predictive simulation based on dynamic optimization is a promising approach to address the problem of assistive device design and control. However, the simulation approach has some challenges. This dissertation aims to develop a predictive simulation tool based on dynamic optimization by tackling those challenges. First, the challenge of the cost function determination in formulating the dynamic optimization problem was addressed using the bilevel optimization approach. The cost functions in both able-bodied and amputee walking simulations were presented. Later, the effects of over-simplified modelling the robotic actuator in the human-robot musculoskeletal model were examined. The results highlight the importance of including the internal dynamics of the device actuator in dynamic simulation of augmented human movements.

First, the dissertation has attempted to address the problem of determining the cost function in the dynamic optimization of human walking. The problem was formulated as a bilevel optimization which was solved through a nested evolutionary approach. The nested approach has effectively and robustly solved different bilevel optimization problems, including a walking simulation. The presented bilevel approach potentially can be used to determine the cost function of other human movement or to address the problems of identifying the parameters in assistive device design and control.

Next, a variety of cost function forms were examined for both able-bodied and amputee walking simulations. The bilevel optimization approach was used to optimize the parameters of some cost functions to ensure the best performance of the cost functions were achieved. The results on both able-bodied and amputee simulations have demonstrated the importance of including gait smoothness and gait stability besides muscle effort in the walking cost function.

This result also suggests that the central nervous system may take multiple performance criteria in consideration during walking.

With the result of the cost function in able-bodied simulation, predictive simulations of human walking augmented by the exoskeleton were done. Both muscle controls and the device controls were optimized simultaneously using the direct collocation method. The results of assistive torque patterns and walking cost reductions were similar to experimental results found in the literature, which suggests the potential of the simulation approach to address the design and control of assistive devices.

Lastly, we examined the effects of including the internal dynamics of the robotics actuator in simulations of augmented human movement. An upper limb, wearing an elbow exoskeleton, lifting an object, was used as a demonstration case. The results have shown that, with DC motor, while the mass and inertia effects may be small, the electromechanics dynamics can considerably affect the simulation results. The simulations with our developed DC motor model may be used to evaluate the design of the device.

In conclusion, the results in this dissertation have contributed the key knowledge about the cost function form used in predictive dynamic optimization approach for human walking. Besides, the results have suggested the potential use of the predictive approach for addressing the problem of assistive device design and control.

7.2 Future work

The work presented in this dissertation has demonstrated the potential of using predictive simulation in studying human gait and in the design and control of the assistive device. Future works involve further investigation in performance criteria in human walking and expand the simulations of human movement augmented by assistive devices.

7.2.1 Cost function in predictive simulation

First, this dissertation examined a variety of cost function forms based on different performance criteria in the dynamic simulations of able-bodied and amputee walking. The best results with these cost functions, however, were still not as good as tracking results, which suggests there may still be additional features of human gait that are not captured by the cost functions such as minimizing joint contact forces (Fey et al. 2012). Moreover, the performance criteria in the examined cost functions could be parameterized in ways other than were done in this dissertation, which may also affect the results. Future studies may tie the modeling and simulation work more directly to research on the neural control of locomotion so that the modeling performance criteria are similar to what humans actually prioritize in walking. In addition, future works may further expand the performance criterion solution space, and consider different ways to parameterize the performance criteria. These expansions, however, will require significant computation time. Therefore, reducing the computation time is important. A solution that could be considered to further address the computation time is implementing parallel computing for both levels (GA in the upper level, direct collocation in lower level) in the bilevel optimization. In this case, using a computer system with multiple CPU, each CPU has multiple cores would be ideal, so that the direct collocation can be parallelized in each CPU, and GA can be parallelized with multiple CPU.

Second, the determination of the performance criteria in the cost function for predictive dynamic optimization of different movements remains challenging. Questions, such as, 1. if the weights among different performance criteria need to be changed when the walking conditions change, 2. if the cost function form for the simulations of running and cycling would be the same as walking, requires further investigation. These questions may potentially be addressed by using the presented bilevel optimization to solve for the inverse optimal control problems of different human movements. The results of cost function forms in different human movements such as

walking at different speeds may give valuable insights into the way central nervous system controls movements.

7.2.2 Application in assistive device design and control

Indeed, assistive device design and control may be in one of the most promising application areas of the predictive simulation approach. Chapter 4 has demonstrated the potential of using predictive simulation to predict optimal assistive ankle torque pattern in human walking with a powered ankle exoskeleton. Furthermore, the simulation approach may be used to evaluate different actuator designs of the assistive device as seen in chapter 6. These simulations may provide valuable insights into the design and control of the devices. Future studies should further expand the use of the predictive dynamic optimization approach such as optimizing the parameters (e.g., stiffness, power) of the ankle exoskeleton, optimizing the design shape of an exoskeleton. Determination of the optimal design may be done by, first, evaluating a set of device parameters based on the simulation. The bilevel optimization approach in this dissertation could also be used to optimize the parameters of the devices. The lower level may solve for predictive simulation of human movement. The upper level may optimize the device parameters such as stiffnesses and assistive torque. Latter, the model predictions of optimal results is evaluated by testing in human subjects. The testing results on human subjects will allow to see if the simulation results actually improve the function of the user, or if the simulations need to be adjusted accordingly.

In chapter 5, we have simulated transtibial amputee walking. Although the amputee musculoskeletal model allows generating human-like walking, there are some remaining limitations. First, the prosthesis model is highly simplified with rigid segments connected via a rotational joint at the ankle. The actual prostheses, however, allow flexion through bending over the area around ankle and foot. Although the effects of an oversimplification of the prothesis ankle are unclear, the quality of the simulation may be improved by capturing more accurately the

dynamic of the device. Adding more details of the device stiffnesses can be done using multiple stiffness points over the foot as seen in (Fey et al. 2012). The second limitation is the assumption of rigid socket-residual limb connection. Experimental studies have shown pistoning and flexion movements of the residual limb within the socket (Sanders et al. 2006)(Eshraghi et al. 2012). These movements may potentially affect amputee gait. Therefore, future studies should account for these movements by using a more detail socket-residual limb model which allows movements of the residual limb respective to the socket. Futhermore, while the performance criterion of minimzing overall socket load was used and found no improvement of the gait solution, it is possible that the amputees actually priorize socket load in other forms such as peak loads at a specific area. Further investigation on parameterizing the socket loads should be considered.

7.2.3 Remaining challenges of the dynamic optimization

In this dissertation, the predictive simulation is based on the dynamic optimization with the musculoskeletal models. The dynamic optimization problem is solved effectively through the direct collocation approach. Nevertheless, the simulation is remaining computationally expensive, which may prevent from using highly complicated musculoskeletal model (e.g., 3D model), or quickly generate multiple simulations. Therefore, further speeding up the simulation is worth to consider in future studies. There are several techniques and approaches has recently gotten attentions. First, a potential approach is implementing parallelization in the direct collocation approach. During solving the NLP problem, evaluation of the dynamic equation of the musculoskeletal model are usually required in some steps such as constraint Jacobian matrix evaluation or cost function gradient evaluation. The dynamic equation evaluation can be time-consuming, especially when the dynamics of musculoskeletal model is complicated. Therefore, evaluation of the dynamic equation at multiple nodes simultaneously with parallel computing can help reduce the computation time. Second, using the implicit representations for the dynamic equation of the musculoskeletal model can improve the speed as well as the robustness of the

optimization (De Groote et al. 2016). Third, approaches such as algorithmic differentiation (Griewank 1989) can be used to replace the finite difference approaches which currently were often used for calculating the constraint Jacobian matrix or objective gradient derivative. Algorithmic differentiation can give the exact results of the derivative, and requires less computation, which may substantially speed up the simulations.

Although the dynamic optimization with the musculoskeletal model has shown great potentials in studying human movements and in assistive device design and control, it is an open-loop, without feedback approach. Therefore, in some cases involving feedback from the environment such as reaching a moving target, walking with disturbances from the ground, the dynamic optimization with such musculoskeletal models may not be enough to used (Mehrabi et al. 2017). Future studies may consider adding the closed-loop feedback with the neural control in the model (Song and Geyer 2018). Or in some specific movement simulations such as hand reaching a target, a closed-loop algorithm such as model predictive control approach may be used (Mehrabi et al. 2017). Furthermore, recent emerging methods in computer science field such as deep learning, and reinforcement learning have given some opportunities to apply in simulation of human movement. For example, deep reinforcement learning has been used to synthesize walking (Peng et al. 2017) and running (Kidziński et al. 2018). These approaches may potentially compensate some limitations of the current approach based on dynamic optimization.

APPENDIX A

SUPPLEMENTARY MATERIALS FOR CHAPTER 2

This supplementary document provides a detailed description of the musculoskeletal model used in chapter 2 and provides additional simulation results of walking using the direct collocation method with a higher grid density than used in the chapter.

Musculoskeletal model

The musculoskeletal model, implemented in OpenSim (Seth et al. 2011), consisted of 12 rigid bodies, namely: torso, pelvis, right and left femur, tibia, talus, calcaneus, and toes. The torso and pelvis were rigidly joined, forming a single trunk segment. The model possessed 11 degrees of freedom, including planar rotation and translation of the pelvis, plus one rotation for each hip, knee, ankle, and metatarsophalangeal joint (Figure S-1a). The model was actuated by 18 muscle-tendon units (nine for each lower limb) which were represented using a Hill-type muscle model described in (Millard et al. 2013). These muscles were the biarticular hamstring (HAM), biceps femoris short head (BFsh), gluteus maximus (GMAX), iliopsoas (IL), rectus femoris (RF), vasti (VAS), gastrocnemius (GAS), soleus (SOL), and dorsiflexor (DOR). The DOR muscle group included the contributions of the tibialis anterior, extensor hallucis longus, and extensor digitorum longus (Figure S-1 b). The body and joint parameters and muscle paths were based on several existing musculoskeletal models (Delp et al. 1990)(Yamaguchi and Zajac 1989)(Anderson and Pandy 1999)(Sasaki, Neptune, and Kautz 2009).

The foot-ground contact model was adopted from the model described by (Porsa et al. 2016). There were eight contact spheres represented in OpenSim as Hunt-Crossley contact elements distributed under each foot. The stiffness and damping coefficients of these contact spheres were optimized to reproduce measured vertical ground reaction forces in walking and running (Porsa et al. 2016).

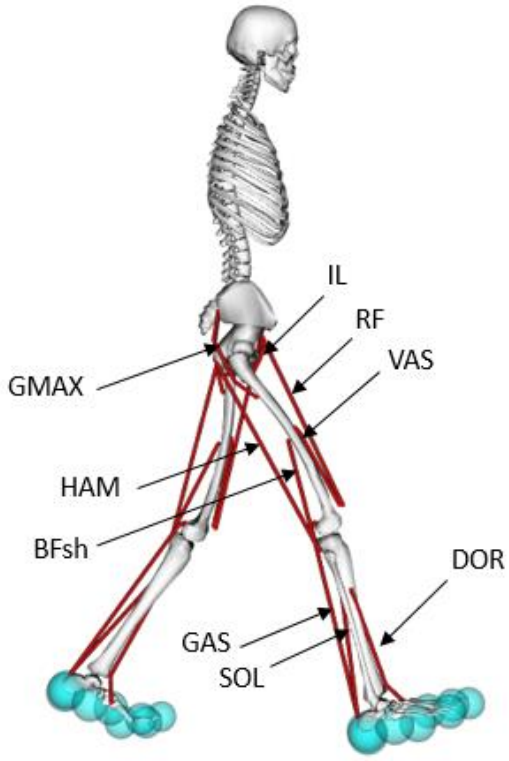

Figure S-1: The model consists of 12 rigid bodies connected through 11 degrees of freedom. The foot-ground contact was modeled by eight OpenSim HuntCrossleyContact spheres under each foot (Porsa et al. 2016) (a). The model is actuated by 18 muscle tendon units (nine on each lower limb) which are represented with Hill-type muscle model (Millard et al. 2013). These muscles are biarticular hamstring (HAM), biceps femoris short head (BFsh), gluteus maximus (GMAX), iliopsoas (IL), rectus femoris (RF), vasti (VAS), gastrocnemius (GAS), soleus (SOL), and dorsiflexor (DOR).

Muscle model parameters

Muscle model parameter values were based on a cadaver study (Ward et al. 2009) and a MRI study with young, healthy subjects (Handsfield et al. 2014) (Table S-1). The muscle optimal fiber lengths (l_0^m) were taken from (Ward et al. 2009). For the muscle groups (HAM, IL, VAS, GAS, DOR), the optimal fiber lengths were calculated as a weighted average of individual muscle optimal fiber length based on muscle volumes (V_m)(Eq. 1).

$$l_0^m = \frac{\sum_{i=1}^{n} V_{m_i} \times l_0^{m_i}}{\sum_{i=1}^{n} V_{m_i}} \quad (1)$$

where l_0^m is the optimal fiber length of the muscle group, V_{m_i} and $l_0^{m_i}$ are the muscle volume and the optimal fiber length of the muscle i^{th}, respectively, in the muscle group.

Muscle volumes were calculated based on data derived from young, healthy subjects using the height-mass metric (Eq. A2) (Handsfield et al. 2014). The muscle physiological cross-sectional areas ($PCSA$) were calculated by diving muscle volumes to the optimal fiber lengths (Eq. 3). Peak isometric muscle force, F_0^m , was calculated through PCSAs (Eq. 4).

$$V_m = b_1 \times (height * mass) + b_2 \tag{2}$$

$$PCSA = {V_m}/{l_0^m} \tag{3}$$

$$F_0^m = PCSA \times \sigma_0^m \tag{4}$$

where b_1 and b_2 were volume prediction coefficients specific to each muscle, taken from (Handsfield et al. 2014); σ_0^m is the muscle specific tension which was set at 60 N/cm^2, similar to other studies (Rajagopal et al. 2016).

The pennation angles α_0 were calculated based on the angles measured by Ward et al. (2009) and the constant muscle volume assumption of Millard muscle model (Millard et al. 2013) (Eq. 5), as was done in (Rajagopal et al. 2016).

$$\alpha_0 = \sin^{-1}\left({L_s}/{2.7\mu m} \times \sin\alpha\right) \tag{5}$$

where α and L_s are the pennation angle and sarcomere length, respectively, taken from (Ward et al. 2009); $2.7\mu m$ represents the optimum sarcomere length of human muscles (Ward et al. 2009)(Lieber, Loren, and Friden 1994). For muscle groups, the pennation angles were equal to the volume weighted average of individual muscle pennation angles.

To set the tendon slack lengths, the model was set at the position reported in (Ward et al. 2009) (7° hip flexion, 0° knee flexion, and 20° plantarflexion). Then the tendon slack lengths were set so that the muscle fiber lengths with 1% activation matched the normalized fiber length reported in (Ward et al. 2009). Using this approach, some muscles had unrealistically high passive fiber

forces. Therefore, we adjusted the tendon slack lengths to reduce the passive fiber forces and match with passive fiber forces in the musculoskeletal model published by Lai et al. 2017. At that point, we generated a walking simulation with the model that tracked kinematic and ground reaction force as described in chapter 2. Based on this simulation, the tendon-slack lengths for some muscles (SOL, GAS, RF) were adjusted so that the muscle fiber lengths over a gait cycle matched with the corresponding data reported by (E. M. Arnold et al. 2013). Thus, the tendon slack lengths were set based on a combination of static and dynamic data. The resulting muscle parameter values are reported in Table S-1. The activation and deactivation time constants for all muscles were assumed to be 55 ms and 65 ms, respectively, based on (Umberger et al. 2003) assuming a mixed fiber type distribution.

Muscle	**Abbreviation**	**Optimal force (N)**	**Optimal fiber length (m)**	**Tendon slack length (m)**	**Pennation angle (°)**
Hamstring	HAM	3373.9	0.121	0.347	13
Biceps fermoris short head	BFsh	586.8	0.110	0.158	15
Gluteus maximus	GMAX	3491.8	0.157	0.083	21
Iliopsoas	IL	2598.6	0.113	0.153	14
Rectus femoris	RF	2267.4	0.076	0.389	12
Vasti	VAS	8573.1	0.115	0.135	15
Gastrocnemius	GAS	4183.5	0.063	0.403	10
Soleus	SOL	6348.6	0.044	0.270	22
Dorsiflexor	DOR	2179.7	0.069	0.256	12

Table S-1: Musculotendon parameters.

Simulation result with a higher grid density

In this study, we solved the lower level optimization problem using the direct collocation method with a relatively coarse grid density (15 nodes), which was necessary for computational efficiency. The results obtained using a grid density of 15 nodes were able to produce simulated gaits that captured the salient features of gait patterns obtained at greater grid density. To demonstrate this, we used the cost function (Eq. 2.7 – chapter 2) with the optimal weights found in the Problem 2 and solved for a walking simulation with a typical grid density of 50 nodes (Ackermann and van den Bogert 2010). The results obtained using 50 nodes were similar to using 15 nodes in term of the kinematics, kinetics, and muscle controls (Figure S-2, Figure S-3). There were slight joint angle differences between the 15 and 50 node results in the swing phase, and for the second peak in the vertical ground reaction force, which was actually closer to the experimental data for the 50-node case. Thus, the cost function weighting results obtained using 15 nodes/step generalize to the denser grids typically used in gait simulation studies.

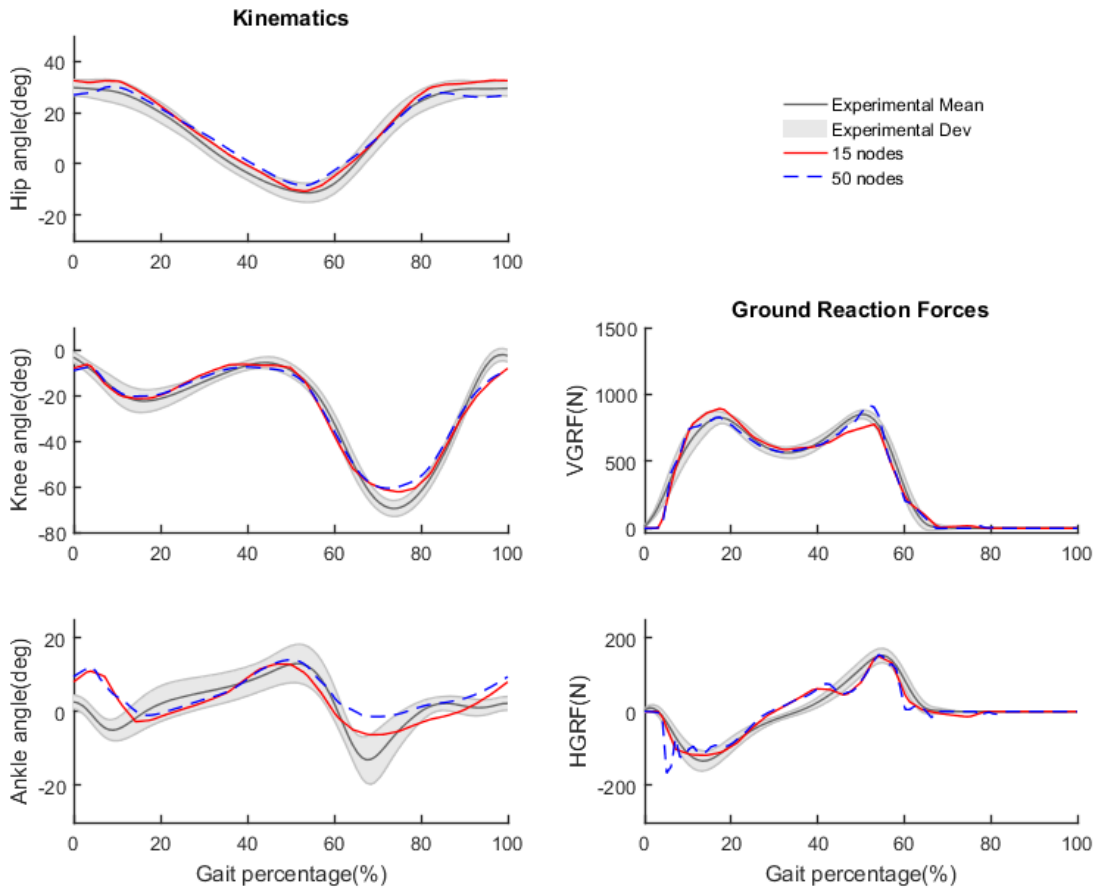

Figure S-2: Predictive joint angles and ground reaction forces using the direct colocation method with the 15 node grid (red, solid lines) and the 50 node grid (blue, dashed lines) are similar. The black lines and gray areas represent the means and one standard deviation of experiments human gaits.

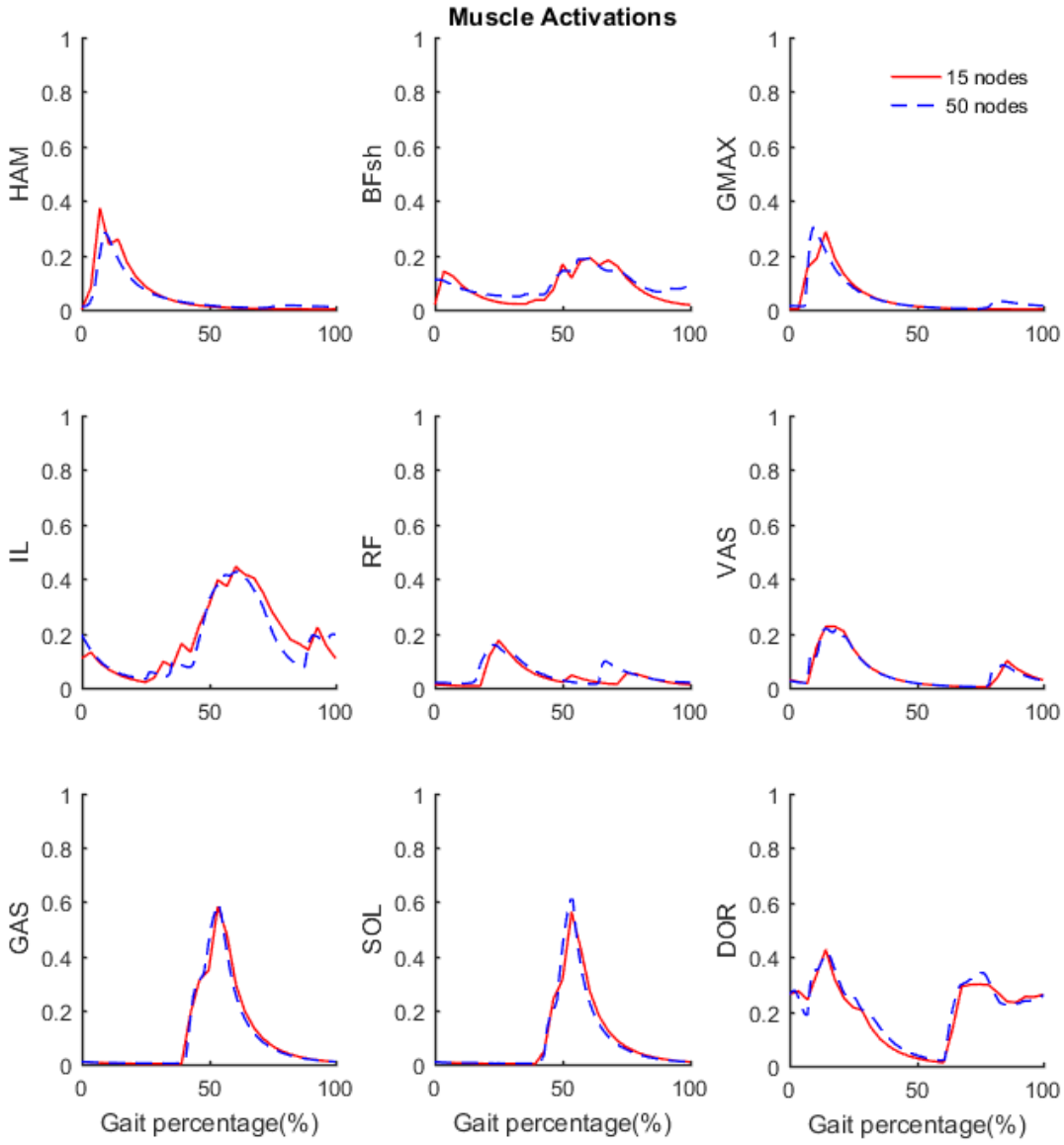

Figure S-3: Predictive muscle activation results using the direct colocation method with the 15 node grid (red, solid lines) and the 50 node grid (blue, dashed lines). The muscle activation patterns and magnitudes are similar using different grid densities.

APPENDIX B

SUPPLEMENTARY MATERIALS FOR CHAPTER 3

This section provides some details of simulation results in chapter 3. The gait kinematics and GRFs error, cost of transports, and stride frequencies of the gait solutions are shown in table S-2. Optimal parameters in the cost functions, found through the bilevel optimization, are shown in table S-3. The gait solutions at different speeds generated with cost function J_{11} were shown in figure S-4.

Gait with cost functions	Kinematics error	GRFs error	CoT	Stride frequency
J_T	0.36	0.38	3.79	0.90
J_1	2.06	2.10	2.36	0.83
J_2	1.55	1.65	2.83	0.90
J_3	3.67	2.24	3.13	1.04
J_4	1.71	1.28	3.27	0.91
J_5	0.88	0.72	3.75	0.82
J_6	1.30	1.05	3.13	0.93
J_7	1.19	1.30	3.38	0.89
J_8	1.91	0.98	3.49	0.78
J_9	1.66	1.30	2.94	0.90
J_{10}	1.70	1.29	2.92	0.89
J_{11}	0.91	0.94	3.38	0.85
J_{12}	1.03	1.04	3.08	0.90
J_{13}	0.85	0.84	3.42	0.84

Table S-2: Gait kinematics and GRFs errors, and the CoT and stride frequencies. The errors were calculated as mean absolute error and reported with SD units. The CoT were calculated using the model of energy expenditure described in (Umberger et al. 2003).

Cost function	HAM	BFsh	GMAX	IL	RF	VAS	GAS	SOL	DOR	w_{s1}	w_{s2}	w_{s3}	w_{s4}
J_4	x	x	x	x	x	x	x	x	x	13.59617	x	x	x
J_5	10.0	40.52879	299.9031	55.09868	43.38198	4.54392	5.51777	0.23440	87.68812	x	x	x	x
J_6	10.0	69.26643	286.1793	102.3467	184.2599	222.9037	5.250276	6.05857	8.10807	x	x	x	x
J_7	10.0	9.746648	298.4637	142.9181	4.424738	1.76867	6.866336	8.177789	0.312561	x	x	x	x
J_8	x	x	x	x	x	x	x	x	x	61.10911	52.56731	x	x
J_9	x	x	x	x	x	x	x	x	x	1.735149	5.574622	x	x
J_{10}	x	x	x	x	x	x	x	x	x	5.977725	12.21293	x	x
J_{11}	x	x	x	x	x	x	x	x	x	93.71989	21.03323	5.127854	41.02795
J_{12}	x	x	x	x	x	x	x	x	x	22.97422	95.04991	49.33517	21.76314
J_{13}	10.0	5.017214	36.25591	49.63796	49.97786	24.58712	5.212011	37.7955	49.6498	152.9006	42.08093	119.0059	207.6781

Table S-3: The optimal parameters in the cost functions. “x” means there is no parameter associated.

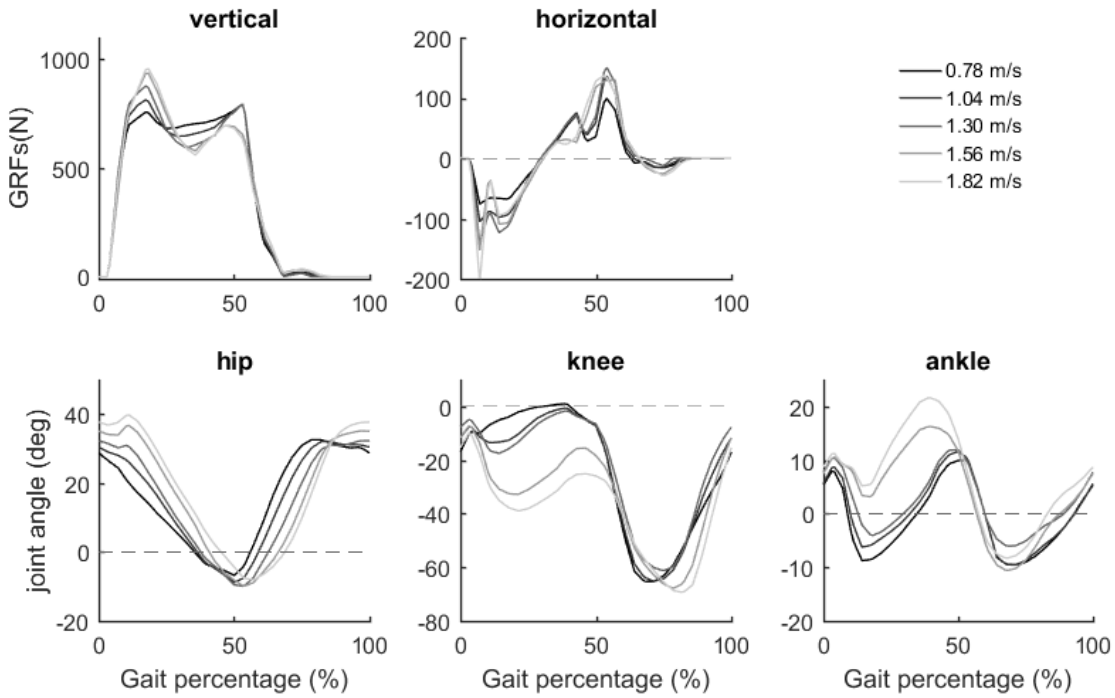

Figure S-4: Predicted kinematics and GRFs at different walking speeds. The solutions were generated using the cost function J_{11} with the optimized weights among different performance criteria. The results predicted some similar trends of changes in kinematics and kinetics compared to the experimental gaits.

APPENDIX C

SUPPLEMENTARY MATERIALS FOR CHAPTER 5

This section provides details of the amputee simulation results in chapter 5. The gait kinematics and GRFs error, cost of transports, and stride frequencies of the gait solutions are shown in table S-4. Optimal weights in the cost functions, found through the bilevel optimization, are shown in table S-5.

Gait with cost functions	Kinematics error	GRFs error	CoT	Stride frequency
J_T	0.99	0.658	3.52	0.77
J_{A1}	3.19	1.75	2.16	0.91
J_{A2}	2.97	1.58	2.64	0.89
J_{A3}	3.12	1.46	2.96	0.91
J_{A4}	1.86	1.27	3.31	0.82
J_{A5}	2.83	1.44	2.73	0.85

Table S-4: Simulated gait kinematics and GRFs errors, and the CoT and stride frequencies. The errors were calculated as mean absolute error and reported with SD units. The CoT were calculated using the model of energy expenditure described in (Umberger et al. 2003).

Cost function	w_1	w_2	w_3	w_4
J_4	0.2069	27.1044	2.1267	72.9974
J_5	47.9002	52.9479	-	-

Table S-5: The optimal weights in the cost functions found through the bilevel optimization approach.

BIBLIOGRAPHY

Ackermann, Marko and Antonie J. van den Bogert. 2010. "Optimality Principles for Model-Based Prediction of Human Gait." *Journal of Biomechanics* 43(6):1055–60.

Alan Hreljac and Philip E. Martin. 1993. "The Relationship between Smoothness and Economy during Walking." *Journal of Biological Cybernetic* 69:213–18.

Albrecht, S., K. Ramírez-Amaro, F. Ruiz-Ugalde, D. Weikersdorfer, M. Leibold, M. Ulbrich, and M. Beetz. 2011. "Imitating Human Reaching Motions Using Physically Inspired Optimization Principles." *IEEE-RAS International Conference on Humanoid Robots* 602–7.

Anderson, Frank C. and Marcus G. Pandy. 1999. "A Dynamic Optimization Solution for Vertical Jumping in Three Dimensions." *Computer Methods in Biomechanics and Biomedical Engineering* 2(3):201–31.

Anderson, Frank C. and Marcus G. Pandy. 2001. "Dynamic Optimization of Human Walking." *Journal of Biomechanical Engineering* 123(5):381–90.

Anon. 2018. "OpenSim Plugin." Retrieved March 29, 2018 (https://simtk-confluence.stanford.edu:8443/display/OpenSim/Using+Plugins).

Anon. 2019. "Maxon Motor Datasheet." Retrieved (https://www.electromate.com/assets/catalog-library/pdfs/maxon/maxonmotor_2014_2015-Brushless-Flat-Motors.pdf).

Arnold, E. M., S. R. Hamner, A. Seth, M. Millard, and S. L. Delp. 2013. "How Muscle Fiber Lengths and Velocities Affect Muscle Force Generation as Humans Walk and Run at Different Speeds." *Journal of Experimental Biology* 216(11):2150–60.

Arnold, Edith M, Samuel R. Hamner, Ajay Seth, Matthew Millard, and Scott L. Delp. 2013. "How Muscle Fiber Lengths and Velocities Affect Muscle Force Generation as Humans Walk and Run at Different Speeds." *The Journal of Experimental Biology* 216(Pt 11):2150–60.

Bessonnet, G. 2005. "A Parametric Optimization Approach to Walking Pattern Synthesis." *The International Journal of Robotics Research* 24(7):523–36.

Betts, John T. 2010. *Practical Methods for Optimal Control and Estimation Using Nonlinear Programming*. Siam.

Van den Bogert, A. J., M. Hupperets, H. Schlarb, and B. Krabbe. 2012. "Predictive Musculoskeletal Simulation Using Optimal Control: Effects of Added Limb Mass on Energy Cost and Kinematics of Walking and Running." *Proceedings of the Institution of Mechanical Engineers, Part P: Journal of Sports Engineering and Technology* 226(2):123–33.

Van Den Bogert, Antonie J., Dimitra Blana, and Dieter Heinrich. 2011. "Implicit Methods for Efficient Musculoskeletal Simulation and Optimal Control." *Procedia IUTAM* 2:297–316.

Bonnefoy-Mazure, Alice and Stephane Armand. 2015. "Normal Gait." Pp. 200–211 in

Orthopedic Management of Children with Cerebral Palsy.

Bottasso, Carlo L., Boris I. Prilutsky, Alessandro Croce, Enrico Imberti, and Stefano Sartirana. 2006. "A Numerical Procedure for Inferring from Experimental Data the Optimization Cost Functions Using a Multibody Model of the Neuro-Musculoskeletal System." *Multibody System Dynamics* 16(2):123–54.

Bruijn, S. M., O. G. Meijer, P. J. Beek, and J. H. Van Dieën. 2013. "Assessing the Stability of Human Locomotion : A Review of Current Measures." *Journal of the Royal Society Interface* 10(83):20120999.

Caputo, Joshua M., Peter G. Adamczyk, and Steven H. Collins. 2015. "Informing Ankle-Foot Prosthesis Prescription through Haptic Emulation of Candidate Devices." *2015 IEEE International Conference on Robotics and Automation (ICRA)* 6445–50.

Cempini, Marco, Levi J. Hargrove, and Tommaso Lenzi. 2017. "Design, Development, and Bench-Top Testing of a Powered Polycentric Ankle Prosthesis." *IEEE International Conference on Intelligent Robots and Systems* 1064–69.

Chelouah, R. and P. Siarry. 2000. "A Continuous Genetic Algorithm Designed for the Global Optimization of Multimodal Functions." *Journal of Heuristics* 6(2):191–213.

Cherry, Michael S., Sridhar Kota, Aaron Young, and Daniel P. Ferris. 2016. "Running with an Elastic Lower Limb Exoskeleton." *Journal of Applied Biomechanics* 32(3):269–77.

Clever, Debora and Katja Mombaur. 2016. "An Inverse Optimal Control Approach for the Transfer of Human Walking Motions in Constrained Environment to Humanoid Robots." *Robotics: Science and Systems (RSS)*.

Colson, Benoît, Patrice Marcotte, and Gilles Savard. 2007. "An Overview of Bilevel Optimization." *Annals of Operations Research* 153(1):235–56.

Crowninshield, Roy D. and Richard A. Brand. 1981. "A Physiologically Based Criterion of Muscle Force Prediction in Locomotion." *Journal of Biomechanics* 14(11):793–801.

Davy, D. T. and M. L. Audu. 1987. "A Dynamic Optimization Technique for Predicting Muscle Forces in the Swing Phase of Gait." *Journal of Biomechanics* 20(2):187–201.

Delp, S. L. L., J. P. P. Loan, M. G. G. Hoy, F. E. Zajac, E. L. Topp, and J. M. Rosen. 1990. "An Interactive Graphics-Based Model of the Lower Extremity to Study Orthopedic Surgical Procedures." *IEEE Transactions on Biomedical Engineering* 37(8):757–67.

Delp, Scott L., Frank C. Anderson, Allison S. Arnold, Peter Loan, Ayman Habib, Chand T. John, Eran Guendelman, and Darryl G. Thelen. 2007. "OpenSim: Open-Source Software to Create and Analyze Dynamic Simulations of Movement." *IEEE Transactions on Biomedical Engineering* 54(11):1940–50.

Delp, Scott L. and J. Peter Loan. 2000. "A Computational Framework for Simulating and Analyzing Human and Animal Movement." *Computing in Science and Engineering* 2(5):46–55.

Dembia, Christopher L., Amy Silder, Thomas K. Uchida, Jennifer L. Hicks, and L. Delp. 2017. "Simulating Ideal Assistive Devices to Reduce the Metabolic Cost of Walking with Heavy Loads." *PLoS ONE* 12(7):e0180320.

Diehl, Moritz, Moritz Diehl, Hans Georg Bock, Holger Diedam, and Et Al. 2005. "Fast Direct Multiple Shooting Algorithms for Optimal Robot Control." *Fast Motions in Biomechanics and Robotics* 65–93.

Ding, Ye, Myunghee Kim, Scott Kuindersma, and Conor J. Walsh. 2018. "Human-in-the-Loop Optimization of Hip Assistance with a Soft Exosuit during Walking." *Science Robotics* 3(15):1–9.

Dorn, Tim W., Jack M. Wang, Jennifer L. Hicks, and Scott L. Delp. 2015. "Predictive Simulation Generates Human Adaptations during Loaded and Inclined Walking." *PLoS ONE* 10(4):e0121407.

Duclos, C., P. Desjardins, S. Nadeau, A. Delisle, D. Gravel, B. Brouwer, and H. Corriveau. 2009. "Destabilizing and Stabilizing Forces to Assess Equilibrium during Everyday Activities." *Journal of Biomechanics* 42(3):379–82.

Dumas, R., L. Cheze, L. Frossard, De Lyon, T. Umr, and Laboratoire De Biome. 2009. "Loading Applied on Prosthetic Knee of Transfemoral Amputee : Comparison of Inverse Dynamics and Direct Measurements." 30(4):560–62.

Electro-Craft Corporation. 1977. *DC Motors, Speed Controls, Servo Systems: An Engineering Handbook*.

Erdemir, A., S. McLean, W. Herzog, and A. J. van den Bogert. 2007. "Model-Based Estimation of Muscle Forces Exerted during Movements." *Clinical Biomech* 22(2):131–54.

Eshraghi, Arezoo, Noor Azuan Abu Osman, Hossein Gholizadeh, Mohammad Karimi, and Sadeeq Ali. 2012. "Pistoning Assessment in Lower Limb Prosthetic Sockets." *Prosthetics and Orthotics International* 36(1):15–24.

Esposito, Elizabeth Russell and Ross H. Miller. 2018. "Maintenance of Muscle Strength Retains a Normal Metabolic Cost in Simulated Walking after Transtibial Limb Loss." *PLoS ONE* 13(1):e0191310.

Esposito, Elizabeth Russell, Kelly M. Rodriguez, Christopher A. Ràbago, and Jason M. Wilken. 2014. "Does Unilateral Transtibial Amputation Lead to Greater Metabolic Demand during Walking?" *Journal of Rehabilitation Research and Development* 51(8):1287–96.

Farris, Dominic James and Gregory S. Sawicki. 2011a. "The Mechanics and Energetics of Human Walking and Running: A Joint Level Perspective." *J. R. Soc. Interface* 9(66):110–18.

Farris, Dominic James and Gregory S. Sawicki. 2011b. "The Mechanics and Energetics of Human Walking and Running: A Joint Level Perspective." *J. R. Soc. Interface* (May 2011):110–18.

Fey, Nicholas P., Glenn K. Klute, and Richard R. Neptune. 2012. "Optimization of Prosthetic

Foot Stiffness to Reduce Metabolic Cost and Intact Knee Loading during Below-Knee Amputee Walking: A Theoretical Study." *Journal of Biomechanical Engineering* 134(11):111005.

Fey, Nicholas P., Glenn K. Klute, and Richard R. Neptune. 2013. "Altering Prosthetic Foot Stiffness Influences Foot and Muscle Function during Below-Knee Amputee Walking: A Modeling and Simulation Analysis." *Journal of Biomechanics* 46(4):637–44.

Flash, Tamar and Neville Hogan. 1985. "The Coordination of Arm Movements: An Experimentally Confirmed Mathematical Model." *Journal of Neuroscience* 5(7):1688–1703.

Galle, S., P. Malcolm, W. Derave, and D. De Clercq. 2013. "Adaptation to Walking with an Exoskeleton That Assists Ankle Extension." *Gait and Posture* 38(3):495–99.

Galle, Samuel, Philippe Malcolm, Steven Hartley Collins, and Dirk De Clercq. 2017. "Reducing the Metabolic Cost of Walking with an Ankle Exoskeleton: Interaction between Actuation Timing and Power." *Journal of NeuroEngineering and Rehabilitation* 14(1):35.

Gard, Steven A. and Dudley S. Childress. 1999. "The Influence of Stance-Phase Knee Flexion on the Vertical Displacement of the Trunk during Normal Walking." *Archives of Physical Medicine and Rehabilitation* 80(1):26–32.

Gardiner, James, Abu Zeeshan Bari, David Howard, and Laurence Kenney. 2017. "Transtibial Amputee Gait Efficiency: Energy Storage and Return versus Solid Ankle Cushioned Heel Prosthetic Feet." *Journal of Rehabilitation Research and Development* 53(6):1133–38.

Genin, Joakim J., Guillaume J. Bastien, Bernard Franck, Christine Detrembleur, and Patrick A. Willems. 2008. "Effect of Speed on the Energy Cost of Walking in Unilateral Traumatic Lower Limb Amputees." *European Journal of Applied Physiology* 103(6):655–63.

Gidley, Alexi D., Anthony P. Marsh, and Brian R. Umberger. 2019. "Performance Criteria for Generating Predictive Optimal Control Simulations of Bicycle Pedaling." *Computer Methods in Biomechanics and Biomedical Engineering* (22):11–20.

Gill, Philip E., Walter Murray, and Michael A. Saunders. 2005. "SNOPT: An SQP Algorithm for Large-Scale Constrained Optimization." *SIAM Journal on Optimization* 12(4):979–1006.

Gordon, Keith E. and Daniel P. Ferris. 2007. "Learning to Walk with a Robotic Ankle Exoskeleton." *Journal of Biomechanics* 40(12):2636–44.

Griewank, Andreas. 1989. "On Automatic Differentiation." *Mathematical Programming: Recent Developments and Applications* 6(6):83–107.

De Groote, Friedl, Allison L. Kinney, Anil V. Rao, and Benjamin J. Fregly. 2016. "Evaluation of Direct Collocation Optimal Control Problem Formulations for Solving the Muscle Redundancy Problem." *Annals of Biomedical Engineering* 44(10):2922–36.

Das Gupta, Sauvik, Maarten F. Bobbert, and Dinant A. Kistemaker. 2019. "The Metabolic Cost of Walking in Healthy Young and Older Adults – A Systematic Review and Meta Analysis." *Scientific Reports* 9.

Hak, Laura, Jaap H. Van Dieën, Peter Van Der Wurff, Maarten R. Prins, Agali Mert, Peter J. Beek, and Han Houdijk. 2013. "Walking in an Unstable Environment: Strategies Used by Transtibial Amputees to Prevent Falling during Gait." *Archives of Physical Medicine and Rehabilitation* 94(11):2186–93.

Handford, Matthew L. and Manoj Srinivasan. 2016. "Robotic Lower Limb Prosthesis Design through Simultaneous Computer Optimizations of Human and Prosthesis Costs." *Scientific Reports* 6(February):19983.

Handford, Matthew L. and Manoj Srinivasan. 2018. "Energy-Optimal Human Walking with Feedback-Controlled Robotic Prostheses: A Computational Study." *IEEE Transactions on Neural Systems and Rehabilitation Engineering* 26(9):1773–82.

Handsfield, Geoffrey G., Craig H. Meyer, Joseph M. Hart, Mark F. Abel, and Silvia S. Blemker. 2014. "Relationships of 35 Lower Limb Muscles to Height and Body Mass Quantified Using MRI." *Journal of Biomechanics* 47(3):631–38.

Haupt, Randy L. and Sue Ellen Haupt. 2004. *Practical Genetic Algorithms*. John Wiley & Sons.

Haxton, H. A. 1944. "Absolute Muscle Force In The Ankle Flexors Of Man." *Physiology* 103:267–73.

Herr, Hugh M. and Alena M. Grabowski. 2012. "Bionic Ankle-Foot Prosthesis Normalizes Walking Gait for Persons with Leg Amputation." *Proceedings. Biological Sciences / The Royal Society* 279(1728):457–64.

Hof, A. L., M. G. J. Gazendam, and W. E. Sinke. 2005. "The Condition for Dynamic Stability." *Journal of Biomechanics* 38(1):1–8.

Huang, Stephanie and Daniel P. Ferris. 2012. "Muscle Activation Patterns during Walking from Transtibial Amputees Recorded within the Residual Limb-Prosthetic Interface." *Journal of NeuroEngineering and Rehabilitation* 9(1):55.

Jackson, Rachel W. and Steven H. Collins. 2015. "An Experimental Comparison of the Relative Benefits of Work and Torque Assistance in Ankle Exoskeletons." *Journal of Applied Physiology* 119(5):541–57.

Kaplan, Matthew L. and Jean H. Heegaard. 2001. "Predictive Algorithms for Neuromuscular Control of Human Locomotion." *Journal of Biomechanics* 34(8):1077–83.

Kidziński, Łukasz, Sharada P. Mohanty, Carmichael F. Ong, Jennifer L. Hicks, Sean F. Carroll, Sergey Levine, Marcel Salathé, and Scott L. Delp. 2018. "Learning to Run Challenge: Synthesizing Physiologically Accurate Motion Using Deep Reinforcement Learning." *The NIPS'17 Competition: Building Intelligent Systems* 101–20.

Kim, Myunghee and Steven H. Collins. 2015. "Once-per-Step Control of Ankle-Foot Prosthesis Push-off Work Reduces Effort Associated with Balance during Walking." *Journal of NeuroEngineering and Rehabilitation* 12(1):43.

Kim, Myunghee, Ye Ding, Philippe Malcolm, Jozefien Speeckaert, Christoper J. Siviy, Conor J. Walsh, and Scott Kuindersma. 2017. "Human-in-the-Loop Bayesian Optimization of

Wearable Device Parameters." *PLoS ONE* 12(9):e0184054.

Koelewijn, Anne D. and Antonie J. van den Bogert. 2016. "Joint Contact Forces Can Be Reduced by Improving Joint Moment Symmetry in Below-Knee Amputee Gait Simulations." *Gait and Posture* 49:219–25.

Koelewijn, Anne D., Eva Dorschky, and Antonie J. van den Bogert. 2018. "A Metabolic Energy Expenditure Model with a Continuous First Derivative and Its Application to Predictive Simulations of Gait." *Computer Methods in Biomechanics and Biomedical Engineering* 21(8):521–31.

Koller, Jeffrey R., Daniel A. Jacobs, Daniel P. Ferris, and C. David Remy. 2015. "Learning to Walk with an Adaptive Gain Proportional Myoelectric Controller for a Robotic Ankle Exoskeleton." *Journal of NeuroEngineering and Rehabilitation* 12(1):97.

LaPrè, A. K., M. A. Price, R. D. Wedge, B. R. Umberger, and Frank C. Sup. 2018. "Approach for Gait Analysis in Persons with Limb Loss Including Residuum and Prosthesis Socket Dynamics." *International Journal for Numerical Methods in Biomedical Engineering* 34(4):e2936.

Laprè, A. K., B. R. Umberger, and F. Sup. 2014. "Simulation of a Powered Ankle Prosthesis with Dynamic Joint Alignment." *IEEE Engineering in Medicine and Biology Society Conference* 1618–21.

Laprè, Andrew K., Vinh Q. Nguyen, Ulvi Baspinar, Michael White, and Frank C. Sup. 2017. "Capturing Prosthetic Socket Fitment: Preliminary Results Using an Ultrasound-Based Device." *IEEE International Conference on Rehabilitation Robotics* 1221–26.

LaPre, Andrew K., Brian R. Umberger, and Frank C. Sup IV. 2016. "A Robotic Ankle Prosthesis with Dynamic Alignment." *Journal of Medical Devices* 10(2):025001.

Lawson, Brian E., Jason Mitchell, Don Truex, Amanda Shultz, Elissa Ledoux, and Michael Goldfarb. 2014. "A Robotic Leg Prosthesis: Design, Control, and Implementation." *IEEE Robotics and Automation Magazine* 21(4):70–81.

Lee, Leng-Feng and Brian R. Umberger. 2016. "Generating Optimal Control Simulations of Musculoskeletal Movement Using OpenSim and MATLAB." *PeerJ* 4:e1638.

Lieber, Richard L., Gregory J. Loren, and Jan Friden. 1994. "In Vivo Measurement of Human Wrist Extensor Muscle Sarcomere Length Changes." *Journal of Neurophysiology* 71(3):874–81.

Lin, Yi-Chung, Jonathan P. Walter, and Marcus G. Pandy. 2018. "Predictive Simulations of Neuromuscular Coordination and Joint-Contact Loading in Human Gait." *Annals of Biomedical Engineering* 46(8):1216–17.

Luc, Martin, Amarantini David, and Violaine Cahou. 2002. "Static Optimal Estimation of Joint Accelerations for Inverse Dynamics Problem Solution." *Journal of Biomechanics* 35(11):1507–13.

Malcolm, Philippe, Wim Derave, Samuel Galle, and Dirk De Clercq. 2013. "A Simple

Exoskeleton That Assists Plantarflexion Can Reduce the Metabolic Cost of Human Walking." 8(2):1–7.

Mansouri, Misagh and Jeffrey A. Reinbolt. 2012. "Short Communication A Platform for Dynamic Simulation and Control of Movement Based on OpenSim and MATLAB." *Journal of Biomechanics* 45(8):1517–21.

McAsey, Michael, Libin Mou, and Weimin Han. 2012. "Convergence of the Forward-Backward Sweep Method in Optimal Control." *Computational Optimization and Applications* 53(1):207–26.

Mehrabi, Naser, Reza Sharif Razavian, Borna Ghannadi, and John McPhee. 2017. "Predictive Simulation of Reaching Moving Targets Using Nonlinear Model Predictive Control." *Frontiers in Computational Neuroscience* 10(January):143.

Millard, Matthew, Thomas Uchida, Ajay Seth, and Scott L. Delp. 2013. "Flexing Computational Muscle: Modeling and Simulation of Musculotendon Dynamics." *Journal of Biomechanical Engineering* 135(2):021005.

Miller, R. H., B. R. Umberger, J. Hamill, and G. E. Caldwell. 2011. "Evaluation of the Minimum Energy Hypothesis and Other Potential Optimality Criteria for Human Running." *Proceedings of the Royal Society B: Biological Sciences* 279(1733):1498–1505.

Miller, Ross H. 2014. "A Comparison of Muscle Energy Models for Simulating Human Walking in Three Dimensions." *Journal of Biomechanics* 47(6):1373–81.

Mitchell, Melanie. 1998. *An Introduction to Genetic Algorithms*. MIT Press.

Mombaur, Katja, Anh Truong, and Jean Paul Laumond. 2010. "From Human to Humanoid Locomotion-an Inverse Optimal Control Approach." *Autonomous Robots* 28(3):369–83.

Murray, M. P., L. A. Mollinger, G. M. Gardner, and S. B. Sepic. 1984. "Kinematic and EMG Patterns During Slow, Free, and Fast Walking." *Journal of Orthopedic Research* 2(3):272–80.

Neill, Matthew C. O., Leng-feng Lee, Brigitte Demes, Nathan E. Thompson, Susan G. Larson, Jack T. Stern, and Brian R. Umberger. 2015. "Three-Dimensional Kinematics of the Pelvis and Hind Limbs in Chimpanzee (Pan Troglodytes) and Human Bipedal Walking." *Journal of Human Evolution* 86:32–42.

Neptune, R. R., S. A. Kautz, and F. E. Zajac. 2001. "Contributions of the Individual Ankle Plantar Flexors to Support, Forward Progression and Swing Initiation during Walking." *Journal of Biomechanics* 34(11):1387–98.

Nguyen, Vinh Q., Russell T. Johnson, Frank C. Sup IV, and Brian R. Umberger. 2019. "Bilevel Optimization for Cost Function Determination in Dynamic Simulation of Human Gait." *IEE Transactions on Neural Systems and Rehabilitation Engineering* ((Accepted)).

Nguyen, Vinh Q., Brian R. Umberger, and Frank C. Sup IV. 2019. "Predictive Simulation of Human Walking Augmented by a Powered Ankle Exoskeleton." *IEEE ... International Conference on Rehabilitation Robotics* ((Accepted)).

Ong, Carmichael F., Jennifer L. Hicks, and Scott L. Delp. 2015. “Simulation-Based Design for Wearable Robotic Systems: An Optimization Framework for Enhancing a Standing Long Jump.” *IEEE Transactions on Biomedical Engineering* 63(5):894–903.

Otten, E. 2003. “Inverse and Forward Dynamics : Models of Multi-Body Systems.” *Philosophical Transactions of the Royal Society B: Biological Sciences* 358(1437):1493–1500.

Panizzolo, Fausto A., Ignacio Galiana, Alan T. Asbeck, Christopher Siviy, Kai Schmidt, Kenneth G. Holt, and Conor J. Walsh. 2016. “A Biologically-Inspired Multi-Joint Soft Exosuit That Can Reduce the Energy Cost of Loaded Walking.” *Journal of NeuroEngineering and Rehabilitation* 13(1):43.

Patriarco, A. G., R. W. Mann, S. R. Simon, and J. M. Mansour. 1981. “An Evaluation of the Approaches of Optimization Models in the Prediction of Muscle Forces during Human Gait.” *Journal of Biomechanics* 14(8):513–525.

Peng, Xue Bin, Glen Berseth, Michiel Van De Panne, and Kangkang Yin. 2017. “DeepLoco: Dynamic Locomotion Skills Using Hierarchical Deep Reinforcement Learning.” *ACM Transactions on Graphics* 36(4).

Porsa, Sina, Yi-Chung Lin, and Marcus G. Pandy. 2016. “Direct Methods for Predicting Movement Biomechanics Based Upon Optimal Control Theory with Implementation in OpenSim.” *Annals of Biomedical Engineering* 44(8):2542–57.

Powell, M. J. D. 2009. “The BOBYQA Algorithm for Bound Constrained Optimization without Derivatives.” *Cambridge NA Report NA2009/06* 26–46.

Prilutsky, Boris I. and Vladimir M. Zatsiorsky. 2002. “Optimization-Based Models of Muscle Coordination.” *Exercise and Sport Sciences Reviews* 30(1):32.

Quesada, Roberto E., Joshua M. Caputo, and Steven H. Collins. 2016. “Increasing Ankle Push-off Work with a Powered Prosthesis Does Not Necessarily Reduce Metabolic Rate for Transtibial Amputees.” *Journal of Biomechanics* 49(14):3452–59.

Quinlivan, B. T., S. Lee, P. Malcolm, D. M. Rossi, M. Grimmer, C. Siviy, N. Karavas, D. Wagner, A. T. Asbeck, I. Galiana, and C. J. Walsh. 2017. “Assistance Magnitude versus Metabolic Cost Reductions for a Tethered Multiarticular Soft Exosuit.” *Science Robotics* 2(2):4416.

Rajagopal, Apoorva, Christopher Dembia, Matthew DeMers, Denny Delp, Jennifer Hicks, and Scott Delp. 2016. “Full Body Musculoskeletal Model for Muscle-Driven Simulation of Human Gait.” *IEEE Transactions on Biomedical Engineering* 63(10):2068–79.

Ralston, H. J. 1976. “Energetics of Human Walking.” Pp. 77–98 in *Neural Control of Locomotion*. Springer US.

Rao, Anil V. 2009. “A Survey of Numerical Methods for Optimal Control.” *Advances in the Astronautical Sciences* 135(1):497–528.

Rasmussen, John, Michael Damsgaard, and Michael Voigt. 2001. “Muscle Recruitment by the Min/Max Criterion - A Comparative Numerical Study.” *Journal of Biomechanics*

34(3):409–15.

Rebula, John R. and Arthur D. Kuo. 2015. “The Cost of Leg Forces in Bipedal Locomotion: A Simple Optimization Study.” *PLoS ONE* 10(2):e0117384.

Sanders, Joan E., Ari Karchin, John R. Fergason, and Elizabeth a Sorenson. 2006. “A Noncontact Sensor for Measurement of Distal Residual-Limb Position during Walking.” *Journal of Rehabilitation Research and Development* 43(4):509.

Sartori, Massimo, Monica Reggiani, Dario Farina, and David G. Lloyd. 2012. “EMG-Driven Forward-Dynamic Estimation of Muscle Force and Joint Moment about Multiple Degrees of Freedom in the Human Lower Extremity.” *PLoS ONE* 7(12):e52618.

Sasaki, K., R. R. Neptune, and S. A. Kautz. 2009. “The Relationships between Muscle, External, Internal and Joint Mechanical Work during Normal Walking.” *Journal of Experimental Biology* 212(5):738–44.

Schmitz, Anne, Amy Silder, Bryan Heiderscheit, Jane Mahoney, and Darryl G. Thelen. 2009. “Differences in Lower-Extremity Muscular Activation during Walking between Healthy Older and Young Adults.” *Journal of Electromyography Kinesiology* 19(6):1085–91.

Serrancolí, Gil, Josep M. Font-Llagunes, and Ana Barjau. 2014. “A Weighted Cost Function to Deal with the Muscle Force Sharing Problem in Injured Subjects: A Single Case Study.” *Proceedings of the Institution of Mechanical Engineers, Part K: Journal of Multi-Body Dynamics* 228(3):241–51.

Serrancolí, Gil, Allison L. Kinney, Benjamin J. Fregly, and Josep M. Font-Llagunes. 2016. “Neuromusculoskeletal Model Calibration Significantly Affects Predicted Knee Contact Forces for Walking.” *Journal of Biomechanical Engineering* 138(8):081001.

Seth, Ajay, Michael Sherman, Jeffrey a. Reinbolt, and Scott L. Delp. 2011. “OpenSim: A Musculoskeletal Modeling and Simulation Framework for in Silico Investigations and Exchange.” *Procedia Iutam* 2:212–32.

Shourijeh, Mohammad S., Naser Mehrabi, and John McPhee. 2017. “Forward Static Optimization in Dynamic Simulation of Human Musculoskeletal Systems: A Proof-of-Concept Study.” *Journal of Computational and Nonlinear Dynamics* 12(September):051005.

Sinha, Ankur, Pekka Malo, and Kalyanmoy Deb. 2017. “A Review on Bilevel Optimization : From Classical to Evolutionary Approaches and Applications.” *IEEE Transactions on Evolutionary Computation* 22(2):276–95.

Sinha, Ankur, Pekka Malo, Anton Frantsev, and Kalyanmoy Deb. 2014. “Finding Optimal Strategies in a Multi-Period Multi-Leader-Follower Stackelberg Game Using an Evolutionary Algorithm.” *Computers and Operations Research* 41:374–85.

Van Soest, A. J. Knoek and L. J. R. Richard Casius. 2003. “The Merits of a Parallel Genetic Algorithm in Solving Hard Optimization Problems.” *TRANSACTIONS-AMERICAN SOCIETY OF MECHANICAL ENGINEERS JOURNAL OF BIOMECHANICAL ENGINEERING* 125(1):141–46.

Song, Seungmoon and Hartmut Geyer. 2018. “Predictive Neuromechanical Simulations Indicate Why Walking Performance Declines with Ageing.” *Journal of Physiology* 596(7):1199–1210.

Sreenivasa, Manish, Matthew Millard, Martin Felis, Katja Mombaur, and Sebastian I. Wolf. 2017. “Optimal Control Based Stiffness Identification of an Ankle-Foot Orthosis Using a Predictive Walking Model.” *Frontiers in Computational Neuroscience* 11(April):23.

Srinivasan, Manoj. 2010. “Fifteen Observations on the Structure of Energy-Minimizing Gaits in Many Simple Biped Models.” *Journal of The Royal Society Interface* 8(54):74–98.

Sugar, Thomas G., Andrew Bates, Matthew Holgate, Jason Kerestes, Marc Mignolet, Philip New, Ragesh K. Ramachandran, Sangram Redkar, and Chase Wheeler. 2015. “Limit Cycles to Enhance Human Performance Based on Phase Oscillators.” *Journal of Mechanisms and Robotics* 7(1):011001.

Suryan, Varun, Ankur Sinha, Pekka Malo, and Kalyanmoy Deb. 2016. “Handling Inverse Optimal Control Problems Using Evolutionary Bilevel Optimization.” *2016 IEEE Congress on Evolutionary Computation (CEC)* 1893–1900.

Thelen, Darryl G. 2003. “Adjustment of Muscle Mechanics Model Parameters to Simulate Dynamic Contractions in Older Adults.” *Journal of Biomechanical Engineering* 125(1):70–77.

Thelen, Darryl G. and Frank C. Anderson. 2006. “Using Computed Muscle Control to Generate Forward Dynamic Simulations of Human Walking from Experimental Data.” *Journal of Biomechanics* 39(6):1107–15.

Thelen, Darryl G., Frank C. Anderson, and Scott L. Delp. 2003. “Generating Dynamic Simulations of Movement Using Computed Muscle Control.” *Journal of Biomechanics* 36(3):321–28.

Uchida, Thomas K., Ajay Seth, Soha Pouya, Christopher L. Dembia, Jennifer L. Hicks, and Scott L. Delp. 2016. “Simulating Ideal Assistive Devices to Reduce the Metabolic Cost of Running.” *PLoS ONE* 11(9):e0163417.

Umberger, B. R. 2010. “Stance and Swing Phase Costs in Human Walking.” *Journal of the Royal Society Interface* 7(50):1329–40.

Umberger, B. R., K. G. M. Gerritsen, and P. E. Martin. 2003. “A Model of Human Muscle Energy Expenditure.” *Computer Methods in Biomechanics and Biomedical Engineering* 6(2):99–111.

Umberger, B. R. and P. E. Martin. 2007. “Mechanical Power and Efficiency of Level Walking with Different Stride Rates.” *Journal of Experimental Biology* 210(18):3255–65.

Umberger, Brian R. and Ross H. Miller. 2017. “Handbook of Human Motion.”

Vaerenbergh, Steven Van, Juan José Murillo-fuentes, Fernando Pérez-cruz, Miguel Lázaro-gredilla, and Ignacio Santamaría. 2013. “Gaussian Process for Nonlinear Signal Processing.” *IEEE Signal Processing Magazine* 30(4):40–50.

Vlassenbroeck, Jacques and Rene Van Dooren. 1988. “A Chebyshev Technique for Solving Nonlinear Optimal Control Problems.” *IEEE Transactions on Automatic Control* 33(4):333–40.

Wächter, Andreas. 2003. “An Interior Point Algorithm for Large-Scale Nonlinear Optimization with Applications in Process Engineering.” *PhD Thesis*.

Wächter, Andreas and Lorenz T. Biegler. 2006. “On the Implementation of Primal-Dual Interior Point Filter Line Search Algorithm for Large-Scale Nonlinear Programming.” *Mathematical Programming* 106(1):25–57.

Ward, Samuel R., Carolyn M. Eng, Laura H. Smallwood, and Richard L. Lieber. 2009. “Are Current Measurements of Lower Extremity Muscle Architecture Accurate?” *Clinical Orthopaedics and Related Research* 467(4):1074–82.

Winter, David A. 2009. *Biomechanics and Motor Control of Human Movement*. John Wiley & Sons.

Witte, Kirby Ann, Juanjuan Zhang, Rachel W. Jackson, and Steven H. Collins. 2015. “Design of Two Lightweight, High-Bandwidth Torque-Controlled Ankle Exoskeletons.” *Proceedings - IEEE International Conference on Robotics and Automation* 2015-June(June):1223–28.

Xiang, Yujiang, Jasbir S. Aora, Salam Rahmatalla, and Karim Abdel-Malek. 2009. “Optimization-Based Dynamic Humanwalking Prediction: One Step Formulation.” *Numerical Methods In Engineering* 79(6):667–95.

Xiang, Yujiang, Jasbir S. Arora, and Karim Abdel-Malek. 2011. “Optimization-Based Prediction of Asymmetric Human Gait.” *Journal of Biomechanics* 44(4):683–93.

Xiang, Yujiang, Hyun-Joon Chung, Joo H. Kim, Rajankumar Bhatt, Salam Rahmatalla, Jingzhou Yang, Timothy Marler, Jasbir S. Arora, and Karim Abdel-Malek. 2010. “Predictive Dynamics: An Optimization-Based Novel Approach for Human Motion Simulation.” *Structural and Multidisciplinary Optimization* 41(3):465–79.

Yamaguchi, Gary T. and Felix E. Zajac. 1989. “A Planar Model of the Knee Joint to Characterize the Knee Extensor Mechanism.” *Journal of Biomechanics* 22(1):1–10.

Yin, Yafeng. 2000. “Genetic Algorithms Based Approach for Bilevel Programming Models.” *Journal of Transportation Engineering* 126(2):115–20.

Zhang, Juanjuan, Pieter Fiers, Kirby A. Witte, Rachel W. Jackson, Katherine L. Poggensee, Christopher G. Atkeson, and Steven H. Collins. 2017. “Human-in-the-Loop Optimization of Exoskeleton Assistance during Walking.” *Science* 356(6344):1280–83.

Zhao, Jie, Karsten Berns, and Roberto De Souza Baptista. 2013. “Design of Variable-Damping Control for Prosthetic Knee Based on a Simulated Biped.” *2013 IEEE 13th International Conference on Rehabilitation Robotics (ICORR)* 1–6.

Zhao, Zhigang and Xinyi Gu. 2006. “Particle Swarm Optimization Based Algorithm for Bilevel Programming Problems.” *International Conference on Intelligent Systems Designs and Applications* 2:951–56.

Zhou, Lelai, Yibin Li, and Shaoping Bai. 2017. “A Human-Centered Design Optimization Approach for Robotic Exoskeletons through Biomechanical Simulation.” *Robotics and Autonomous Systems* 91:337–47.

Zmitrewicz, Robert J., Richard R. Neptune, and Kotaro Sasaki. 2007. “Mechanical Energetic Contributions from Individual Muscles and Elastic Prosthetic Feet during Symmetric Unilateral Transtibial Amputee Walking: A Theoretical Study.” *Journal of Biomechanics* 40(8):1824–31.